February 1, 2008
hep-ph/0311186
Freiburg-THEP 03/20

Two-Loop Vertices in Quantum Field Theory: Infrared Convergent Scalar Configurations*

Andrea Ferroglia†

Fakultät für Physik, Albert-Ludwigs Universität, Freiburg, Germany
Institut für Theoretische Teilchenphysik, Universität Karlsruhe, Karlsruhe, Germany

Massimo Passera‡

Dipartimento di Fisica, Università di Padova and INFN–Padova, Italy
Departament de Física Teòrica and IFIC, Universitat de València – CSIC, Spain
Institut für Theoretische Physik, Universität Bern, Bern, Switzerland

Giampiero Passarino§ and Sandro Uccirati¶

Dipartimento di Fisica Teorica, Università di Torino, Italy
INFN, Sezione di Torino, Italy

A comprehensive study is performed of general massive, scalar, two-loop Feynman diagrams with three external legs. Algorithms for their numerical evaluation are introduced and discussed, numerical results are shown for all different topologies, and comparisons with analytical results, whenever available, are performed. An internal cross-check, based on alternative procedures, is also applied. The analysis of infrared divergent configurations, as well as the treatment of tensor integrals, will be discussed in two forthcoming papers.

Key words: Feynman diagrams, Multi-loop calculations, Vertex diagrams

PACS Classification: 11.10.-z; 11.15.Bt; 12.38.Bx; 02.90.+p; 02.60.Jh; 02.70.Wz

*Work supported by the European Union under contract HPRN-CT-2000-00149, by MIUR under contract 2001023713_006 and by the MCyT grant FPA 2002-00612.

†andrea.ferroglia@physik.uni-freiburg.de
‡massimo.passera@pd.infn.it
§giampiero@to.infn.it
¶uccirati@to.infn.it

Contents

1 Introduction

This paper is the fourth in a series devoted to numerical evaluation of the multi-loop, multi-leg Feynman diagrams that appear in any renormalizable quantum field theory. In [1] (hereafter I) the general strategy has been designed and in [2] (hereafter II) a complete list of results has been derived for two-loop functions with two external legs, including their infrared divergent on-shell derivatives. Results for one-loop multi-leg diagrams have been shown in [3] and additional material can be found in [4].

In a new series of papers we will present a complete set of results for the class of fully general three-point, two-loop diagrams. There has been an extensive writing on the subject and known results in this area are given in [5]; however, to the best of our knowledge, we are still missing some general attempt to systematize the field (with the noticeable exception of [6]).

Due to the complexity of the problem, six different topologies with up to six propagators, see Fig. 7, we have found natural to split our presentation into three parts: in this paper we will analyze general, scalar, massive configurations, while the treatment of the corresponding tensor integrals [7] and infrared divergent two-loop vertices [8] will be discussed in two forthcoming papers (for recent numerical tests of existing analytical results see [9] and [10]). Furthermore, there are parallel developments in our project: a FORM [11] code is being created for the generation of all one- and two-loop diagrams (so far only in the context of the standard model [12]), and all the numerical algorithms are being assembled into a FORTRAN code [13]. Well-known packages for diagram handling are in [14].

Any Feynman diagram is built, starting from the rules fixed by the Lagrangian of the theory under study, using two ingredients: vertices and propagators. The latter are represented in momentum space by

$$\frac{N(p)}{p^2 + m^2 - i\,\delta}, \tag{1}$$

where $\delta \to 0_+$ and $N(p)$ is a structure depending on spin. For a selected number of external legs and a given order in perturbation theory, the diagrams are constructed from propagators and vertices according to the allowed topologies, and are then endowed with signs and combinatorial factors [15].

Despite the dramatic recent progress in the field of analytical evaluation of Feynman integrals, Mellin-Barnes techniques [16], shifting dimensions [17], differential [18] and difference [19] equations, non-recursive solutions of recurrence equations [20], just to name a few, we firmly believe that sooner or later we will achieve the structural limit of the field and that a general solution can only be numerical.

Our general approach toward the numerical evaluation of an arbitrary Feynman diagram G, a typical example of a multi-scale problem, is to use a Feynman parameter representation and to obtain – diagram-by-diagram – some integral representation of the following form:

$$G = \frac{1}{B_G} \int_S dx\, \mathcal{G}(x), \tag{2}$$

where x is a vector of Feynman parameters, S is some simplex, $\mathcal{G}$ is an integrable function (in the limit $\delta \to 0$) and B_G is a function of masses and external momenta whose zeros correspond to true singularities of G, if any. The Bernstein-Tkachov (hereafter BT) functional relations [21] are one example but, in this work, we will consider other realizations of Eq.(2). One example will be enough to characterize the criterion of smoothness. Although the integral

$$I = \int_0^1 dx \left[V(x) - i\,\delta\right]^{-1+\epsilon} = \int_0^1 dx \left(h\,x^2 + 2\,k\,x + l - i\,\delta\right)^{-1+\epsilon} \tag{3}$$

is well defined through the $i\,\delta$ prescription, it is not convenient to attempt a direct numerical integration because poles may be dangerously close to the real axis. However, after some algebraic manipulation we

can write $V_\delta = V - i\,\delta$,

$$I = \frac{h}{h\,l - k^2}\left\{1 - \frac{1}{2}\left(1 + \frac{k}{h}\right)\,\ln V_\delta(1) + \frac{k}{2h}\,\ln V_\delta(0) + \frac{1}{2}\int_0^1 dx\,\ln\,V_\delta(x) + \mathcal{O}\left(\epsilon\right)\right\}, \tag{4}$$

which is much easier to evaluate and where $h\,l = k^2$ represents a pinch singularity [22] for I. One drawback of Eq.(4) is that the behavior around the singularity is overestimated. Therefore, whenever in the presence of a true singularity of G, we took particular care in investigating the integral representation with the correct behavior since, as well-known and as shown in our specific example, most if not all of the methods currently employed tend to overestimate the singular behavior.

Smoothness requires that the kernel in Eq.(2) and its first N derivatives be continuous functions and, ideally, N should be as large as possible. However, in most of the cases we will be satisfied with absolute convergence, e.g. logarithmic singularities of the kernel. This is particularly true around the zeros of B_G where the large number of terms required by obtaining continuous derivatives of higher order leads to large numerical cancellations.

There are other alternative approaches to the numerical evaluation of multi-loop Feynman diagrams where differential equations are written and solved but, to our knowledge, they have been applied – so far – only to two-point functions or to QED/QCD examples [23].

In any realistic calculation tensor integrals will appear and we distinguish between two different applications: before assembling all terms into the S-matrix element associated with some physical process we must verify the complete set of Ward-Slavnov-Taylor identities (hereafter WST) and this requires reduction, often called scalarization, of the corresponding expressions. While at one-loop level we only need reduction to standard scalar functions $A_0, B_0, \cdots$ [24], here the number of scalar expressions which are required is larger because of irreducible numerators, i.e. we have less propagators in a diagrams than scalar products, and the adjective "scalar" should be used only when we enlarge the class of functions to arbitrary space-time dimension and arbitrary powers for the propagators. However, in [7] we will be able to show that this is only a semantic question and we will present our version for a scheme of scalarization. After checking that the relevant WST identities are satisfied, we plan to organize our calculation for physical observables according to gauge-parameter independent blocks $\mathcal{B}_i$, each of which will be mapped into one integral of the form

$$\mathcal{B}_i = \int_S dx \sum_{j\,\in\,i} \frac{1}{B_G^{ij}}\,P^{ij}(x)\,\mathcal{G}^{ij}(x), \tag{5}$$

where P are polynomials in the Feynman parameters. Of course, checking unrenormalized WST identities is only a test on having correctly generated and evaluated the diagrams and, in the end, we will have to control also renormalized WST identities.

We mention here that, in our approach, numerical evaluation of infrared divergent vertices is always understood as numerical evaluation of the residues of the infrared (or even collinear) poles at space-time dimension $n = 4$ and of the corresponding finite parts. In any realistic calculation infrared (and, eventually, collinear poles) will be combined with real emission of both photons and gluons according to some scheme, e.g. dipole-formalism [25]. Our strategy, to be fully described in [8], will always start with techniques which aim to extract the infrared/collinear divergent part of two-loop vertices, with a finite remainder. To summarize we either express the diagram through hypergeometric functions in arbitrary space-time dimensions that are subsequently expanded around $n = 4$ (cf. with Sect 7.4 of [2]) or we use sector decomposition (a technique introduced in [26]). In both cases we are able to obtain results valid in all regions, not only in the unphysical one.

Finally we stress that, whenever possible, we have been seeking for at least two independent algorithms per diagram in order to allow for an internal cross-check of our results.

The outline of the paper will be as follows: in Section 2 we describe our conventions for a general definition of two-loop diagrams. Special cases and special topologies are discussed in Section 3. The class of G^{1N1} diagrams is analyzed in Section 4. All two-loop vertex-like topologies and the related derivatives of self-energy diagrams needed in the wave function renormalization factors are described and evaluated in Section 5 – 10. Numerical results are shown in Section 11. Several technical details, ranging from solutions of Landau equations [27] to recurrent integrals encountered in the text are analyzed in several appendices.

2 General definitions and conventions

In this section we present basic definitions and properties of Feynman diagrams. An arbitrary two-loop scalar diagram can be cast in the following form:

$$(\alpha; m_1, \ldots, m_\alpha; \eta_1 | \gamma; m_{\alpha+1}, \ldots, m_{\alpha+\gamma}; \eta_{12} | \beta; m_{\alpha+\gamma+1}, \ldots, m_{\alpha+\gamma+\beta}; \eta_2) =$$
$$\frac{\mu^{2\epsilon}}{\pi^4} \int d^n q_1 \, d^n q_2 \prod_{i=1}^{\alpha} (k_i^2 + m_i^2)^{-1} \prod_{j=\alpha+1}^{\alpha+\gamma} (k_j^2 + m_j^2)^{-1} \prod_{l=\alpha+\gamma+1}^{\alpha+\gamma+\beta} (k_l^2 + m_l^2)^{-1}, \tag{6}$$

where $n = 4 - \epsilon$, n is the space-time dimension, and α, β and γ give the number of lines in the q_1, q_2 and $q_1 - q_2$ loops, respectively. Furthermore we have

$$\begin{array}{ll} k_i = q_1 + \sum_{j=1}^{N} \eta_{ij}^1 \, p_j, & i = 1, \ldots, \alpha \\ k_i = q_1 - q_2 + \sum_{j=1}^{N} \eta_{ij}^{12} \, p_j, & i = \alpha + 1, \ldots, \alpha + \gamma \\ k_i = q_2 + \sum_{j=1}^{N} \eta_{ij}^{2} \, p_j, & i = \alpha + \gamma + 1, \ldots, \alpha + \gamma + \beta, \end{array}$$

where N is the number of vertices, $\eta^a = \pm 1$, or 0, $\{p\}$ is the set of external momenta and μ is the arbitrary unit of mass. Diagrams that can always be reduced to combinations of other diagrams with less internal lines will never receive a particular name. Otherwise we will denote a two-loop scalar diagram with $G^{\alpha\beta\gamma}$ where $G = S, V, B$ etc. stands for two-, three-, four-point etc. Family of diagrams with the same number N of internal lines will be denoted collectively by S_N, etc.

Next we recall few basic properties of two-loop diagrams [28]. In any two-loop diagram there are three one-loop sub-diagrams, called $\alpha\gamma, \beta\gamma$ and $\alpha\beta$ sub-diagrams respectively.

Definition 1: the $\alpha\beta\gamma$ diagram is overall ultraviolet (UV) convergent if $\alpha + \beta + \gamma > 4$, logarithmically divergent if $\alpha + \beta + \gamma = 4$, linearly divergent if $\alpha + \beta + \gamma = 3$, and so on.

Definition 2: the $\alpha\beta$ sub-diagram is convergent if $\alpha + \beta > 2$, logarithmically divergent if $\alpha + \beta = 2$, linearly divergent if $\alpha + \beta = \frac{3}{2}$, and so on.

If any of the one-loop sub-diagrams diverge, we will have counter-terms associated with them. Therefore, in addition to the $\alpha\beta\gamma$ diagram we will also consider the subtraction diagrams of Fig. 1, $G^{\underline{\alpha}\beta\underline{\gamma}}$ etc. More specifically, an arbitrary vertex diagram (often referred to as a three-point function) is depicted in Fig. 2 where, in our conventions, all external momenta are flowing inward and $P = p_1 + p_2$ [1]. The sign of the invariants is left unspecified and each external mass squared can represent not only a mass squared but one of the Mandelstam invariants, $s \geq 0$ and $t \leq 0$. We also introduce scaled quantities

$$\mu_i^2 = \frac{m_i^2}{|\, -P^2 \,|}, \quad i = 1, \ldots, N, \qquad \nu_j^2 = \mid \frac{p_j^2}{P^2} \mid, \quad j = 1, 2, \tag{7}$$

[1] In our metric, space-like p implies $p^2 = \vec{p}^{\,2} + p_4^2 > 0$. Also, it is $p_4 = i\, p_0$ with p_0 real for a physical four-momentum.

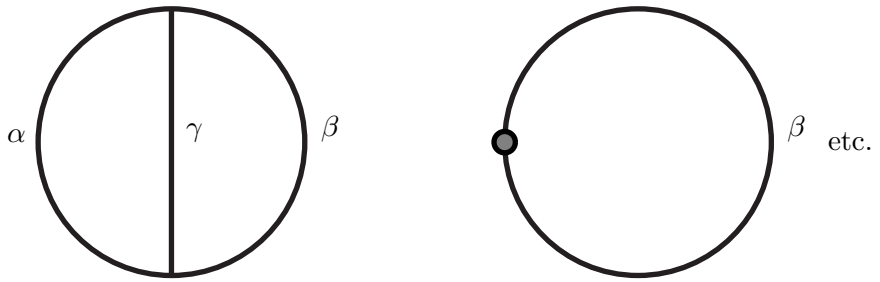

Figure 1: The arbitrary two-loop diagram $G_L^{\alpha\beta\gamma}$ of Eq.(6) and one of the associated subtraction sub-diagrams.

where $m_i,\ i = 1, \ldots, N$ are the internal masses and Mandelstam invariants

$$P^2 = -\, s_p\, M^2, \qquad p_i^2 = -\, s_i\, M_i^2, \qquad s_p, s_i = \pm 1, \tag{8}$$

where M^2 and M_i^2 are positive. The diagrams are evaluated within dimensional regularization where the space-time dimensionality is $n = 4 - \epsilon$. Therefore, we define a two-loop $\overline{MS}$ factor

$$\Delta_{UV} = \gamma + \ln \pi + \ln \frac{M^2}{\mu^2}, \tag{9}$$

where $\gamma = 0.577216\cdots$ is the Euler's constant. We will also use the shorthand notation

$$\mathcal{G}(n) = \left(\frac{\mu^2}{\pi}\right)^{\epsilon} \Gamma\left(n + \epsilon\right), \qquad \mathcal{G}(n, M^2) = \left(\frac{\mu^2}{\pi\, M^2}\right)^{\epsilon} \Gamma\left(n + \epsilon\right), \tag{10}$$

where Γ denotes the Euler's gamma-function. Note that in this paper we will use the van der Bij-Veltman parametrization [29] of two-loop integrals rather than the more familiar Cvitanovic-Kinoshita one [30]. Finally, to keep our results as compact as possible, we introduce the following notations where $x_0 = y_0 = 1$

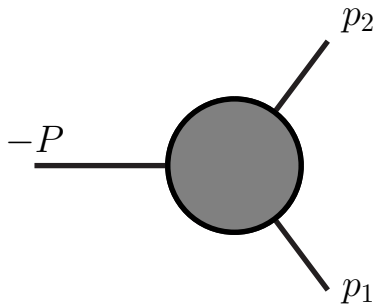

Figure 2: The three-point Green function. All external momenta are flowing inward, $P = p_1 + p_2$.

$$\begin{aligned}
\int dS_n(\{x\})\, f(x_1, \cdots, x_n) &\equiv \prod_{i=1}^{n} \int_0^{x_{i-1}} dx_i\, f(x_1, \cdots, x_n), \\
\int dC_n(\{x\})\, f(x_1, \cdots, x_n) &\equiv \int_0^1 \prod_{i=1}^{n} dx_i\ f(x_1, \cdots, x_n), \\
\int dCS\left(\{x\}\,;\, \{y\}\right)\, f(x_1, \cdots, x_{n_1}, y_1, \cdots, y_{n_2}) &\equiv \int_0^1 \prod_{i=1}^{n_1} dx_i \prod_{j=1}^{n_2} \int_0^{y_{j-1}} dy_j\, f(x_1, \cdots, x_{n_1}, y_1, \cdots, y_{n_2}).
\end{aligned} \tag{11}$$

When no confusion arises we will, eventually, omit the list of arguments which will be, otherwise, made compact by using the following notation:

$$f(\{x\}\,;\,[y\,z\,u]_i) = \begin{cases} f(\{x\}\,;\,y,z) \text{ for } i=0 \\ f(\{x\}\,;\,z,z) \text{ for } i=1 \\ f(\{x\}\,;\,z,u) \text{ for } i=2 \end{cases}. \tag{12}$$

Furthermore the so-called $'+'$-distribution will be extensively used, e.g.

$$\int d\{z\} \int_0^1 dx\, \frac{f(x,\{z\})}{x}\,|_+ = \int d\{z\} \int_0^1 dx\, \frac{f(x,\{z\}) - f(0,\{z\})}{x}, \tag{13}$$

etc. Gram's determinants associated with N vectors $p_1, \cdots, p_2$ are always denoted by

$$G_{1\cdots N} = -\det(p_i \cdot p_j). \tag{14}$$

Quite often we are interested in the condition $G_{12} \geq 0$ which requires that p_1 and/or p_2 and/or $p_1 + p_2$ be time-like. Therefore the condition is violated only if the momenta occurring in G_{12} are all space-like, indeed time-like momenta and $G_{12} < 0$ cannot happen for $p_{1,2}$ real.

2.1 Alphameric classification of diagrams

As we have seen any scalar two-loop diagram is identified by a capital letter (S, V etc) indicating the number of external legs and by a triplet of numbers (α, β and γ) giving the number of internal lines (in the q_1, q_2 and $q_1 - q_2$ loops respectively). There is a compact way of representing this triplet: assume that $\gamma \neq 0$, i.e. that we are dealing with non-factorisable diagrams, then we introduce the integer

$$\kappa = \gamma_{\max}\left[\alpha_{\max}\,(\beta - 1) + \alpha - 1\right] + \gamma \tag{15}$$

for each diagram. For $G = V$ we have $\alpha_{\max} = 2$ and $\gamma_{\max} = 2$. We can then associate a letter of the alphabet to each value of κ, thus introducing the following correspondence between $\alpha\beta\gamma$ and κ:

$$121 \to E, \quad 131 \to I, \quad 141 \to M, \quad 221 \to G, \quad 231 \to K, \quad 222 \to H. \tag{16}$$

This classification is extensively used throughout the paper.

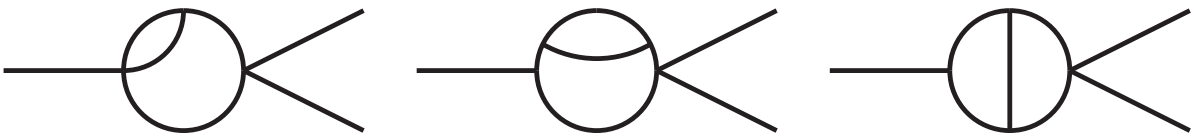

Figure 3: Examples of two-loop vertices that are topologically equivalent to self-energies.

3 Special kinds of diagrams

In this section we introduce special diagrams, topologically equivalent to either one-loop or two-loop configurations, which are naturally connected with two-loop vertices. First of all we have two-loop vertices with the topology of a self-energy (i.e., diagrams with only two vertices connected to the external legs) which are shown in Fig. 3. They are given by $S^{121}(P), S^{131}(P)$ and $S^{221}(P)$, with $P = p_1 + p_2$, and have been evaluated in [2].

3.1 One-loop counter-terms in two-loop diagrams

Renormalization in quantum field theory is a order-by-order procedure, therefore we also have to consider those one-loop vertices with the insertion of a counter-term, which are associated with the two-loop vertices of Fig. 7. There are several subtraction diagrams, for instance three associated with one-loop

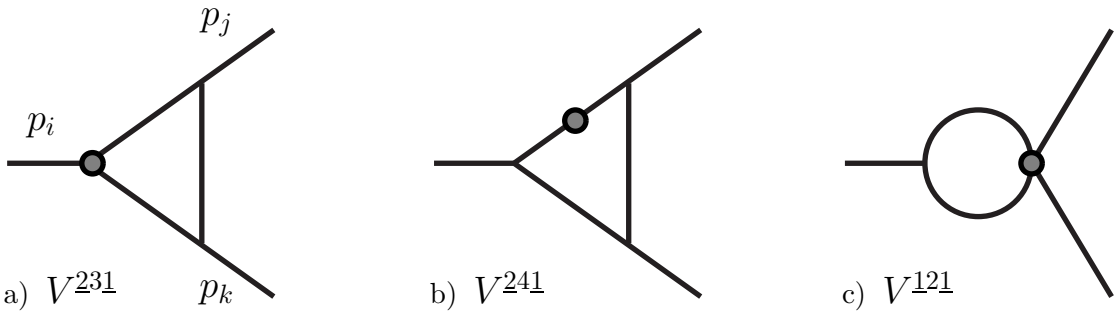

Figure 4: Examples of one-loop vertices with counter-terms (gray circles). Permutations are understood.

vertex counter-terms, Fig. 4(a),

$$V^{\rm sub}_{v;i} = \frac{\mu^\epsilon}{i\,\pi^2}\,\delta V_i \int d^n q\,\frac{1}{(q^2+m_k^2)\,((q+p_i)^2+m_i^2)\,((q+p_i+p_j)^2+m_j^2)}, \tag{17}$$

where $i = 1,\ldots,3$, and three associated with one-loop self-energy counter-terms, Fig. 4(b),

$$V^{\rm sub}_{s;i} = \frac{\mu^\epsilon}{i\,\pi^2}\,\delta S_i \int d^n q\,\frac{1}{(q^2+m_k^2)\,((q+p_i)^2+m_i^2)^2\,((q+p_i+p_j)^2+m_j^2)}, \tag{18}$$

where $i = 1,\ldots,3$. We easily obtain

$$V^{\rm sub}_{v;i} = \delta V_i\,C_0(1,1,1\,|\,p_i^2,p_j^2,p_k^2;m_k,m_i,m_j), \quad V^{\rm sub}_{s;i} = \delta S_i\,C_0(1,2,1\,|\,p_i^2,p_j^2,p_k^2;m_k,m_i,m_j), \tag{19}$$

where $\delta V_i, \delta S_i$ have been fixed, for instance in the $\overline{MS}$-scheme, by a one-loop calculation and contain an ultraviolet pole. C_0 is the generalized, scalar, form factor with arbitrary powers in the propagators which must be evaluated up to $\mathcal{O}(\epsilon)$, contrary to the one-loop case. According to the findings of [3] all one-loop diagrams are evaluated, at any order in ϵ, according to the BT-algorithm. Counter-terms associated with one-loop four-point vertices, Fig. 4(c), will be included as well:

$$V^{\rm sub}_{v;jk} = \delta V^q_{jk}\,B_0(p_i^2;m_1,m_2). \tag{20}$$

Note that subtractions associated with the diagrams of Fig. 3 have not been explicitly included in Fig. 4.

3.2 Wave function renormalization

To perform two-loop wave function renormalization we need the p^2 derivatives of two-point functions which are always a combination of scalar and tensor self-energies (those with powers of irreducible scalar products in the numerator) where one of the propagators containing the external momentum p has power -2, as depicted in Fig. 5.

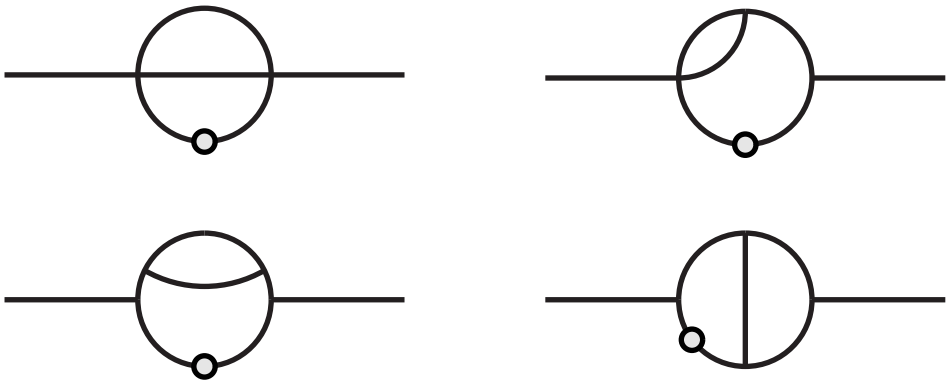

Figure 5: The two-loop topologies that contribute to wave-function renormalization (permutations are not included). The '$\circ$' refers to propagators with non-canonical power -2.

All the diagrams of Fig. 5 represent special cases of two-loop vertices with one external momentum set to zero. By referring to Fig. 7 we obtain the following set of equivalences:

$$\begin{aligned} S_p^{111} &\equiv V^{121}(p_1 = 0\,;\, m_3 = m_4), \quad S_p^{121} \equiv V^{131}(p_2 = 0\,;\, m_4 = m_5), \\ S_p^{131} &\equiv V^{141}(p_2 = 0\,;\, m_4 = m_5), \quad S_p^{221} \equiv V^{231}(p_2 = 0\,;\, m_5 = m_6), \end{aligned} \tag{21}$$

where S_p is the self-energy type of diagram where the propagator containing momentum p has non-canonical power -2. The previous relations have been derived for the scalar case, but they hold for tensor integrals too. The infrared divergent configurations for on-shell derivatives of two-loop two-point functions have been previously considered in II while the infrared finite ones will be treated, in this paper, as a special case of vertices.

4 The $G^{1N\,1}$ class of diagrams

$G^{1N\,1}$ is a general class of two-loop diagrams with $N+2$ internal lines which are overall ultraviolet convergent for $N > 2$ and contain the $\alpha\gamma$ logarithmically divergent sub-diagram. We have

$$\pi^4\, G^{1N\,1} = \mu^{2\epsilon} \int d^n q_1\, d^n q_2\, \left(q_1^2 + m_1^2\right)^{-1} \left((q_1 - q_2)^2 + m_2^2\right)^{-1} \prod_{i=0}^{N-1} \left((q_2 + k_i)^2 + m_{i+3}^2\right)^{-1}, \tag{22}$$

where the momenta k_i are linear combinations of the external momenta P_j, $k_i \equiv P_0 + P_1 + \ldots + P_i$. Often, we are going to use a special notation: p_{ij}^2 denotes the square of the difference of the four-momenta flowing through propagators i and j. Since three out of six V-topologies belong to this family, we found it appropriate do give a detailed description of its properties. In order to evaluate this specific class of diagrams we introduce Feynman parameters z_i for the propagators of the q_2 loop and also a $\{z_i\}$-dependent momentum and mass

$$dz_L = \prod_{i=0}^{N-1} dz_i\, \delta\left(1 - z_L\right), \quad z_L = \sum_{i=0}^{N-1} z_i, \quad P_\mu = \sum_{i=0}^{N-1} z_i k_{i\mu}, \quad M^2 = \sum_{i=0}^{N-1} z_i \left(k_i^2 + m_{i+3}^2\right), \tag{23}$$

and obtain

$$G^{1N\,1} = -2\,\frac{\mathcal{G}(N-1)}{\epsilon}\int d[P]\Big[\left(m_x^2+P^2y^2\right)\,\chi^{1-N-\epsilon}+\frac{1}{2}\,\frac{4-\epsilon}{N-2+\epsilon}\,\chi^{2-N-\epsilon}\Big], \tag{24}$$

where x and y parameters have been introduced to combine all propagators arising after the q_2 integration. Additional quantities are as follows:

$$\chi = -P^2y^2+(M^2-m_x^2)y+m_x^2, \qquad m_x^2=\frac{(1-x)\,m_1^2+x\,m_2^2}{x\,(1-x)}, \tag{25}$$

$$\int d[P] = \int dC_2(x,y)\int dz_{_L}\,\Big[x(1-x)\Big]^{-\epsilon/2}y^{N-1}(1-y)^{\epsilon/2}. \tag{26}$$

The G^{1N1} family has special properties and the corresponding diagrams are particularly easy to handle within the BT method. First of all, due to the presence of the factor $m_x^2+P^2\,y^2$ we can apply for the first term of Eq.(24) the following BT relation:

$$\left(m_x^2+P^2\,y^2\right)\,\chi^{1-N-\epsilon} = \Big(1+\frac{1}{N-2+\epsilon}\,y\,\partial_y\Big)\,\chi^{2-N-\epsilon} \tag{27}$$

Henceforth, an integration by parts gives

$$\int_0^1 dy\,y^{N-1}(1-y)^{\epsilon/2}\,\Big(m_x^2+P^2\,y^2\Big)\chi^{1-N-\epsilon} = \int_0^1 dy\,y^{N-1}(1-y)^{\epsilon/2-1}\,\frac{\epsilon-(4-\epsilon)\,(1-y)}{2\,(N-2+\epsilon)}\chi^{2-N-\epsilon}. \tag{28}$$

It is easily seen that the term proportional to $4-\epsilon$ in Eq.(28) cancels the equivalent term in Eq.(24). Henceforth, using well-known properties of the Euler's Γ function we obtain the following compact result:

$$G^{1N1} = -\mathcal{G}(N-2)\,\int_0^1 dx\int_0^1 dy\int dz_{_L}\,\Big[x(1-x)\Big]^{-\epsilon/2}\,y^{N-1}\,(1-y)^{\epsilon/2-1}\,\chi^{2-N-\epsilon} \tag{29}$$

As expected, for $N>2$ the diagram is overall ultraviolet convergent while the sub-divergence is hidden in the y-integration. We use the δ-function to carry through the integration over $z_{_N}$ and introduce a new set of variables defined by

$$y=u_0, \qquad z_i=\frac{u_i-u_{i+1}}{u_0}, \qquad u_{_N}=0, \tag{30}$$

obtaining $0\le u_{N-1}\le\ldots\le u_1\le u_0\le 1$. Furthermore:

$$G^{1N1} = -\,\mathcal{G}(N-2)\,\int_0^1\,dx\,\int\,dS_N(u_0,\cdots,u_{N-1})\,\Big[x(1-x)\Big]^{-\epsilon/2}\,(1-u_0)^{\epsilon/2-1}\,\chi^{2-N-\epsilon} \tag{31}$$

where the quadratic form χ has been rewritten as $\chi = u^t\mathcal{H}u+2\mathcal{K}^tu+\mathcal{L}$,

$$\mathcal{H}_{ij}=-P_i\cdot P_j, \quad \mathcal{K}_0=\frac{1}{2}\,(k_0^2+m_3^2-m_x^2), \quad \mathcal{K}_i=\frac{1}{2}\,\left(k_i^2-k_{i-1}^2+m_{i+3}^2-m_{i+2}^2\right), \quad \mathcal{L}=m_x^2. \tag{32}$$

There is a special case, $P_0=k_0=0$, where we redefine $u_0=y$, and obtain

$$G^{1N1} = -\,\mathcal{G}(N-2)\,\int_0^1\,dx\,\int\,dS_N(y,u_1,\cdots,u_{N-1})\,\Big[x(1-x)\Big]^{-\epsilon/2}\,(1-y)^{\epsilon/2-1}\,\chi^{2-N-\epsilon}, \tag{33}$$

$$\chi = u^t\mathcal{H}u+2\mathcal{K}^tu+(m_x^2-m_3^2)\,(1-y)+m_3^2, \tag{34}$$

where $\mathcal{H}$ etc are given by

$$\mathcal{H}_{ij} = -P_i \cdot P_j, \quad \mathcal{K}_i = \frac{1}{2}\,(k_i^2 - k_{i-1}^2 + m_{i+3}^2 - m_{i+2}^2), \quad i,j = 1,\ldots,N-1. \tag{35}$$

In this case the following relation holds:

$$\chi^\mu = \frac{1}{b}\,\left\{1 - \frac{1}{\mu+1}\left[(y-1)\partial_y + \frac{1}{2}(u^t - U^t)\partial_u\right]\right\}\,\chi^{\mu+1} \tag{36}$$

where $U^t = -\mathcal{K}^t\mathcal{H}^{-1}$ and $b = m_3^2 - \mathcal{K}^t\mathcal{H}^{-1}\mathcal{K}$. Alternatively we may introduce new variables v with

$$u = v - \mathcal{H}^{-1}\,\mathcal{K}, \qquad \chi = v^t\mathcal{H}v + (m_x^2 - m_3^2)\,(1-y) + b, \tag{37}$$

where χ is now an homogeneous form in v.

For each topology there is a maximum value for N, denoted by $N_{\max}$, corresponding to every two-loop diagram $\in G^{1N1}$, i.e. $N_{\max}(S) = 3$, $N_{\max}(V) = 4$, etc. They all correspond to an internal line with a one-loop self-energy insertion and we are always interested in the case where the masses in the two propagators adjacent to the insertion are equal, otherwise the diagram can be expressed through the difference of other (simpler) diagrams.

There are alternative assignments of internal momenta: consider the case of V^{141}, as given in Fig. 7 (d). With the momentum assignment of Fig. 2 we may have $k_0 = 0$ and

$$k_1 = p_1, \quad k_2 = p_1 + p_2, \quad k_3 = 0, \quad \text{or} \quad k_1 = 0, \quad k_2 = p_1, \quad k_3 = p_1 + p_2. \tag{38}$$

Accordingly, the momenta $P_i, i = 1,\ldots,3$ are

$$P_1 = p_1, \quad P_2 = p_2, \quad P_3 = -P = -p_1 - p_2, \quad \text{or} \quad P_1 = 0, \quad P_2 = p_1, \quad P_3 = p_2, \tag{39}$$

and H, K of Eq.(35) should be consistently evaluated.

When $N = N_{\max}$ and the masses in the two propagators adjacent to the self-energy insertion are equal, we are in the special case where two propagators coincide. As a consequence, one of the u-integrations in Eq.(33) is trivial and can be shifted to the innermost position so that we can write

$$\int dS_N(y, u_1, \cdots, u_{N-1}) \quad \to \quad \int dS_{N-1}(y, u_1, \cdots, u_{N-2})\,u_{N-1}, \tag{40}$$

in Eq.(33), with some important consequence to be discussed in the next section.

4.1 Power-counting for G^{1N1} when $b \approx 0$

The G^{1N1} diagrams are evaluated with repeated applications of Eq.(36). When $b \to 0$, the diagram could show a singularity if $0 \le U_{N-1} \le \cdots \le U_1 \le 1$, with $U = -\mathcal{H}^{-1}\,\mathcal{K}$, see Eq.(35).

The BT procedure that we have described will overestimate the nature of the singularity[2] and we have to find some general algorithm to derive the leading behavior of the diagram for $b \to 0$. With $N \ge 3$ we can write

$$\begin{aligned} G^{1N1} &= -\,\mathcal{G}(N-2)\,\int_0^1 dx\,\Big[x(1-x)\Big]^{-\epsilon/2}\,\mathcal{G}^{1N1}, \\ \mathcal{G}^{1N1} &= \int dS_N(y, u_1, \cdots, u_{N-1})\;(1-y)^{\epsilon/2-1}\,\Big[(u-U)^t\,\mathcal{H}\,(u-U) + K\,(1-y) + b\Big]^{2-N-\epsilon}, \end{aligned} \tag{41}$$

[2]Any other known procedure will also overestimate the nature of the singularity.

where the quantities U and b have been defined after Eq. (36), while $K = m_x^2 - m_3^2$. If the point P of coordinates $\{u_i = U_i\}$ is internal to the integration domain $\mathcal{D}$, we can complete $\mathcal{D}$ to the unit hypercube since the integral will be regular in the complementary part $[0,1]^N - \mathcal{D}$ where the diagram can be computed with standard methods. Therefore we arrive at the following set of relations, where the integration is now over the hypercube:

$$\begin{aligned}
\mathcal{G}_C^{1N1} &= \int dC_N\, y^{\epsilon/2-1} \Big[(u-U)^t\, \mathcal{H}\,(u-U) + K\,y + b\Big]^{2-N-\epsilon} \\
&= \int_0^1 dy \Big[\prod_{i=1}^{N-1} \sum_{n=1}^{2} (-1)^n \int_0^{\alpha_i^{(n)}} du_i\Big]\, y^{\epsilon/2-1}\, (u^t\, \mathcal{H}\, u + K\, y + b)^{2-N-\epsilon} \\
&= \sum_{n_1=1}^{2} \cdots \sum_{n_{N-1}=1}^{2} \int_0^1 dy \Big[\prod_{i=1}^{N-1} (-1)^{n_i}\, \alpha_i^{(n_i)} \int_0^1 du_i\Big]\, y^{\epsilon/2-1}\, (Q_{n_1 \cdots n_{N-1}} + K\, y + b)^{2-N-\epsilon}. \quad (42)
\end{aligned}$$

We have introduced

$$\alpha_i^{(1)} = -U_i, \qquad \alpha_i^{(2)} = 1 - U_i, \qquad Q_{n_1 \cdots n_{N-1}} \equiv \sum_{i,j=1}^{N-1} H_{ij}\, \alpha_i^{(n_i)}\, \alpha_j^{(n_j)}\, u_i\, u_j. \quad (43)$$

In the following we suppress this string of indices in Q. Using the well-known Mellin-Barnes technique [31], we obtain

$$\begin{aligned}
\mathcal{G}_C^{1N1} &= \frac{1}{2\,\pi\, i} \int_{-i\,\infty}^{+i\,\infty} ds\, B(s, N-2+\epsilon-s)\, \rho^{N-2+\epsilon-s}\, I(s0, \qquad\qquad \rho = b^{-1}, \\
I(s) &= \sum_{n_1=1}^{2} \cdots \sum_{n_{N-1}=1}^{2} \int_0^1 dy \Big[\prod_{i=1}^{N-1} (-1)^{n_i}\, \alpha_i^{(n_i)} \int_0^1 du_i\Big]\, y^{\epsilon/2-1}\, (Q + K\, y)^{-s}. \quad (44)
\end{aligned}$$

This relation is valid for $0 \le \mathrm{Re}\, s \le N - 2 + \epsilon$ ($N \ge 3$) and B denotes the Euler's beta-function.

The I- integral appearing in Eq.(44) is computed via sector decomposition [26]: it is the sum of N contributions, the first given by

$$\begin{aligned}
I^0 &= \sum_{n_1=1}^{2} \cdots \sum_{n_{N-1}=1}^{2} \int_0^1 dy \Big[\prod_{i=1}^{N-1} (-1)^{n_i}\, \alpha_i^{(n_i)} \int_0^{y} du_i\Big]\, y^{\epsilon/2-1}\, (Q + K\, y)^{-s} \\
&= \int dC_N(y, u_1, \cdots, u_{N-1})\; y^{N-2-s} \Big[(u^t - U^t)\, \mathcal{H}\,(u-U)\, y + K\Big]^{-s}, \quad (45)
\end{aligned}$$

where we performed the transformation $u_i \to y\,(u_i - U_i)/\alpha_i^{(n_i)}$ and we have been able to set $\epsilon = 0$. We obtain

$$I^0 = \frac{f^0(s)}{s - N + 1}, \qquad f^0(s) = -\,K^{-s} \int dC_{N-1}\; {}_2F_1(s\,,\, N-1-s\,;\, N-s\,;\, -\frac{Q^R}{K}). \quad (46)$$

where $Q^R = (u^t - U^t)\, \mathcal{H}\,(u-U)$ and ${}_2F_1$ denotes the hypergeometric function. Since we are interested in the behavior of the diagram for $|\rho| \to \infty$ we close the contour over the right-hand complex half-plane at infinity. The poles of the integrand are at $s = N - 2 + k$ with $k \ge 0$ integer; they are all simple but for $k = 1$ which is double. From this we obtain

$$\mathcal{G}_0^{1N1} = \mathrm{const} + \mathcal{O}\,(b)\,, \quad \text{for} \quad b \to 0. \quad (47)$$

The remaining $N-1$ contributions for I of Eq.(44) have the following form:

$$I^m = \sum_{n_1=1}^{2} \cdots \sum_{n_{N-1}=1}^{2} (-1)^{n_m}\, \alpha_m^{(n_m)} \int_0^1 du_m \int_0^{u_m} dy \Big[\prod_{i\neq m} (-1)^{n_i}\, \alpha_i^{(n_i)} \int_0^{u_m} du_i \Big]\, y^{\epsilon/2-1}\, (Q + K\, y)^{-s}$$
$$= \sum_{n=1}^{2} (-1)^n\, \alpha_m^{(n)} \int dC_N(y, u_1, \cdots, u_{N-1})\; y^{\epsilon/2-1}\, u_m^{N-2+\epsilon/2-s}\, (Q_m^{R\,(n)}\, u_m + K\, y)^{-s}, \tag{48}$$

where we changed variables according to $y \to u_m\, y$ and $u_i \to u_m\, (u_i - U_i)/\alpha_i^{(n_i)}$ for $(i \neq m)$. We introduced:

$$Q_m^{R\,(n)} = \sum_{i,j\neq m} \mathcal{H}_{ij}\, (u_i - U_i)\, (u_j - U_j) + 2 \sum_{i\neq m} \mathcal{H}_{im}\, \alpha_m^{(n)}\, (u_i - U_i) + \mathcal{H}_{mm}\, [\alpha_m^{(n)}]^2. \tag{49}$$

We complete first the y-integration, obtaining as a result

$$I_y = \int_0^1 dy\, y^{\epsilon/2-1}\, (Q_m^{R\,(n)}\, u_m + K\, y)^{-s} = \frac{2}{\epsilon}\, (Q_m^{R\,(n)}\, u_m)^{-s}\, {}_2F_1(s\,,\, \frac{\epsilon}{2}\,;\, 1+\frac{\epsilon}{2}\,;\, -\frac{K}{Q_m^{R\,(n)}\, u_m}), \tag{50}$$

Using well-known properties of the hypergeometric function [31] we derive

$$I^m = \sum_{n=1}^{2} (-1)^n\, \alpha_m^{(n)} \int dC_{N-2}(u_1, \cdots, u_{m-1}, u_{m+1}, \cdots, u_{N-1})\; J_m$$
$$J_m = -\frac{K^{-s}}{s} \int_0^1 du_m\, u_m^{N-2+\epsilon/2-s}\, {}_2F_1(s\,,\, s\,;\, 1+s\,;\, \frac{Q_m^{R\,(n)}\, u_m}{K})$$
$$+ \Gamma\left(\frac{\epsilon}{2}\right) \frac{\Gamma\,(s-\epsilon/2)}{\Gamma\,(s)}\, K^{-\epsilon/2} \left[Q_m^{R\,(n)}\right]^{\epsilon/2-s} \int_0^1 du_m\, u_m^{N-2+\epsilon-2\,s}. \tag{51}$$

Note that $Q_m^{R\,(n)}$ is u_m-independent, allowing for u_m integration. In particular,

$$\int_0^1 du_m\, u_m^{N-2-s}\, {}_2F_1(s\,,\, s\,;\, 1+s\,;\, q_{nm}\, u_m) = B(1, N-1-s)\, {}_3F_2(s\,,\, s\,,\, N-1-s\,;\, s+1\,,\, N-1\,;\, q_{nm}), \tag{52}$$

with $q_{nm} = Q_m^{R\,(n)}/K$ and where ${}_3F_2$ is a generalized hypergeometric function. The general expression will be

$$\mathcal{G}_m^{1N1} = \frac{1}{2\,\pi\, i} \sum_{n=1}^{2} (-1)^n\, \alpha_m^{(n)} \int dC_{N-2} \int_{-i\,\infty}^{+i\,\infty} ds \Big[B(s, N-2-s)\, B(1, N-1-s)\, \frac{f_1^m(s)}{s} \rho^{N-2-s}$$
$$+ \Gamma\left(\frac{\epsilon}{2}\right) \frac{\Gamma\,(s-\epsilon/2)}{\Gamma\,(s)}\, B(s, N-2+\epsilon-s)\, \frac{f_2^m(s)}{N-1+\epsilon-2\,s}\, \rho^{N-2+\epsilon-s}\Big], \tag{53}$$

where the functions f_i^m are

$$f_1^m(s) = -\,K^{-s}\, {}_3F_2(s\,,\, s\,,\, N-1-s\,;\, s+1\,,\, N-1\,;\, \frac{Q_m^{R\,(n)}}{K}), \qquad f_2^m(s) = K^{-\epsilon/2} \left[Q_m^{R\,(n)}\right]^{\epsilon/2-s}. \tag{54}$$

Closing once again the contour over the right-hand complex half-plane at infinity we have (for $\epsilon = 0$)

$N = 3$: a single pole at $s = 1$, double poles at $s = 2 + k$, with $k \geq 0$ for the first term in Eq.(53); a double pole at $s = 1$ and single poles at $s = 2 + k$ $(k \geq 0)$ for the second one.

$N > 3$: a single pole at $s = N - 2$ and double poles at $s = N - 1 + k\,(k \geq 0)$ for the first term in Eq.(53); simple poles at $s = (N-1)/2$ and $s = N - 2 + k\,(k \geq 0)$ for the second one.

As a result, and taking into account the correct ϵ dependence, we obtain

$$\mathcal{G}_m^{131} \sim \ln b(\ln^2 b) \quad \text{for divergent(finite) part,}$$

$$\mathcal{G}_m^{1N1} \sim b^{(3-N)/2}(b^{(3-N)/2}\,\ln b)\;(N > 3) \quad \text{for divergent(finite) part,} \tag{55}$$

for $b \to 0$. Eq.(55) is derived under the condition that we have $N+2$ different propagators in the diagram which is not the case if there is a self-energy insertion with equal masses in the two propagators adjacent to the insertion, e.g. for S^{131} or V^{141}. When this happens we have to distinguish between N_L and N_I, i.e. the number of internal lines and the number of integration variables in $\mathcal{G}^{1N1}$ of Eq.(41). For S^{131} or V^{141} we have $N_I = N_L - 1$ since one integration is trivial and produces some extra factor in the integrand for $\mathcal{G}^{1N1}$ which, however, is irrelevant from the point of view of power counting. The most important consequence is that, in these cases, in Eq.(53) we will have

$$\frac{1}{N - 2 + \epsilon - 2\,s}\,\rho^{N-2+\epsilon-s} \tag{56}$$

with a pole at $s = N/2 - 1 + \epsilon/2$. Taking into account the ultraviolet pole of Eq.(53) we have a corresponding leading behavior of

$$\Gamma\left(\frac{\epsilon}{2}\right)\,b^{1-N/2}\,(1 - \frac{\epsilon}{2}\,\ln b). \tag{57}$$

Having discussed the simplest class of two-loop vertices in more detail, we now proceed to an exhaustive classification and description of all the vertices, from V^{121} to V^{222}.

5 The V^{121} diagram

The V^{121} diagram of Fig. 7(a) is representable as

$$\pi^4\,V^{121} = \mu^{2\epsilon}\int d^n q_1 \int d^n q_2\,\frac{1}{[1][2][3][4]}, \tag{58}$$

$$[1] \equiv q_1^2 + m_1^2, \quad [2] \equiv (q_1 - q_2)^2 + m_2^2, \quad [3] \equiv (q_2 - p_2)^2 + m_3^2, \quad [4] \equiv (q_2 - P)^2 + m_4^2. \tag{59}$$

Therefore it is a special case of G^{1N1}, Eq.(33), with $k_0 = -p_2$ and $k_1 = -p_2 - p_1$. The discussion of the relative Landau equations is shown in Appendix F.

5.1 Evaluation of V^{121}

Following our discussion of $G^{1N\,1}$ of Section 4 we are able to derive immediately the result for V^{121}. By performing an expansion in ϵ we have:

$$V_{DP}^{121} = -\frac{2}{\epsilon^2} - \Delta_{UV}^2, \quad V_{SP}^{121} = 2\,\frac{\Delta_{UV}}{\epsilon} + \left(\Delta_{UV} - \frac{1}{\epsilon}\right)\Big[1 - 2\int dC_2\,\ln\chi_{_E}(x,1,y)\Big],$$
$$V_{\rm fin}^{121} = \int dCS\,(x\,;\,y,z)\,\Big[\frac{\ln\chi_{_E}(x,y,z)}{1-y}\Big]_+ + \int dC_2\,\ln\chi_{_E}(x,1,y)\,L_{1;E}(x,y) - \frac{3}{2} - \frac{1}{2}\,\zeta(2), \tag{60}$$

where ζ is the Riemann's zeta-function, Δ_{UV} is defined in Eq.(9) and the subscripts DP, SP and fin denote the double and single ultraviolet pole (in dimensional regularization) and finite part (as $n \to 4$), respectively, and where the auxiliary quantities are

$$L_{1;E}(x,y) = \ln(1-y) - \ln x - \ln(1-x) - \ln \chi_E(x,1,y). \tag{61}$$

For the complete list of different kinematic configurations we recall Eq.(8): in general we have

$$\begin{aligned}\chi_E(x,y,z) = {} & s_2\,\nu_2^2\,y^2 + s_1\,\nu_1^2\,z^2 + (s_p - s_1\,\nu_1^2 - s_2\,\nu_2^2)\,y\,z + (\mu_3^2 - s_2\,\nu_2^2)\,y \\ & + (s_2\,\nu_2^2 - s_p - \mu_3^2 + \mu_4^2)\,z + \mu_x^2\,(1-y).\end{aligned} \tag{62}$$

We report the explicit result for the situation where s_p and $s_{1,2}$ are positive. Here we have

$$\chi_E(x,y,z) = \nu_2^2\,y^2 + \nu_1^2\,z^2 + (1-\nu_2^2-\nu_1^2)\,y\,z - (\nu_2^2 + \mu_x^2 - \mu_3^2)\,y + (\nu_2^2 - \mu_{34}^2)\,z + \mu_x^2, \tag{63}$$

where we used the auxiliary quantities

$$\mu_x^2 = \frac{\mu_1^2(1-x) + \mu_2^2 x}{x(1-x)}, \quad \mu_{ij}^2 = 1 + \mu_i^2 - \mu_j^2. \tag{64}$$

Note that Eq.(60) defines V^{121} everywhere. For the first integral in Eq.(60) we may use the fact that, thanks to the $i\,\delta$ prescription, both $\chi_E(x,y,z)$ and $\chi_E(x,1,z)$ have the same imaginary part and therefore

$$\ln \chi_E(x,y,z)\ |_+ = \sum_{i=\pm} \ln(y - y_i)\ |_+, \tag{65}$$

where $y_\pm(x,z)$ are the roots of the equation $\chi_E(x,y,z) = 0$. In this way we obtain an expression which is more appropriate for numerical integration,

$$\int dS_2(y,z) \Big[\frac{\ln \chi_E(x,y,z)}{1-y}\Big]_+ = -\sum_{i=\pm} \int_0^1 dz\, \mathrm{Li}_2\left(\frac{1-z}{1-y_i}\right), \tag{66}$$

$\mathrm{Li}_2\,(z)$ denoting the standard di-logarithm [32].

5.2 Wave function renormalization: S_p^{111}

The evaluation of the derivative S_p^{111} follows immediately from Eq.(60) with $\nu_1^2 = 0$, $\nu_2^2 = 1$ and $\mu_3 = \mu_4$, i.e. with

$$\chi_E \to \chi_E(x,y) = y^2 - (1 + \mu_x^2 - \mu_3^2)\,y + \mu_x^2, \tag{67}$$

where we assumed $M^2 \geq 0$. Therefore we have

$$S_{p;\,DP}^{111} = -\frac{2}{\epsilon^2} - \Delta_{UV}^2 \quad S_{p;\,SP}^{111} = 2\,\frac{\Delta_{UV}}{\epsilon} + \left(\Delta_{UV} - \frac{1}{\epsilon}\right)\left(1 - 2\,\ln \mu_3^2\right) \tag{68}$$

$$S_{p;\,\mathrm{fin}}^{111} = \int dC_2\; y \Big[\frac{\ln \chi_E(x,y)}{1-y}\Big]_+ + \int dC_2\; \ln \mu_3^2\, L_{1;E}(x,y) - \frac{3}{2} - \frac{1}{2}\,\zeta(2), \tag{69}$$

where $L_{1;E} = \ln(1-y) - \ln x - \ln(1-x) - \ln \mu_3^2$. Finally we have

$$S_{p;\,\mathrm{fin}}^{111} = \int dC_2\; y \Big[\frac{\ln \chi_E(x,y)}{1-y}\Big]_+ + \ln \mu_3^2\,(1 - \ln \mu_3^2) - \frac{3}{2} - \frac{1}{2}\,\zeta(2). \tag{70}$$

giving our result for the finite part of S_p^{111}.

6 The V^{131} diagram

The V^{131} diagram of Fig. 7(c) is representable as

$$\pi^4\, V^{131} = \mu^{2\epsilon} \int d^n q_1 \int d^n q_2 \, \frac{1}{[1][2][3][4][5]}, \tag{71}$$

with propagators

$$[1] \equiv q_1^2 + m_1^2, \qquad [2] \equiv (q_1 - q_2)^2 + m_2^2, \qquad [3] \equiv q_2^2 + m_3^2,$$

$$[4] \equiv (q_2 + p_1)^2 + m_4^2, \qquad [5] \equiv (q_2 + P)^2 + m_5^2. \tag{72}$$

This topology represents a special case of G^{1N1}, Eq.(33), with $k_0 = 0$, $k_1 = p_1$ and $k_2 = p_1 + p_2$. The corresponding Landau equations are discussed in Appendix G. Two methods for the evaluation of V^{131} will be presented in the following sections.

6.1 Evaluation of V^{131}: method I

Our first method for evaluating V^{131} uses the BT-method of Appendix A for increasing the powers in the integrand. Here we describe in more detail the derivation for time-like momenta. First we introduce the quadratic form

$$\begin{aligned}\chi_{_I}(x, y, z_1, z_2) = {} & \nu_1^2\, z_1^2 + \nu_2^2\, z_2^2 + (1 - \nu_1^2 - \nu_2^2)\, z_1\, z_2 - (\nu_1^2 + \mu_3^2 - \mu_4^2)\, z_1 \\ & + (\nu_1^2 - \mu_{45}^2)\, z_2 + (\mu_3^2 - \mu_x^2)\, y + \mu_x^2,\end{aligned} \tag{73}$$

with ν_i^2 defined in Eq.(7) and μ_{ij}^2 in Eq.(64). Observing that $\chi_{_I}(x, 1, y, z)$ does not depend on x we will use $\chi_{_I}(y, z) \equiv \chi_{_I}(x, 1, y, z)$. Furthermore, the coefficient $b_{_I}$ is defined as

$$b_{_I} = (\nu_1^2 + \mu_3^2 - \mu_4^2)^2 - \mu_{35}^2\, (1 + \nu_1^2 - \nu_2^2)\, (\nu_1^2 + \mu_3^2 - \mu_4^2) + \mu_{35}^4\, \nu_1^2 + \lambda_{_I} \mu_3^2, \tag{74}$$

where we have set $\lambda_{_I} = \lambda(1, \nu_1^2, \nu_2^2)$ and λ denotes the familiar Källen's lambda-function $\lambda(x, y, z) = x^2 + y^2 + z^2 - 2xy - 2xz - 2yz$. BT co-factors (Eq.(269)) are

$$\begin{aligned} & Z_{0;I} = -\lambda_{_I}, \qquad Z_{3;I} = 0, \qquad Z_{1;I} = (1 - \nu_1^2 - \nu_2^2)\, (\nu_1^2 - \mu_{45}^2) + 2\, (\nu_1^2 + \mu_3^2 - \mu_4^2)\, \nu_2^2 \\ & Z_{2;I} = -(1 - \nu_1^2 - \nu_2^2)\, (\nu_1^2 + \mu_3^2 - \mu_4^2) - 2\, (\nu_1^2 - \mu_{45}^2)\, \nu_1^2, \quad Z_{i;I}^- = Z_{i;I} - Z_{i+1;I}. \end{aligned} \tag{75}$$

An integration by parts is performed before the ϵ-expansion and this leads to the following result:

$$V_{SP}^{131} = (-\frac{1}{\epsilon} + \Delta_{UV})\, \frac{1}{M^2\, b_{_I}} \Big\{ 2\, \lambda_{_I} \int dS_2\, \ln \chi_{_I}(y, z) + \int dC_1 \sum_{i=0}^{2} Z_{i;I}^-\, \ln \chi_{_I}([1\, y\, 0]_i) + \lambda_{_I} \Big\}. \tag{76}$$

The $[x, y, z]_i$ notation has been introduced in Eq.(12). Note that the expression multiplying the ultraviolet factor (Δ_{UV} defined in Eq.(9)) has the form of a C_0-function, the one-loop scalar vertex. For the ultraviolet finite part of the diagram we obtain the following expression:

$$V_{\rm fin}^{131} = \frac{1}{M^2\, b_{_I}} \Big[\int dCS\,(x\,;\, y, \{z\})\; I_{_I}^4 + \int dCS\,(x\,;\, y, z)\; I_{_I}^3 + \int dC_2\, I_{_I}^2 - \frac{1}{4}\, \lambda_{_I} \Big]. \tag{77}$$

The various I-functions of Eq.(77) are given by

$$I_I^4 = -\lambda_I \Big[\frac{\ln\chi_I(x,y,z_1,z_2)}{1-y}\Big]_+, \quad I_I^2 = -\frac{1}{2}\sum_{i=0}^{2} Z_{i;I}^- L_{i+2;I}(x,y)\,\ln\chi_I([1\,y\,0]_i),$$
$$I_I^3 = \lambda_I\Big\{\frac{1}{2}\ln\chi_I(x,y,y,z) + \ln\chi_I(y,z)\Big[1-L_{1;I}(x,y,z)\Big]\Big\} - \frac{1}{2}\sum_{i=0}^{2} Z_{i;I}^-\Big[\frac{\ln\chi_I(x,y\,;\,[y\,z\,0]_i)}{1-y}\Big]_+ \quad (78)$$

with an additional set of auxiliary functions defined by

$$L_{1;I}(x,y,z) = \mathcal{L}(x,y) - \ln\chi_I(y,z), \quad L_{2;I}(x,y) = \mathcal{L}(x,y) - \ln\chi_I(1,y),$$
$$L_{3;I}(x,y) = \mathcal{L}(x,y) - \ln\chi_I(y,y), \quad L_{4;I}(x,y) = \mathcal{L}(x,y) - \ln\chi_I(y,0), \quad (79)$$

where $\mathcal{L}(x,y) = \ln(1-y) - \ln(x) - \ln(1-x)$. Note that no modification of the algorithm is needed when the H-matrix becomes singular, i.e. for $\lambda_I = 0$. This method fails when b_I, defined in Eq.(74), is zero. For a general configuration, Eq.(8), we have

$$\chi_I(x,y,z_1,z_2) = s_1\,\nu_1^2\,z_1^2 + s_2\,\nu_2^2\,z_2^2 + (s_p - s_1\,\nu_1^2 - s_2\,\nu_2^2)\,z_1\,z_2 - (s_1\,\nu_1^2 + \mu_3^2 - \mu_4^2)\,z_1$$
$$+ (s_1\,\nu_1^2 - s_p - \mu_4^2 + \mu_5^2)\,z_2 + (\mu_3^2 - \mu_x^2)\,y + \mu_x^2, \quad (80)$$

Henceforth we seek for a second, alternative, algorithm which allows for internal cross-check.

6.2 Evaluation of V^{131}: method II

Method I, described in the previous section, fails when we are around $b_I = 0$ or, equivalently around

$$2\,\mu_3^2\,\nu_2^2 = -\nu_1^2\,(1-\mu_3^2-\mu_5^2) + \mu_4^2\,(1-\mu_5^2+\mu_3^2) + \mu_3^2\,(1-\mu_3^2+\mu_5^2) \pm \Big[\lambda(\nu_1^2,\mu_3^2,\mu_4^2)\,\lambda(1,\mu_3^2,\mu_5^2)\Big]^{1/2}, \quad (81)$$

which corresponds to the leading Landau singularity for all time-like momenta (other configurations follow with the appropriate change in signs).

In [3] we have given a complete discussion of the different options that one has in dealing with integrals where the related BT-factor is approaching zero. If we introduce $Z = -\mathcal{H}^{-1}\,\mathcal{K}$, with $\mathcal{H},\mathcal{K}$ defined in Eq.(35), then

$$\chi = A_{x;I}\,(1-y) + (z-Z)^t\,\mathcal{H}\,(z-Z) + b. \quad (82)$$

If $b_I = 0$ but the condition $0 \le Z_2 \le Z_1 \le 1$ is not fulfilled, V^{131} is regular and we can perform a Taylor expansion around $b_I = 0$. If, instead, the condition is satisfied, V^{131} is singular and we implement a Laurent expansion via Mellin-Barnes techniques following again [3]. Also in [3] we have shown that for one-loop, multi-leg diagrams new integral representations can be constructed which encompass the need for expansion.

In order to deal with V^{131} we start from the relation

$$V^{131} = -\mathcal{G}(1)\int dCS\,(x\,;\,y,\{z\})\,\Big[x(1-x)\Big]^{-\epsilon/2}\,(1-y)^{\epsilon/2-1}\,\chi^{-1-\epsilon}, \quad (83)$$

where $\mathcal{G}$ is defined in Eq.(10) and we rewrite χ as

$$\chi = A_{x;I}\,(1-y) + B_I(z_1,z_2), \qquad B_I(z_1,z_2) = z^t\mathcal{H}z + 2\mathcal{K}^t z + m_3^2, \quad A_{x;I} = m_x^2 - m_3^2. \quad (84)$$

Now we introduce (always assuming time-like external momenta)

$$\mathcal{A}_{x;I} = \mu_x^2 - \mu_3^2, \qquad \mathcal{B}_I = \chi_I(x, y, z_1, z_2). \tag{85}$$

The innermost integral in Eq.(83) will then become

$$J_I = \int_0^{1-z_1} dy\, y^{\epsilon/2-1} \Big[\mathcal{A}_{x;I}\, y + \mathcal{B}_I(z_1, z_2)\Big]^{-1-\epsilon}. \tag{86}$$

A similar result holds for all G^{1N1} diagrams. The integral appearing in Eq.(86) is evaluated explicitly in Appendix C. The result is

$$J_I = \frac{2}{\epsilon}\,(1 - \frac{\epsilon}{2}\,\ln \mathcal{A}_{x;I})\, C_0(\frac{1}{2}) - \frac{1}{\mathcal{B}_I(z_1, z_2)}\,\ln(1 + Q_{x;I}), \quad Q_{x;I} = \frac{\mathcal{B}_I(z_1, z_2)}{\mathcal{A}_{x;I}\,(1 - z_1)}, \tag{87}$$

where the C_0-function is defined in Eq.(282) and, in the limit $\epsilon \to 0$, corresponds to a one loop vertex of arguments $\{p_1^2\,,\, p_2^2\,,\, P^2\,;\, m_3\,,\, m_4\,,\, m_5\}$. Recalling Eq.(286) of Appendix E, the whole diagram is therefore represented by

$$\begin{aligned} V^{131} &= -\frac{\mathcal{G}(1, M^2)}{M^2} \int dCS\,(x\,;\, z_1, z_2)\, \Big[x(1-x)\Big]^{-\epsilon/2} J_I \\ &= \frac{1}{M^2}\Big\{2\,(\Delta_{UV} - \frac{1}{\epsilon})\, C_{00} + C_{00} \int_0^1 dx \Big[\ln \mathcal{A}_{x;I} + \ln x + \ln(1-x)\Big] + \frac{1}{2}\, C_{01} \\ &+ \int dCS\,(x\,;\, z_1, z_2)\, \frac{1}{\mathcal{B}_I(z_1, z_2)}\,\ln(1 + Q_{x;I})\Big\}. \end{aligned} \tag{88}$$

In Eq.(88) we have a one-loop three-point function to be evaluated up to $\mathcal{O}\,(\epsilon)$ (Δ_{UV} is defined in Eq.(9)). The corresponding BT factor is as in Eq.(74) and, therefore, this function can be computed according to the methods of Sect. 4 of [3] or by using the new result of Appendix E. In any case, the behavior for $b_I \to 0$ is under control.

6.3 Wave function renormalization: S_p^{121}

To obtain an expression for the derivative of S^{121} we follow Eqs.(76)–(77) with $\nu_1^2 = 1$, $\nu_2^2 = 0$ and $\mu_4 = \mu_5$, i.e. with the replacement

$$\chi_I(x, y, z_1, z_2) \quad \to \quad \xi_I = z_1^2 - \mu_{34}^2\, z_1 + (\mu_3^2 - \mu_x^2)\, y + \mu_x^2. \tag{89}$$

However, being $b_I = \lambda_I = 0$, it is more convenient to start from Eq.(83) since ξ_I is z_2-independent; introducing

$$\mathcal{A}_{x;I} = \mu_x^2 - \mu_3^2, \quad \mathcal{B}_I(z) = z^2 - \mu_{34}^2\, z + \mu_3^2, \tag{90}$$

we obtain the same result as in Eq.(88) but with C-functions replaced by B-functions (one-loop two-point functions) of the following type:

$$\begin{aligned} B_{\{0;1\}} &= B_{\{0;1\}0} - \frac{\epsilon}{2}\, B_{\{0;1\}1} + \mathcal{O}\left(\epsilon^2\right) = \int_0^1 dz\,\{1\,;\, z\}\,\mathcal{B}_I^{-1-\epsilon/2}(z), \\ B_{\{0;1\}_L}(x) &= \int_0^1 dz\,\{1\,;\, z\}\,\mathcal{B}_I^{-1}(z)\,\ln\Big[1 + \frac{\mathcal{B}_I(z)}{\mathcal{A}_x\,(1-z)}\Big]. \end{aligned} \tag{91}$$

With their help we write

$$S_p^{121} = \frac{1}{M^2}\left\{2\,(\Delta_{UV} - \frac{1}{\epsilon})\,B_{10} + B_{10}\int_0^1 dx\,\Big[\ln A_{x;I} + \ln x + \ln(1-x) + B_{1L}(x)\Big] + \frac{1}{2}\,B_{11}\right\}. \quad (92)$$

Note that B_{1L} is well-behaved for $\mathcal{B} = 0$ and that the simultaneous occurrence of $\mathcal{B} = 0$ and of $\mathcal{A}_x = 0$ or of $z = 1$ can be treated according to the results of Appendix D. Furthermore, $B_{1,\{0;1\}}$ are generalized one-loop two-point functions that have been described in [3].

7 The V^{221} diagram

This topology, corresponding to Fig. 7(b), can be written as

$$\pi^4\,V^{221} = \mu^{2\epsilon}\int d^nq_1\int d^nq_2\,\frac{1}{[1][2][3][4][5]}, \quad (93)$$

where we have introduced the following notation:

$$[1] \equiv q_1^2 + m_1^2, \quad [2] \equiv (q_1+p_1)^2 + m_2^2, \quad [3] \equiv (q_1-q_2)^2 + m_3^2,$$
$$[4] \equiv (q_2+p_1)^2 + m_4^2, \quad [5] \equiv (q_2+P)^2 + m_5^2, \quad (94)$$

and where $P = p_1 + p_2$ (with all momenta are flowing inward). The related Landau equations are given in Appendix H. This diagram, not belonging to the V^{1N1}-class, will represent the first example of application of a smoothness algorithms different from the BT one.

7.1 Evaluation of V^{221}

In evaluating this diagram the first step consists in combining propagators $[1]-[3]$ of Eq.(94) with Feynman parameters x_1, x_2,

$$\pi^4\,V^{221} = \mu^{2\epsilon}\,\Gamma(3)\int d^nq_1\int d^nq_2\int dS_2\,\frac{1}{[4][5]}\,\frac{1}{(q_1^2 + 2\,R_x\cdot q_1 + Q_x^2)^3}. \quad (95)$$

We have introduced the $x_{1,2}$-dependent quantities

$$R_x = (1-x_1)\,p_1 - x_2\,q_2, \quad Q_x^2 = x_1\,(m_1^2 - m_2^2) + x_2\,(q_2^2 + m_3^2 - m_1^2) + m_2^2 + (1-x_1)\,p_1^2. \quad (96)$$

Integrating over q_1 in Eq.(95) gives

$$\pi^2\,V^{221} = i\,\pi^{-\epsilon/2}\,\mu^{2\epsilon}\,\Gamma\Big(1+\frac{\epsilon}{2}\Big)\int dS_2\,\Big[x_2(1-x_2)\Big]^{-1-\epsilon/2}\int\frac{d^nq_2}{(q_2^2 + 2\,P_x\cdot q_2 + M_x^2)^{1+\epsilon/2}\,[4][5]}, \quad (97)$$

where the new $\{x\}$-dependent parameters are

$$P_x = \frac{1-x_1}{1-x_2}\,p_1 = X\,p_1, \quad M_x^2 = \frac{-p_1^2\,x_1^2 + x_1\,(p_1^2 + m_1^2 - m_2^2) + x_2\,(m_3^2 - m_1^2) + m_2^2}{x_2\,(1-x_2)}. \quad (98)$$

Next we combine the remaining propagators with Feynman parameters $y_i, i = 1,2$. It follows

$$\pi^2\,V^{221} = i\,\pi^{-\epsilon/2}\,\mu^{2\epsilon}\,\Gamma\Big(3+\frac{\epsilon}{2}\Big)\int dS_2(x_1,x_2)\,\Big[x_2(1-x_2)\Big]^{-1-\epsilon/2}\int dS_2(y_1,y_2)\,y_2^{\epsilon/2}$$
$$\times\int d^nq_2\,\Big[y_2\,[123] + (y_1-y_2)\,[4] + (1-y_1)\,[5]\Big]^{-3-\epsilon/2}. \quad (99)$$

In the above equation $[123] = q_2^2 + 2\,P_x \cdot q_2 + M_x^2$. After the q_2-integration we obtain the following result:

$$V^{221} = -\,\frac{\mathcal{G}(1,M^2)}{M^2}\int dS_2(x_1,x_2)\,\Big[x_2(1-x_2)\Big]^{-1-\epsilon/2}\int dS_2(y_1,y_2)\,y_2^{\epsilon/2}\,\chi_G^{-1-\epsilon}, \tag{100}$$

where $\mathcal{G}$ is defined in Eq.(10). Since the diagram is ultraviolet finite we set $\epsilon = 0$ and get

$$V^{221} = -\,\frac{1}{M^2}\int dS_2(x_1,x_2)\int dS_2(y_1,y_2)\,\chi_G^{-1}. \tag{101}$$

where the quadratic form χ_G is given by

$$\chi_G = x_2\,\Big(A\,y_1^2 + B\,y_2^2 + C\,y_1y_2 + D\,y_1 + E\,y_2 + F\Big), \tag{102}$$

and its coefficients are

$$\begin{aligned} &A = \overline{x}_2^2\,s_2\,\nu_2^2, \quad B = \overline{x}^2\,s_1\,\nu_1^2, \quad C = \overline{x}_2\,\overline{x}\,(s_p - s_1\,\nu_1^2 - s_2\,\nu_2^2), \quad D = \overline{x}_2^2\,(\mu_4^2 - \mu_5^2 - s_2\,\nu_2^2),\\ &E = \overline{x}_2\,(\overline{x}_1\,(s_p + s_1\,\nu_1^2 - s_2\,\nu_2^2) + \overline{x}_2\,(s_2\,\nu_2^2 - s_p) - \overline{x}_2\,\mu_4^2 + \mu_x^2/x_2), \quad F = \overline{x}_2^2\,\mu_5^2, \end{aligned} \tag{103}$$

where $\overline{x}_i = 1 - x_1$ and $\overline{x} = x_1 - x_2$. Furthermore,

$$\mu_x^2 = s_1\,\nu_1^2\,x_1^2 + x_1\,(\mu_1^2 - \mu_2^2 - s_1\,\nu_1^2) + x_2\,(\mu_3^2 - \mu_1^2) + \mu_2^2. \tag{104}$$

Note that the y_1, y_2 integral is exactly a generalized C_0-function of Appendix E. For internal cross-checking we use instead Eq.(264), based on a procedure of numerical differentiation, to be discussed in Section 10.4.

8 The V^{141} diagram

The V^{141} topology of Fig. 7(d) can be written as the following integral:

$$\pi^4\,V^{141} = \mu^{2\epsilon}\int d^nq_1\int d^nq_2\,\frac{1}{[1][2][3][4][5][6]}, \tag{105}$$

where the propagators are

$$[1] \equiv q_1^2 + m_1^2, \quad [2] \equiv (q_1 - q_2)^2 + m_2^2, \quad [3] \equiv (q_2^2 + m_3^2),$$

$$[4] \equiv (q_2 + p_1)^2 + m_4^2, \quad [5] \equiv (q_2 + P)^2 + m_5^2, \quad [6] \equiv q_2^2 + m_6^2. \tag{106}$$

If $m_3 \neq m_6$ then V^{141} is the difference of two V^{131} diagrams,

$$V^{141} = \frac{1}{m_6^2 - m_3^2}\,\Big[V^{131}(P^2; m_1, m_2, m_3, m_4, m_5) - V^{131}(P^2; m_1, m_2, m_6, m_4, m_5)\Big], \tag{107}$$

otherwise it is a special case of G^{141}, Eq.(33), with $k_0 = k_1 = 0$, and $k_2 = p_1$, $k_3 = P$. This choice of the rooting of momenta has the advantage of making the z_1 integration trivial. The corresponding quadratic form χ_M will be $\chi_M = \chi_I$ where we have used $z_0 = y - z_1 - z_2 - z_3$ and, moreover, we have performed the integration over z_1, further renaming z_2, z_3 as z_1, z_2. Since we are only interested in the non-trivial case $m_3 = m_6$ the Landau equations and their solution for V^{141} are identical to those for V^{131},see Appendix G.

8.1 Evaluation of V^{141} for $m_3 = m_6$

We proceed with the calculation of V^{141}, always assuming that all external momenta are time-like. In this case we use the special set of BT relations which are valid for $G^{1N\,1}$ (Section 4) when $k_0 = 0$. For this diagram we will choose $k_1 = 0, k_2 = p_1$ and $k_3 = P$. As a consequence the z_1 integration becomes trivial and we obtain

$$V^{141} = -\frac{\mathcal{G}(2, M^2)}{M^4} \int dCS\,(x\,;\,y, z_1, z_2)\,\Big[x\,(1-x)\Big]^{-\epsilon/2}\,(1-y)^{\epsilon/2-1}\,(y-z_1)\,\chi_M^{-2-\epsilon}(x, y, z_1, z_2), \quad (108)$$

where $\mathcal{G}$ is defined in Eq.(10) and $\chi_M \equiv \chi_I$. The BT-relation that we need is as follows:

$$\chi_M^{-2-\epsilon} = \frac{1}{b_{0;M}}\Big\{\lambda_M + \frac{1}{1+\epsilon}\Big[(y-1)\,\lambda_M\partial_y + \frac{1}{2}\sum_{i=1,2}(\lambda_M\,z_i - Z_{i;M})\partial_{z_i}\Big]\Big\}\,\chi_M^{-1-\epsilon}, \quad (109)$$

where, similarly to the treatment of the V^{131} case, we have introduced some special combination, where the ν_i^2 are defined in Eq.(7) and μ_{ij}^2 in Eq.(64):

$$\begin{aligned}
Z_{1;M} &= -(1-\nu_1^2-\nu_2^2)\,(\nu_1^2-\mu_{45}^2) - 2\,(\nu_1^2+\mu_3^2-\mu_4^2)\,\nu_2^2,\\
Z_{2;M} &= (1-\nu_1^2-\nu_2^2)\,(\nu_1^2+\mu_3^2-\mu_4^2) + 2\,(\nu_1^2-\mu_{45}^2)\,\nu_1^2,\\
b_{0;M} &= (\nu_1^2+\mu_3^2-\mu_4^2)^2 - \mu_{35}^2\,(1+\nu_1^2-\nu_2^2)\,(\nu_1^2+\mu_3^2-\mu_4^2) + \mu_{35}^4\,\nu_1^2 + \lambda_M\mu_3^2.
\end{aligned} \quad (110)$$

Furthermore, we have $\lambda_M \equiv \lambda_I = \lambda(1, \nu_1^2, \nu_2^2)$ and moreover $b_{0;M} \equiv b_I$. After performing integration by parts we introduce secondary quadratic forms:

$$\begin{aligned}
\chi_{1;M} &= \chi_M(z_2 = z_1) = z_1^2 - \mu_{35}^2\,z_1 + (\mu_3^2 - \mu_x^2)\,y + \mu_x^2,\\
\chi_{2;M} &= \chi_M(z_2 = 0) = \nu_1^2\,z_1^2 - (\nu_1^2+\mu_3^2-\mu_4^2)\,z_1 + (\mu_3^2-\mu_x^2)\,y + \mu_x^2
\end{aligned} \quad (111)$$

with μ_x^2 defined in Eq.(64). The following BT-relations are available for these functions:

$$\chi_{i;M}^{-1-\epsilon} = \frac{1}{b_{i;M}}\Big\{1 + \frac{1}{\epsilon}\Big[(y-1)\partial_y + \frac{1}{2}(z_1 - Z_{1i;M})\partial_{z_1}\Big]\Big\}\,\chi_{i;M}^{-\epsilon} \quad (112)$$

where additional BT factors and co-factors (Eq.(269) have been introduced:

$$\begin{aligned}
Z_{11;M} &= \frac{\mu_{35}^2}{2}, \qquad Z_{12;M} = \frac{\nu_1^2+\mu_3^2-\mu_4^2}{2\,\nu_1^2},\\
b_{1;M} &= -\frac{1}{4}\,\lambda(1, \mu_3^2, \mu_5^2). \qquad b_{2;M} = -\frac{1}{4\,\nu_1^2}\,\lambda(\nu_1^2, \mu_3^2, \mu_4^2).
\end{aligned} \quad (113)$$

To write our result in a compact form we introduce $Z_{0;M} = \lambda_M$, $Z_{3;M} = 0$ and also

$$\begin{aligned}
L_{+;M}(x, y, z_1, z_2) &= \Big[\frac{\ln\chi_M(x, y, z_1, z_2)}{1-y}\Big]_+, \qquad Z_{i;M}^- = Z_{i;M} - Z_{i+1;M},\\
L_M(x, y, z) &= \ln(1-y) - \ln(x) - \ln(1-x) - \ln\chi_I(y, z).
\end{aligned} \quad (114)$$

Once more we integrate by parts and, after a Laurent expansion around $\epsilon = 0$, we obtain the following expression for the single ultraviolet pole:

$$V_{SP}^{141} = \frac{1}{2\,M^4\,b_{0;M}}\,(\frac{1}{\epsilon} - \Delta_{UV})\,\mathcal{V}_{SP}^{141},$$

$$\mathcal{V}^{141}_{SP} = \frac{1}{b_{0;M}}\Big[-\frac{3}{2}\,\lambda_M\int dS_2\,\mathcal{Z}_{1;M}(y)\,\ln\chi_M(y,z)$$
$$+\frac{1}{2}\sum_{i=0}^{2}\int dC_1\,Z^-_{i;M}\,\mathcal{Z}_{i;M}(y)\,\ln\chi_M([1,y,0]_i)+\frac{1}{2}\,\lambda_M\,(Z_{1;M}-\frac{2}{3}\,\lambda_M)\Big]$$
$$-\sum_{i=1}^{2}\frac{Z^-_{i;M}}{b_{i;M}}\Big[1-Z_{1i;M}\,\ln\mu_3^2+\int dC_2\,(1+Z_{1i;M}-2\,y)\,\ln\chi_M([1,y,0]_i)\Big], \qquad (115)$$

where we have used Δ_{UV} from Eq.(9) and

$$\mathcal{Z}_{0;M}(y)=\lambda_M-Z_{1;M},\qquad \mathcal{Z}_{1,2;M}(y)=\lambda_M\,y-Z_{1;M},\qquad \chi_M(y,z)\equiv\chi_M(x,1,y,z). \qquad (116)$$

For the finite part the result is as follows:

$$V^{141}_{\rm fin}=-\frac{1}{4\,M^4\,b_{0;M}}\Big[\int dCS\,(x\,;\,y,\{z\})\;\mathcal{V}_{4;M}-\int dCS\,(x\,;\,y,z)\;\mathcal{V}_{3;M}-\int dC_2\,\mathcal{V}_{2;M}-\mathcal{V}_{0;M}\Big]. \qquad (117)$$

Collecting all terms the final answer can be cast into the following form:

$$\mathcal{V}_{4;M}=\frac{\lambda_M}{b_{0;M}}\Big[8\,\lambda_M\,\ln\chi_M(x,y,z_1,z_2)+3\,\mathcal{Z}_{1;M}(z_1)\,L_{+;M}(x,y,z_1,z_2)\Big]$$
$$\mathcal{V}_{3;M}=\sum_{i=0}^{2}\frac{Z^-_{i;M}}{b_{0;M}}\Big[\mathcal{Z}_{i;M}(z)\,L_{+;M}(x,y\,;\,[y,z,0]_i)+2\,\lambda_M\,\ln\chi_M(x,y\,;\,[y,z,0]_i)\Big]$$
$$+\frac{\lambda_M}{b_{0;M}}\Big\{\ln\chi_M(y,z)\Big[4\,(2\,y-1)\,\lambda_M-4\,Z_{1;M}-3\,\mathcal{Z}_{1;M}(y)\,L_M(x,y,z)\Big]$$
$$+\lambda_M\,(1-y)\,\ln\chi_M(x,y,y,z)\Big\}+\sum_{i=1}^{2}\frac{Z^-_{i;M}}{b_{i;M}}\Big[(2\,z-1-Z_{1i;M})\,L_{+;M}(x,y\,;\,[y,z,0]_i)$$
$$+3\,\ln\chi_M(x,y\,;\,[y,z,0]_i)\Big],$$
$$\mathcal{V}_{2;M}=\Big[\sum_{i=0}^{2}\mathcal{Z}_{i;M}(y)\,L_M(x,1\,;\,[1,y,0]_i)+2\sum_{i=1}^{2}\lambda_M\,(1-y)\Big]\,\frac{Z^-_{i;M}}{b_{0;M}}\,\ln\chi_M([1,y,0]_i)$$
$$+\sum_{i=1}^{2}\frac{Z^-_{i;M}}{b_{i;M}}\Big[Z_{1i;M}\,L_{+;M}(x,y,0,0)+(2\,y-1-Z_{1i;M})\,L_M(x,1\,;\,[1,y,0]_i)$$
$$\times\ln\chi_M([1,y,0]_i)-Z_{1i;M}\,\ln\chi_M(x,y,0,0)+2\,(1-y)\,\ln\chi_M([1,y,0]_i)\Big],$$
$$\mathcal{V}_{0;M}=\frac{\lambda_M}{b_{0;M}}\,(\frac{1}{2}\,Z_{1;M}-\frac{13}{9}\,\lambda_M)+\sum_{i=1}^{2}\frac{Z^-_{i;M}}{b_{0;M}}\,\Big[-\frac{1}{2}+Z_{1i;M}\,\ln\mu_3^2\,(2-\ln\mu_3^2)\Big]. \qquad (118)$$

The method will fail for $b_{0;M}=0$ but also for $b_{0;M}\neq 0$ and $\lambda(\nu_1^2,\mu_3^2,\mu_4^2)=0$ and/or $\lambda(1,\mu_3^2,\mu_5^2)=0$ which are non-leading Landau singularities representing normal and pseudo thresholds for reduced V^{141}-diagrams. To occur, they require either p_1 or P to be time-like.

8.2 Evaluation of V^{141}: method II

When $b_{0;M}=0$, with $b_{0;M}$ defined in Eq.(110), method I as described in the previous section cannot be applied. This is not yet a sign that the diagram is singular, since a singularity will appear only if the

point of coordinates $z_i = Z_i$ (Eq.(82)) is internal to the integration domain. From general arguments presented in Section 4.1, see in particular Eq.(55), we know that in this case $V^{141} \sim 1/b_{0;M}$ for $b_{0;M} \to 0$. Therefore the correct procedure amounts to applying the BT algorithm of Appendix A, only once; after that we change $y \to 1-y$ and carry out the y-integration. Some care is needed because a pole at $\epsilon = 0$ is hidden in the parametric integration: for this case we use Eq.(274) of Appendix C. As a result we obtain an integral representation with the correct asymptotic behavior which requires the introduction of generalized one-loop two- and three-point functions. After putting $\chi_M = A_x\,(1-y) + B(z_1, z_2)$ these functions are given in the following list:

$$C_{\{0;1\}}(\alpha) = C_{\{0;1\}0} - \alpha\,\epsilon\,C_{\{0;1\}1} + \mathcal{O}\left(\epsilon^2\right) = \int dS_2\,\{1\,;\,z_1\}\,B^{-1-\alpha\epsilon}(z_1, z_2), \tag{119}$$

and they correspond to the generalized functions of Appendix E. Furthermore we define

$$C_{\{0;1\}_L} = \int dS_2\,\frac{\{1\,;\,z_1\}}{B(z_1, z_2)}\,\ln\Big[1 + \frac{B(z_1, z_2)}{A_x}\Big], \tag{120}$$

which is well-behaved for $B = 0$ and where the case $B = A_x = 0$ will be treated according to Appendix D. Finally we introduce

$$B^i_{\{0;1\}}(\beta) = B^i_{\{0;1\}0} - \beta\,\epsilon\,B^i_{\{0;1\}1} + \mathcal{O}\left(\epsilon^2\right) = \int_0^1 dz\,\{1\,;\,z\}\,B^{-1-\beta\epsilon}([1, z, 0]_i), \tag{121}$$

which are the generalized two-point functions presented in Eq. (10) of [3] (with $\alpha = -1-\epsilon$) and also

$$B^i_{\{0;1\}_L} = \int_0^1 dz\,\{1\,;\,z\}\,B^{-1}([1, z, 0]_i)\,\ln\Big[1 + \frac{B([1, z, 0]_i)}{A_x}\Big], \tag{122}$$

which are also well behaved for $B = 0$. Collecting the various terms we obtain:

$$V^{141} = -\,\frac{1}{b_{0;M}\,M^4}\int_0^1 dx\,\Big[\mathcal{V}_{SP;M}\,(\frac{1}{\epsilon} - \Delta_{UV}) + \mathcal{V}_{f;M}\Big]. \tag{123}$$

where the residue of the ultraviolet pole (Δ_{UV} is defined in Eq.(9)) and the finite part are given by

$$\begin{aligned}
\mathcal{V}_{SP;M} &= \lambda_M\,C_{10} - Z_{1;M}\,C_{00} + \sum_{i=1}^{2} Z^-_{i;M}\,\Big[B^i_{00} - B^i_{10}\Big], \\
\mathcal{V}_{f;M} &= \lambda_M\,(C_{00} - C_{10}) + \frac{1}{2}\,\Big[Z_{1;M}\,C_{0L} - \lambda_M\,C_{1L} + Z_{1;M}\,C_{01} - \lambda_M\,C_{11} \\
&\quad + \ln(X\,A_x)\,(Z_{1;M}\,C_{00} - \lambda_M\,C_{10})\Big] - \frac{1}{2}\sum_{i=1}^{2} Z^-_{i;M}\,\Big[B^i_{0L} - B^i_{1L} + B^i_{01} - B^i_{11} \\
&\quad + \ln(X\,A_x)\,(B^i_{00} - B^i_{10})\Big] + \frac{\lambda_M}{A_x}\,\Big\{\int dS_2\,\ln\Big[A_z\,(1-z_1) + B(z_1, z_2)\Big] \\
&\quad - \frac{1}{2}\int dC_1\,\sum_{i=1}^{2} Z^-_{i;M}\,\ln\Big[A_x\,(1-z_1) + B([1, z, 0]_i)\Big]\Big\}_+,
\end{aligned} \tag{124}$$

and $X = x\,(1-x)$ and $'+'$ refers to the subtraction at $A_x = 0$.

8.3 Wave function renormalization: S_p^{131}

The derivative of S^{131} follows from Eq.(73) with $\nu_1^2 = 1$, $\nu_2^2 = 0$ and $\mu_4 = \mu_5$, i.e. with the replacement $\chi_I \to \xi_I$ of Eq.(89). Therefore, we write

$$S_p^{131} = -\frac{1}{M^4}\int_0^1 dx\, \mathcal{S}_p^{131}(x), \quad \mathcal{S}_p^{131}(x) = \mathcal{G}(2,M^2)\int dS_2 \Big[x\,(1-x)\Big]^{-\epsilon/2}(1-y)^{\epsilon/2-1}\,z\,(y-z)\,\xi_I^{-2-\epsilon}. \tag{125}$$

where $\mathcal{G}$ is defined in Eq.(10). The most convenient way of evaluating this integral is to change variable, $y \to 1-y'$, and to write

$$\xi_I = \mathcal{A}_x\, y + \mathcal{B}_I(z), \qquad \mathcal{B}_I(z) = h\,z^2 + 2\,k\,z + l, \qquad \lambda = h\,l - k^2, \quad Z = -\frac{k}{h}. \tag{126}$$

Next we use one BT-iteration, incrementing the power form $-2-\epsilon$ to $-1-\epsilon$, and the results of Appendix C. With

$$\begin{aligned} B_n &= B_{n0} + \frac{\epsilon}{2}\,B_{n1} + \mathcal{O}\left(\epsilon^2\right) = \int_0^1 dz\, z^n\, \mathcal{B}_I^{-1-\epsilon/2}(z), \\ B_{nL}(x) &= \int_0^1 dz\, z^n\, \mathcal{B}_I^{-1}(z)\,\ln\Big[1 + \frac{\mathcal{B}_I(z)}{\mathcal{A}_x\,(1-z)}\Big], \end{aligned} \tag{127}$$

we obtain

$$\begin{aligned} \lambda\,\mathcal{S}_p^{131}(x) &= h\,(\frac{1}{\epsilon} - \Delta_{UV})\,(Z\,B_{00} - 2\,Z\,B_{10} + B_{20}) + h\,(\frac{1}{2}\,Z\,B_{01} + B_{10} - Z\,B_{11} - B_{20} + \frac{1}{2}\,B_{21}) \\ &- h\,(\frac{1}{2}\,Z\,B_{0L} - Z\,B_{1L} + \frac{1}{2}\,B_{2L}) + \frac{h}{\mathcal{A}_x}\int_0^1 dz\,(z - \frac{1}{2}\,Z)\,\ln\Big[1 + \frac{\mathcal{A}_z\,(1-z)}{\mathcal{B}_I(z)}\Big] \\ &- h\,(\frac{1}{2}\,Z\,B_{00} - Z\,B_{10} + \frac{1}{2}\,B_{20})\,\ln\Big[x\,(1-x)\,\mathcal{A}_x\Big]. \end{aligned} \tag{128}$$

which give our result for this function, with Δ_{UV} defined in Eq.(9).

9 The V^{231} diagram

This topology, depicted in Fig. 7(e), can be written as

$$\pi^4\,V^{231} = \mu^{2\epsilon}\int d^nq_1\int d^nq_2\,\frac{1}{[1][2][3][4][5][6]}, \tag{129}$$

where we have introduced the following notation for propagators:

$$\begin{aligned} &[1] \equiv q_1^2 + m_1^2, \quad [2] \equiv (q_1+P)^2 + m_2^2, \quad [3] \equiv (q_1-q_2)^2 + m_3^2, \\ &[4] \equiv q_2^2 + m_4^2, \quad [5] \equiv (q_2+p_1)^2 + m_5^2, \quad [6] \equiv (q_2+P)^2 + m_6^2, \end{aligned} \tag{130}$$

where $P = p_1 + p_2$ and all momenta are flowing inward. The corresponding set of Landau equations are discussed in Appendix I. An algorithm to evaluate this diagram is discussed in the following section.

9.1 Evaluation of V^{231}

As a first step in the evaluation of V^{231} we combine propagators [1] – [3] with Feynman parameters x_1, x_2,

$$\pi^4\, V^{231} = \Gamma\,(3)\;\mu^{2\epsilon} \int d^n q_1 \int d^n q_2 \int dS_2\, \frac{1}{[4][5][6]}\, \frac{1}{(q_1^2 + 2\,R_x \cdot q_1 + Q_x^2)^3}. \tag{131}$$

Here we have introduced the x-dependent quantities

$$R_x = (1-x_1)\,P - x_2\,q_2, \qquad Q_x^2 = x_1\,(m_1^2 - m_2^2) + x_2\,(q_2^2 + m_3^2 - m_1^2) + m_2^2 + (1-x_1)\,P^2. \tag{132}$$

Integrating over q_1 gives

$$\pi^2\, V^{231} = i\,\frac{\mu^{2\epsilon}}{\pi^{\epsilon/2}}\,\Gamma\left(1+\frac{\epsilon}{2}\right) \int dS_2 \left[x_2(1-x_2)\right]^{-1-\epsilon/2} \int \frac{d^n q_2}{(q_2^2 + 2\,P_x \cdot q_2 + M_x^2)^{1+\epsilon/2}\,[4][5][6]}, \tag{133}$$

where new x-dependent parameters are

$$P_x = \frac{1-x_1}{1-x_2}\,P = X\,P, \quad M_x^2 = \frac{-P^2\,x_1^2 + x_1\,(P^2 + m_1^2 - m_2^2) + x_2\,(m_3^2 - m_1^2) + m_2^2}{x_2\,(1-x_2)}. \tag{134}$$

Next we combine the remaining propagators with Feynman parameters $y_i, i = 1, \ldots, 3$. It follows

$$\begin{aligned}\pi^2\, V^{231} = {} & i\,\frac{\mu^{2\epsilon}}{\pi^{\epsilon/2}}\,\Gamma\left(4+\frac{\epsilon}{2}\right) \int dS_2(x_1,x_2) \left[x_2(1-x_2)\right]^{-1-\epsilon/2} \int dS_3(y_1,y_2,y_3)\, y_3^{\epsilon/2} \\ & \times \int d^n q_2 \left[y_3\,[123] + (y_2-y_3)\,[4] + (y_1-y_2)\,[5] + (1-y_1)\,[6]\right]^{-4-\epsilon/2}. \end{aligned} \tag{135}$$

In the above equation, $[123] = q_2^2 + 2\,P_x \cdot q_2 + M_x^2$. After the q_2-integration we obtain the following result:

$$V^{231} = -\,\frac{\mathcal{G}(2, M^2)}{M^4} \int dS_2(\{x\}) \left[x_2(1-x_2)\right]^{-1-\epsilon/2} \int dS_3(\{y\})\, y_3^{\epsilon/2}\, U_K^{-2-\epsilon}, \tag{136}$$

where we use Eq.(8) and where the quadratic form U_K is given by $U_K = y^t\,H\,y + 2\,K^t\,y + L$ or

$$U_K = A y_1^2 + B y_2^2 + C y_3^2 + D y_1 y_2 + E y_1 y_3 + F y_2 y_3 + G y_1 + I y_2 + J y_3 + N, \tag{137}$$

with coefficients

$$\begin{aligned} & A = s_2\,\nu_2^2, \quad B = s_1\,\nu_1^2, \quad C = X^2\,s_p, \quad D = s_p - s_1\,\nu_1^2 - s_2\,\nu_2^2, \\ & E = X(-s_p + s_1\,\nu_1^2 - s_2\,\nu_2^2), \quad F = X(-s_p - s_1\,\nu_1^2 + s_2\,\nu_2^2), \quad G = -s_2\,\nu_2^2 + \mu_5^2 - \mu_6^2, \\ & I = -s_p + s_2\,\nu_2^2 + \mu_4^2 - \mu_5^2, \quad J = 2\,X\,s_p + \mu_x^2 - \mu_4^2, \quad N = \mu_6^2, \end{aligned} \tag{138}$$

where $m_i^2 = M^2\,\mu_i^2$. It is easily seen that the matrix H of Eq.(137) is singular and we may change variables $y_1 = y_1' + X\,y_3, y_2 = y_2' + X\,y_3$ and $y_3 = y_3'$, with $P_x = X\,P$. The transformed quadratic form becomes

$$U_K' = y_r^t\,H_r\,y_r + 2\,K_r^t\,y_r + f\,y_3 + L, \tag{139}$$

where $y_r^t = (y_1, y_2)$, and the reduced matrix H_r has elements h_{ij} with diagonal elements $s_2\,\nu_2^2$, $s_1\,\nu_1^2$ and off-diagonal elements $(s_p - s_1\,\nu_1^2 - s_2\,\nu_2^2)/2$. Moreover we have

$$\begin{aligned} 2\,K_{r1} = -s_2\,\nu_2^2 + \mu_5^2 - \mu_6^2, \qquad & 2\,K_{r2} = -s_p + s_2\,\nu_2^2 + \mu_4^2 - \mu_5^2, \\ f = X\,(\mu_4^2 - \mu_6^2 + s_p) + \mu_x^2 - \mu_4^2, \qquad & L = \mu_6^2. \end{aligned} \tag{140}$$

Due to the singular nature of the original matrix H, we have been able to confine the x_1, x_2-dependence in the term linear in y_3 and there are no terms proportional to y_3^2 or $y_1 y_3, y_2 y_3$. In this case we can use the following relation

$$\Big\{1 + \frac{1}{1+\epsilon}\Big[y_3 \frac{\partial}{\partial\, y_3} + \frac{1}{2}\sum_{i=1}^{2}(y_i - Y_i)\frac{\partial}{\partial\, y_i}\Big]\Big\}\, U_K^{-2-\epsilon} = b_K\, U_K^{-1-\epsilon}, \tag{141}$$

with a vector $Y_i = -\,H_r^{-1}\, K_r$. As a result b_K is x_1, x_2-independent,

$$b_K = \mu_6^2 - (h_{11}\, k_2^2 + h_{22}\, k_1^2 - 2\, h_{12}\, k_1\, k_2)\, G_{12}^{-1} \tag{142}$$

where $H_r \equiv h$, $K_r \equiv k$ and $G_{12} = h_{11}\, h_{22} - h_{12}^2$ is the usual Gram determinant. After the transformation the innermost integral appearing in Eq.(136) is written as

$$I_K = \int_0^1 dy_3\, y_3^{\epsilon/2} \int_{\overline{X}\, y_3}^{1-X\, y_3} dy_1 \int_{\overline{X}\, y_3}^{y_1} dy_2\, U_K^{-2-\epsilon}, \tag{143}$$

where, as usual, $\overline{X} = 1 - X$ and where we can increment the exponent from $-2-\epsilon$ to $-1-\epsilon$ with a x_1, x_2-independent BT factor. The original quadratic form will be denoted by

$$Q_{0;K}(y_1, y_2, y_3) = U_K(y_1, y_2, y_3), \tag{144}$$

but after integration by parts the result contains 6 new quadratic forms. One is the original quadric after the transformation,

$$Q_{1;K}(y_1, y_2, y_3) = U'_K(y_1, y_2, y_3), \tag{145}$$

while the remaining 5 arise from surface terms. Among them a special role is played by

$$\begin{aligned} Q_{2;K}(y_1, y_2) &= s_p\, y_2^2 + (-s_p + \mu_4^2 - \mu_6^2)\, y_2 + \Big[X\,(\mu_4^2 - \mu_6^2 + s_p) + \mu_x^2 - \mu_4^2\Big]\, y_1 + \mu_6^2 \\ &= H_2\, y_2^2 + 2\, K_2\, y_2 + F_2\, y_1 + L_2. \end{aligned} \tag{146}$$

Indeed the quadratic form $Q_{2;K}$ is also incomplete – the matrix of the quadratic part is singular – and moreover the x_1, x_2-dependent part is confined in the coefficient of y_1. Finally we have

$$Q_{i;K}(y_1, y_2) = y^t\, H_i\, y + 2\, K_i^t\, y + L_i, \qquad y^t = (y_1, y_2), \qquad i = 3, \cdots, 6. \tag{147}$$

Our strategy will be as follows: the term proportional to $Q_{1;K}$ can be transformed according to Eq.(141) with $1 + \epsilon \to \epsilon$, i.e. from power $-1-\epsilon$ to power $-\epsilon$. Furthermore, the form of $U_{2;K}$ makes it possible to increment once again its power with a BT factor which is x_1, x_2-independent; this is possible because when we have a quadratic in two variables of the form $V = hz^2 + 2\, k_1 z + 2\, k_2 y + l$ then we may use

$$\Big[1 - \frac{y}{\mu+1}\,\partial_y - \frac{1}{2\,(\mu+1)}\,\Big(z + \frac{k_1}{h}\Big)\,\partial_z\Big]\, V^{\mu+1} = \frac{hl - k_1^2}{h}\, V^{\mu}. \tag{148}$$

The remaining quadratic forms in two variables, from 3 to 6, contain all terms and Eq.(148) is not active. Therefore, the strategy will be to transform all double integrations into the standard form, $y_1 \in [0, 1]$ and $y_2 \in [0, y_1]$ and to use suitable integral representations for the corresponding generalized C-functions. The final result will be as follows:

$$V^{231} = -\,\frac{1}{M^4} \int dS_2(x_1, x_2) \sum_{i=1}^{3} I_K^{(i)}. \tag{149}$$

For the first term, where the BT-algorithm can be applied twice, we expand around $\epsilon = 0$ and transform back the integration variables to the standard simplexes, obtaining

$$I_K^{(1)} = \frac{1}{b_K^2}\Big[\frac{\mathcal{I}_K^{(1)}}{x_2}\mid_+ + \frac{\mathcal{I}_K^{(1)}}{1-x_2}\Big] \qquad \mathcal{I}_K^{(1)} = \frac{1}{2}\sum_{k=2}^{3}\int dS_k\,\mathcal{I}_K^{(1;k)} + \frac{1}{2}\int dC_2\mathcal{J}_K^{(1)} - \frac{1}{6}. \tag{150}$$

The functions $\mathcal{I}$ of Eq.(150) are given by

$$\mathcal{I}_K^{(1;3)} = -4\,\ln\,\mathcal{Q}_{1;K}^0, \tag{151}$$

$$\begin{aligned}\mathcal{I}_K^{(1;2)} &= X\,(Y_1 - Y_2)\,\ln\mathcal{Q}_{1;K}^a + \Big[X(\bar{Y}_1 - y_1\,\bar{X}) - \bar{Y}_1\Big]\,\ln\mathcal{Q}_{1;K}^b \\ &+ X\,(y_2\,\bar{X} + Y_2)\,\ln\mathcal{Q}_{1;K}^c + X\,(\bar{Y}_1 + X\,y_2)\,\mathcal{Q}_{1;K}^d \\ &+ \Big\{y_1 - Y_2 + X\,\Big[(X-2)\,y_1 + Y_2\Big]\Big\}\,\ln\mathcal{Q}_{1;K}^e + \Big\{y_2 + Y_2 + X\,\Big[(X-2)\,y_2 - Y_2\Big]\Big\}\,\ln\mathcal{Q}_{1;K}^f \\ &+ \Big\{y_2 - Y_1 + X\,\Big[(X-2)\,y_2 + Y_1\Big]\Big\}\,\ln\mathcal{Q}_{1;K}^g\end{aligned} \tag{152}$$

$$\mathcal{J}_K^{(1)} = \Big[\bar{Y}_1 + X\,(y_1\,\bar{X} - \bar{Y}_1)\Big]\,\ln\mathcal{Q}_{1;K}^b + \Big\{Y_1 - y_2 - X\,\Big[(X-2)\,y_2 + Y_1\Big]\Big\}\,\ln\mathcal{Q}_{1;K}^g, \tag{153}$$

where $\bar{Y}_i = 1 - Y_i$ etc. Note that, in Eq.(150) the '+'-distribution only applies to the logarithms. Integration by parts has introduced new quadratic forms:

$$\begin{aligned}&\mathcal{Q}_{1;K}^0 = C_X\,Q_{0;K}(y_1,y_2,y_3), \qquad \mathcal{Q}_{1;K}^a = C_X\,Q_{1;K}(1-X\,y_1, 1-X\,y_1, y_2),\\ &\mathcal{Q}_{1;K}^b = C_X\,Q_{1;K}(1-X\,y_1, \overline{X}\,y_2, y_1), \qquad \mathcal{Q}_{1;K}^c = C_X\,Q_{1;K}(1-X\,y_1, \overline{X}\,y_2, y_2),\\ &\mathcal{Q}_{1;K}^d = C_X\,Q_{1;K}(1-X\,y_2, 1-X\,y_1, y_2), \qquad \mathcal{Q}_{1;K}^e = C_X\,Q_{1;K}(\overline{X}\,y_1, \overline{X}\,y_1, y_2),\\ &\mathcal{Q}_{1;K}^f = C_X\,Q_{1;K}(\overline{X}\,y_1, \overline{X}\,y_2, y_2), \qquad \mathcal{Q}_{1;K}^g = C_X\,Q_{1;K}(\overline{X}\,y_2, \overline{X}\,y_2, y_1),\end{aligned} \tag{154}$$

$C_X = x_2\,(1-x_2)^2$. The rearrangement of terms in Eq.(150) makes evident that no particular problem arises at $x_2 \to 0$. For the second term in Eq.(149) we have from Eq.(146)

$$Y_2' = -\frac{K_2}{H_2} \quad b_K' = L_2 - \frac{K_2^2}{H_2}, \quad I_K^{(2)} = \Big[\frac{\mathcal{I}_K^{(2)}}{x_2}\mid_+ + \frac{\mathcal{I}_K^{(2)}}{1-x_2}\Big], \tag{155}$$

and, correspondingly

$$\begin{aligned}\mathcal{I}_K^{(2)} = \frac{1}{4}\,\frac{Y_1 - Y_2}{b_K\,b_K'}\Big\{1 + 3\int dS_2\Big[X\,\ln\,\mathcal{Q}_{2;K}^a + \overline{X}\,\ln\,\mathcal{Q}_{2;K}^b\Big] \\ - \int dC_1\,\Big[(1 - Y_2' + X\,y_1)\,\ln\,\mathcal{Q}_{2;K}^c + (\overline{X}\,y_1 + Y_2')\,\ln\,\mathcal{Q}_{2;K}^c\Big]\Big\},\end{aligned} \tag{156}$$

where the quadratic forms are

$$\begin{aligned}&\mathcal{Q}_{2;K}^a = C_X\,Q_{1;K}(y_2, 1-X\,y_1), \qquad \mathcal{Q}_{2;K}^b = C_X\,Q_{1;K}(y_2, \overline{X}\,y_1),\\ &\mathcal{Q}_{2;K}^c = C_X\,Q_{1;K}(y_1, 1-X\,y_1), \qquad \mathcal{Q}_{2;K}^d = C_X\,Q_{1;K}(y_1, \overline{X}\,y_1).\end{aligned} \tag{157}$$

For the last term in Eq.(149) we introduce form-factors of the C-family, defined by

$$C_{0\,;11\,;12} = \int dS_2 \,\{1\,;\,x\,;\,y\} \left(a\,x^2 + b\,y^2 + c\,xy + d\,x + e\,y + f - i\,\delta\right)^{-1}, \tag{158}$$

and obtain the following expression:

$$\begin{aligned} I_K^{(3)} &= -\bar{Y}_1 \left[\overline{x}_1\, C_0(a) + \overline{x}\, C_0(b)\right] - Y_2\, C_0(d)\,\overline{x}_1 - 2\,\overline{x}^2\, C_0(e) + 2\, C_0(f) - \overline{x}\, Y_2\, C_0(h) \\ &+ \overline{x}_2 \left[\bar{Y}_1\, C_0(i) + Y_2\, C_0(j) + Y_2\, C_0(l)\right] + \overline{x}_2\, \bar{Y}_1\, C_0(m) + \frac{\overline{x}_1^2}{\overline{x}_2}\, C_{11}(a) \\ &- \overline{x}_1 \frac{\overline{x}}{\overline{x}_2} \left[C_{11}(b) - C_{11}(d)\right] + 2\,\frac{\overline{x}^3}{\overline{x}_2}\, C_{11}(e) - 2\, C_{11}(f) + \frac{\overline{x}^2}{\overline{x}_2}\, C_{11}(h) \\ &- \overline{x}_1\, C_{11}(i) - \overline{x}\, C_{11}(j) + 2\,\overline{x}_1 \frac{\overline{x}}{\overline{x}_2}\, C_{12}(c) + 2\,\frac{\overline{x}^2}{\overline{x}_2}\, C_{12}(g) - \overline{x}\, C_{12}(l) - \overline{x}_1\, C_{12}(m), \end{aligned} \tag{159}$$

where $\overline{x}_i = 1 - x_i$ and $\overline{x} = x_1 - x_2$. Labels from a to m in Eq.(159) characterize different C form-factors and the corresponding expressions for $a, \cdots, f$ are given in Tab. 1.

label	a/x_2	b/x_2	c/x_2	d	e	f
a	$\overline{x}_1^2\, h_{11}$	$\overline{x}_1^2\, h_{22}$	$2\,\overline{x}_1^2\, h_{12}$	$\overline{x}_2(F - 2x_2\,\overline{x}_1\,\sigma_1)$	$-2\,x_2\,\overline{x}_1\,\overline{x}_2\,\sigma_2$	$x_2\,\overline{x}_2^2\,\Sigma$
b	$\overline{x}_1^2\, h_{11}$	$\overline{x}^2\, h_{22}$	$-2\,\overline{x}_1\,\overline{x}\, h_{12}$	$\overline{x}_2(F - 2x_2\,\overline{x}_1\,\rho_1)$	$2\,x_2\,\overline{x}_2\,\overline{x}\,\rho_2$	$x_2\,\overline{x}_2^2\,\omega$
c	$\overline{x}_1^2\, h_{11}$	$\overline{x}^2\, h_{22}$	$-2\,\overline{x}_1\,\overline{x}\, h_{12}$	$-2\,x_2\,\overline{x}_1\,\overline{x}_2\,\rho_1$	$\overline{x}_2(F + 2x_2\,\overline{x}\,\rho_2)$	$x_2\,\overline{x}_2^2\,\omega$
d	$\overline{x}^2\, h_{22}$	$\overline{x}_1^2\, h_{11}$	$-2\,\overline{x}_1\,\overline{x}\, h_{12}$	$\overline{x}_2(F + 2x_2\,\overline{x}\,\rho_2)$	$-2\,x_2\,\overline{x}_1\,\overline{x}_2\,\rho_1$	$x_2\,\overline{x}_2^2\,\omega$
e	$\overline{x}_1\,\overline{x}^2\, h_{11}$	$\overline{x}_1\,\overline{x}^2\, h_{22}$	$2\,\overline{x}_1\,\overline{x}^2\, h_{12}$	$-\overline{x}_2\overline{x}(F - 2x_2\,\overline{x}_1\, k_1)$	$2\,x_2\,\overline{x}_1\,\overline{x}_2\,\overline{x}\, k_2$	$\overline{x}_2^2(F + x_2\,\overline{x}_1\, l)$
f	$\overline{x}_1\, h_{11}$	$\overline{x}_1\, h_{22}$	$2\,\overline{x}_1\, h_{12}$	$-F + 2\,x_2\,\overline{x}_1\, k_1$	$2\,x_2\,\overline{x}_1\, k_2$	$F + x_2\,\overline{x}_1\, l$
g	$\overline{x}^2\, h_{11}$	$\overline{x}^2\, h_{22}$	$2\,\overline{x}^2\, h_{12}$	$2\,x_2\,\overline{x}_2\,\overline{x}\, k_1$	$\overline{x}_2(F + 2x_2\,\overline{x}\, k_2)$	$x_2\,\overline{x}_2^2\, l$
h	$\overline{x}^2\, h_{22}$	$\overline{x}^2\, h_{11}$	$2\,\overline{x}^2\, h_{12}$	$\overline{x}_2(F + 2x_2\,\overline{x}\, k_2)$	$2\,x_2\,\overline{x}_2\,\overline{x}\, k_1$	$x_2\,\overline{x}_2^2\, l$
i	$\overline{x}_1^2\, h_{11}$	$\overline{x}_2^2\, h_{22}$	$2\,\overline{x}_1\,\overline{x}_2\, h_{12}$	$\overline{x}_2(F - 2x_2\,\overline{x}_1\,\sigma_1$	$-2\,x_2\,\overline{x}_2^2\,\sigma_2$	$x_2\,\overline{x}_2^2\,\Sigma$
j	$\overline{x}^2\, h_{22}$	$\overline{x}_2^2\, h_{11}$	$-2\,\overline{x}_2\,\overline{x}\, h_{12}$	$\overline{x}_2(F + 2x_2\,\overline{x}\,\rho_2)$	$-2\,x_2\,\overline{x}_2^2\,\rho_1$	$x_2\,\overline{x}_2^2\,\omega$
l	$\overline{x}_2^2\, h_{11}$	$\overline{x}^2\, h_{22}$	$-2\,\overline{x}_2\,\overline{x}\, h_{12}$	$-2\,x_2\,\overline{x}_2^2\,\rho_1$	$\overline{x}_2(F + 2x_2\,\overline{x}\,\rho_2)$	$x_2\,\overline{x}_2^2\,\omega$
m	$\overline{x}_2^2\, h_{22}$	$\overline{x}_1^2\, h_{11}$	$2\,\overline{x}_1\,\overline{x}_2\, h_{12}$	$-2\,x_2\,\overline{x}_2^2\,\sigma_2$	$\overline{x}_2(F - 2x_2\,\overline{x}_1\,\sigma_1)$	$x_2\,\overline{x}_2^2\,\Sigma$

Table 1: Parameters for the C-functions arising from Eq.(158).

We have introduced the auxiliary quantities

$$\begin{aligned} h_{11} &= -s_2\,\nu_2^2, \quad h_{22} = -s_1\,\nu_1^2, \quad h_{12} = \frac{1}{2}\,(s_p - s_1\,\nu_1^2 - s_2\,\nu_2^2) \\ k_1 &= \frac{1}{2}\,(\mu_5^2 - \mu_6^2 - s_2\,\nu_2^2), \quad k_2 = \frac{1}{2}\,(\mu_4^2 - \mu_5^2 - s_p + s_2\,\nu_2^2), \quad l = \mu_6^2, \end{aligned} \tag{160}$$

as well as the combinations

$$\begin{aligned}
&\Sigma = h_{11} + h_{22} + 2\,h_{12} + 2\,k_1 + 2\,k_2 + l,\\
&\sigma_1 = h_{11} + h_{12} + k_1, \qquad \sigma_2 = h_{22} + h_{12} + k_2,\\
&\rho_1 = h_{11} + k_1, \qquad \rho_2 = h_{12} + k_2, \qquad \omega = h_{11} + 2\,k_1 + l.
\end{aligned} \tag{161}$$

Finally we have defined

$$f = X\,(\mu_4^2 - \mu_6^2 + s_p) - \mu_4^2 + \mu_x^2 = \frac{F}{x_2\,(1-x_2)}. \tag{162}$$

One can see that, for any of the above functions, the corresponding determinant is proportional to G_{12}. All C-functions are computed according to the procedure of Appendix E, including a preliminary sector decomposition in order to avoid numerical instabilities at the end points of the $x_1 - x_2$ integration. Finally, note that the sub-leading BT-factor is given by $b'_{K} = -1/4\,\lambda(s_p, \mu_4^2, \mu_6^2)$. An alternative representation will be studied in the next section.

9.2 Evaluation of V^{231}: method II

There is a second integral representation for this diagram where we start from Eq.(143), exchange the order of integration and directly perform the y_3 integration. After that the $y_1 - y_2$ interval is mapped into the standard triangle $0 \le y_2 \le y_1 \le 1$ and the net result for I_K is a combination of 10 C_0 functions with $\{x\}$ dependent parameters. We write h_{ij} for the elements of H_r and k_i for those of K_r, see Eq.(139): the ten quadratic forms in two variables are

$$Q_i(y_1, y_2) = a_i\,y_1^2 + b_i\,y_2^2 + c_i\,y_1\,y_2 + d_i\,y_1 + e_i\,y_2 + f_i, \tag{163}$$

and the coefficients are given in Tab. 2. The result is

$$I_{K} = \frac{1}{M^4\,f}\int dS_2\,x_2\,\mathcal{I}_{K}, \tag{164}$$

$$\mathcal{I}_{K} = \overline{x}_1^2\,C_0([1-2]) - \overline{x}_1\,\overline{x}_2\,C_0([3-4]) - \overline{x}_1\,\overline{x}_2\,C_0([5-6]) - \overline{x}^2\,C_0([7-8]) + \overline{x}_1\,\overline{x}\,C_0([9-10]), \tag{165}$$

where $C_0([i-j]) = C_0(i) - C_0(j)$. Furthermore we have

$$\begin{aligned}
&f = \frac{\Delta(x_1,x_2)}{x_2\,(1-x_2)} \quad \Delta(x_1,x_2) = \nu_x^2 - x_2\,(1-x_2)\,\mu_4^2 + x_2\,(1-x_1)\,(\mu_4^2 - \mu_6^2 + s_p),\\
&\nu_x^2 = -s_p\,x_1^2 + x_1\,(-s_p + \mu_1^2 - \mu_2^2) + x_2\,(\mu_3^2 - \mu_1^2) + \mu_2^2.
\end{aligned} \tag{166}$$

As a result our second expression for the V^{231} diagram is

$$V^{231} = -\frac{1}{M^4}\int dS_2(x_1,x_2)\,\frac{x_2}{\Delta(x_1,x_2)}\int dS_2(y_1,y_2)\,\mathcal{I}_{K}. \tag{167}$$

Note that there is no severe problem when $\Delta(x_1,x_2) \to 0$ because, as seen from Eq.(165) and Tab. 2, the differences $C_0(i) - C_0(i+1)$ vanish in the same limit. For technical details regarding the evaluation of C_0 we refer once more to Appendix E.

i	a	b	c	d	e	f
1	$x_2\,\overline{x}_1^2\,h_{11}$	$x_2\,\overline{x}_1^2\,h_{22}$	$2\,x_2\,\overline{x}_1^2\,h_{12}$	$-2\,x_2\,\overline{x}_1\,\overline{x}_2\,\sigma_1+\overline{x}_2\,\Delta$	$-2\,x_2\,\overline{x}_1\,\overline{x}_2\,\sigma_2$	$x_2\,\overline{x}_2^2\,\Sigma$
2	$x_2\,\overline{x}_1^2\,h_{11}$	$x_2\,\overline{x}_1^2\,h_{22}$	$2\,x_2\,\overline{x}_1^2\,h_{12}$	$-2\,x_2\,\overline{x}_1\,\overline{x}_2\,\sigma_1$	$-2\,x_2\,\overline{x}_1\,\overline{x}_2\,\sigma_2$	$x_2\,\overline{x}_2^2\,\Sigma$
3	$x_2\,\overline{x}_1^2\,h_{11}$	$x_2\,\overline{x}_2^2\,h_{22}$	$2\,x_2\,\overline{x}_1\,\overline{x}_2\,h_{12}$	$-2\,x_2\,\overline{x}_1\,\overline{x}_2\,\sigma_1+\overline{x}_2\,\Delta$	$-2\,x_2\,\overline{x}_2^2\,\sigma_2$	$x_2\,\overline{x}_2^2\,\Sigma$
4	$x_2\,\overline{x}_1^2\,h_{11}$	$x_2\,\overline{x}_2^2\,h_{22}$	$2\,x_2\,\overline{x}_1\,\overline{x}_2\,h_{12}$	$-2\,x_2\,\overline{x}_1\,\overline{x}_2\,\sigma_1$	$-2\,x_2\,\overline{x}_2^2\,\sigma_2$	$x_2\,\overline{x}_2^2\,\Sigma$
5	$x_2\,\overline{x}_2^2\,h_{22}$	$x_2\,\overline{x}_1^2\,h_{11}$	$2\,x_2\,\overline{x}_1\,\overline{x}_2\,h_{12}$	$-2\,x_2\,\overline{x}_2^2\,\sigma_2$	$-2\,x_2\,\overline{x}_1\,\overline{x}_2\,\sigma_1+\overline{x}_2\,\Delta$	$x_2\,\overline{x}_2^2\,\Sigma$
6	$x_2\,\overline{x}_2^2\,h_{22}$	$x_2\,\overline{x}_1^2\,h_{11}$	$2\,x_2\,\overline{x}_1\,\overline{x}_2\,h_{12}$	$-2\,x_2\,\overline{x}_2^2\,\sigma_2$	$-2\,x_2\,\overline{x}_1\,\overline{x}_2\,\sigma_1$	$x_2\,\overline{x}_2^2\,\Sigma$
7	$x_2\,\overline{x}^2\,h_{11}$	$x_2\,\overline{x}^2\,h_{22}$	$2\,x_2\,\overline{x}^2\,h_{12}$	$2\,x_2\,\overline{x}_2\,\overline{x}\,k_1$	$2\,x_2\,\overline{x}_2\,\overline{x}\,k_2+\overline{x}_2\,\Delta$	$x_2\,\overline{x}_2^2\,l$
8	$x_2\,\overline{x}^2\,h_{11}$	$x_2\,\overline{x}^2\,h_{22}$	$2\,x_2\,\overline{x}^2\,h_{12}$	$2\,x_2\,\overline{x}_2\,\overline{x}\,k_1$	$2\,x_2\,\overline{x}_2\,\overline{x}\,k_2$	$x_2\,\overline{x}_2^2\,l$
9	$x_2\,\overline{x}_1^2\,h_{11}$	$x_2\,\overline{x}_1^2\,h_{22}$	$-2\,x_2\,\overline{x}_1\,\overline{x}\,h_{12}$	$-2\,x_2\,\overline{x}_1\,\overline{x}_2\,\rho_1+\overline{x}_2\,\Delta$	$2\,x_2\,\overline{x}_2\,\overline{x}\,\rho_2$	$x_2\,\overline{x}_2^2\,\omega$
10	$x_2\,\overline{x}_1^2\,h_{11}$	$x_2\,\overline{x}^2\,h_{22}$	$-2\,x_2\,\overline{x}_1\,\overline{x}\,h_{12}$	$-2\,x_2\,\overline{x}_1\,\overline{x}_2\,\rho_1$	$2\,x_2\,\overline{x}_2\,\overline{x}\,\rho_2+\overline{x}_2\,\Delta$	$x_2\,\overline{x}_2^2\,\omega$

Table 2: Coefficients $a\cdots f$ for the 10 quadratic forms in two variables of Eq.(165). Here $\Sigma = h_{11}+2h_{12}+h_{22}+2k_1+2k_2+l$. Furthermore, $\sigma_1 = h_{11}+h_{12}+k_1$, $\sigma_2 = h_{22}+h_{12}+k_2$, $\rho_1 = h_{11}+k_1$, $\rho_2 = h_{12}+k_2$ and $\omega = h_{11}+2\,k_1+l$.

9.3 Wave function renormalization: S_p^{221}

The derivative S_p^{221} is computed from Eq.(136) when we put $p_2 = 0$ and $m_5 = m_6$, using Eqs.(164)–(167) with $p_2 = 0$ and $m_5 = m_6$. This is equivalent to say that all C_0 functions in Eq.(165) have vanishing Gram's determinant. We briefly recall the strategy to evaluate a one-loop vertex when the Gram determinant is zero [3]: let us write $y^t\,H_i\,y+2\,K_i^t\,y+L_i$ for any of the quadratic forms of Eq.(163). Let us introduce also

$$b_i = \lim_{G_{12}\to 0} G_{12}\,B_i, \qquad B_i = L_i - K_i^t\,H_i^{-1}\,K_i, \qquad \mathcal{X}_i = -\,\Delta_i\,K_i, \tag{168}$$

where G_{12} is the Gram's determinant and $\Delta_{i,kl}$ is the co-determinant of the element $H_{i,kl}$. For each $b_i \neq 0$ we obtain

$$C_i(G_{12}=0) = -\,\frac{1}{2\,b_i}\,\int_0^1 dy\,\sum_{j=0}^{2}\,(\mathcal{X}_{i,j}-\mathcal{X}_{i,j+1})\,\ln Q_i(\widehat{j\;j+1}), \tag{169}$$

where $\mathcal{X}_{i0}=1$, $\mathcal{X}_{i3}=0$, and $Q_i(\widehat{j\;j+1})$ denotes contractions, i.e.

$$Q_i(\widehat{0\;1}) = Q_i(1,y), \quad Q_i(\widehat{1\;2}) = Q_i(y,y), \quad Q_i(\widehat{2\;3}) = Q_i(y,0). \tag{170}$$

When $b_i = 0$ in Eq.(169) we have to distinguish between two sub-cases (the subscript i is left understood), a) $e - cd/(2\,a) \neq 0$ where the integration is trivial and b) $e - cd/(2\,a) = 0$ where the vertex reduces to a combination of generalized two-point functions [3] showing a possible singularity of the form $(a\,f - d^2/4)^{-1/2}$.

10 The V^{222} diagram

The V^{222} topology of Fig. 7(f) is a non-planar one, therefore showing a novel feature with respect to all other two-loop vertices, namely there are two lines in common between any of the one-loop subdiagrams. The expression is

$$\pi^4\, V^{222} = \mu^{2\epsilon} \int d^n q_1 \int d^n q_2\, \frac{1}{[1][2][3][4][5][6]}, \tag{171}$$

where we have introduced the following notation for propagators:

$$\begin{aligned} &[1] \equiv q_1^2 + m_1^2 \qquad [2] \equiv (q_1 - p_2)^2 + m_2^2 \qquad [3] \equiv (q_1 - q_2 + p_1)^2 + m_3^2, \\ &[4] \equiv (q_1 - q_2 - p_2)^2 + m_4^2 \qquad [5] \equiv q_2^2 + m_5^2 \qquad [6] \equiv (q_2 - p_1)^2 + m_6^2. \end{aligned} \tag{172}$$

The corresponding Landau equations are discussed in Appendix J. All the techniques that we have adopted so far in evaluating two-loop diagrams will have severe drawbacks when applied to V^{222}. Consider, for instance, the standard parametrization:

10.1 V^{222}: parametrization I

As usually done, in the first step we combine the propagators $[1] - [4]$ of Eq.(172) with Feynman parameters $y_i, i = 1, \ldots, 3$, obtaining

$$\pi^4\, V^{221} = \mu^{2\epsilon}\, \Gamma(4) \int d^n q_1 d^n q_2 \int dS_3\, \frac{1}{[5][6]}\, \frac{1}{(q_1^2 + 2\, R_y \cdot q_1 + Q_y^2)^4}, \tag{173}$$

with y-dependent quantities defined by

$$\begin{aligned} R_y = (y_2 - y_3)\, p_1 - (y_1 - y_2 + y_3)\, p_2 - y_2\, q_2, \quad Q_y^2 = y_1\, (p_2^2 + m_2^2 - m_1^2) + y_2\, ((q_2 - p_1)^2 - p_2^2 + m_3^2 - m_2^2) \\ + y_3\, (2P \cdot q_2 - p_1^2 + p_2^2 + m_4^2 - m_3^2) + m_1^2. \end{aligned} \tag{174}$$

Integrating over q_1 gives

$$\pi^2\, V^{222} = i\, \frac{\mu^{2\epsilon}}{\pi^{-\epsilon/2}}\, \Gamma\left(2 + \frac{\epsilon}{2}\right) \int dS_3 \Big[y_2(1 - y_2)\Big]^{-2-\epsilon/2} \int \frac{d^n q_2}{(q_2^2 + 2\, P_y \cdot q_2 + M_y^2)^{2+\epsilon/2}\, [5][6]}, \tag{175}$$

where the y-dependent internal and external masses are given by

$$\begin{aligned} P_y &= (\frac{y_3}{y_2} - 1)\, p_1 + (\frac{y_3}{y_2} - \frac{y_1 - y_2}{1 - y_2})\, p_2, \\ M_y^2 &= \frac{1}{y_2\, (1 - y_2)} \Big[-y_1^2\, p_2^2 - (y_2 - y_3)\, P^2 + 2\, y_1\, (y_2 - y_3)\, P \cdot p_2 \\ &\quad + y_1\, (p_2^2 - m_1^2 + m_2^2) + y_2\, (p_1^2 - p_2^2 - m_2^2 + m_3^2) - y_3\, (p_1^2 - p_2^2 + m_3^2 - m_4^2) + m_1^2\Big]. \end{aligned} \tag{176}$$

Next we combine the remaining propagators with Feynman parameters $x_i, i = 1, 2$. After the q_2-integration, it follows

$$V^{222} = -\,\mathcal{G}(2) \int dS_3(\{y\}) \Big[y_2(1 - y_2)\Big]^{-2-\epsilon/2} \int dS_2(\{x\})\, x_2^{1+\epsilon/2}\, U_H^{-2-\epsilon} \tag{177}$$

where $\mathcal{G}$ is defined in Eq.(10) and the quadratic form is given by

$$U_H = x^t\, H_H\, x + 2\, K_H^t\, x + L_H = A x_1^2 + B x_2^2 + C x_1 x_2 + D x_1 + E x_2 + F, \tag{178}$$

and where the coefficients are

$$A = -\,p_1^2, \quad B = -\,P_y^2, \quad C = -2\,p_1\cdot P_y,$$
$$D = p_1^2 + m_5^2 - m_6^2, \quad E = 2\,p_1\cdot P_y - m_5^2 + M_y^2, \quad F = m_6^2. \tag{179}$$

The fact that we have a quadratic form in two variables for the internal integration, in a context where there are two external momenta, makes H non-singular, in contrast to the planar topology V^{231}. The consequence is that when we increase the power of the integrand using only internal variables this will, inevitably, result into a denominator which depends on external Feynman parameters. A BT functional relation of Appendix A applied to the quadratic form U_H produces a coefficient b_H which can be written in a compact form as

$$b_H = \frac{n_H}{p_1^2\,P_y^2 - (p_1\cdot P_y)^2}, \tag{180}$$

$$n_H = -\,\frac{1}{4\,m_5^2}\,\Big\{\Big[(p_1^2 - m_5^2 - m_6^2)\,P_y^2 - \frac{1}{2}\,(p_1^2 + m_5^2 - m_6^2)\,M_y^2$$
$$-\,\frac{1}{2}\,(m_5^2 + m_6^2 - 3\,p_1^2)\,m_5^2 - 2\,m_5^2\,p_1\cdot P_y\Big]^2 - \frac{1}{4}\,\lambda(-P_y^2, M_y^2 - P_y^2, m_5^2)\,\lambda(-p_1^2, m_6^2, m_5^2)\Big\}. \tag{181}$$

Note that the solutions for $(p_1 + P_y)^2$ of the equation $b_H = 0$ correspond to the anomalous threshold (the leading Landau singularity) for the vertex with external momenta p_1, P_y and internal masses squared $M_y^2 - P_y^2, m_5^2$ and m_6^2. We have real solutions for $(p_1 + P_y)^2$ if and only if

$$-\,p_1^2 \le (m_5 - m_6)^2 \quad \text{or} \quad -\,p_1^2 \ge (m_5 + m_6)^2, \quad \lambda(-P_y^2, M_y^2 - P_y^2, m_5^2) \ge 0. \tag{182}$$

In principle the proper strategy in dealing with y-dependent BT factors consists in deforming the corresponding integration contour, a technique introduced in [33]. In practice the high dimensionality of the hyper-contour makes it extremely hard to obtain a distortion with the requested causal properties. An alternative parametrization will be discussed in the following section.

10.2 V^{222}: parametrization II

As it is well-known, any two-loop diagram can be cast into the form of an integral representation where the kernel is a generalized sunset diagram. Starting from the definition of V^{222} Eqs. (171-172) we combine propagators $[1]-[2]$ with a parameter z_1, propagators $[3]-[4]$ with z_2 and $[5]-[6]$ with z_3. Next we introduce auxiliary variables

$$R_1^2 = z_1\,(p_2^2 + m_2^2) + (1 - z_1)\,m_1^2, \quad R_2^2 = z_2\,(p_1^2 + m_3^2) + (1 - z_2)\,(p_2^2 + m_4^2),$$
$$R_3^2 = z_3\,(p_1^2 + m_6^2) + (1 - z_3)\,m_5^2,$$
$$K_1 = -z_1\,p_2, \quad K_2 = z_2\,p_1 - (1 - z_2)\,p_2, \quad K_3 = -z_3\,p_1. \tag{183}$$

As a second step we change variables, $q_1 \to q_1 - K_1$ and $q_2 \to q_2 - K_3$ and combine the q_1 and $q_1 - q_2$ propagators with a parameter x. After the q_1-integration we combine the residual propagators with a parameter y and carry out the q_2 integration obtaining

$$V^{222} = -\,\mathcal{G}(2)\int dC_5\,y^{1+\epsilon/2}\,(1-y)\,\Big[x(1-x)\Big]^{-1-\epsilon/2}\,\Big[-Q^2\,y^2 + (M_x^2 - M^2 + Q^2)\,y + M^2\Big]^{-2-\epsilon}, \tag{184}$$

where $\mathcal{G}$ is defined in Eq.(10) and where we have introduced the following quantities

$$Q = K_1 - K_2 - K_3, \qquad M^2 = R_3^2 - K_3^2, \qquad M_x^2 = \frac{x\,(R_1^2 - K_1^2) + (1-x)\,(R_2^2 - K_2^2)}{x\,(1-x)}. \tag{185}$$

Since there are no ultraviolet poles we can put $\epsilon = 0$ and increase twice the power of the quadratic form in y, obtaining

$$V^{222} = \int dC_5\, \frac{1}{B_H^2\, x(1-x)}\, \mathcal{V}^{222}, \tag{186}$$

where the explicit expression for $\mathcal{V}^{222}$ will not be reported explicitly and where the BT factor is

$$B_H = \lambda\left(-Q^2, M^2, M_x^2\right). \tag{187}$$

This formulation has the advantage that, for fixed $\{z_i\}$, we could distort the x-integration in order to avoid the zeros of B_H and the study of these zeros follows directly from the analysis of S^{111} [1]. We assume that all external momenta are time-like and put $Q^2 = -\,P^2\,\nu_Q^2$, with $P = p_1 + p_2$: it follows that

$$\begin{aligned}\nu_Q^2 = {} & \nu_2^2\, z_1^2 - z_2^2 + \nu_2^2\, z_3^2(\nu_1^2 - \nu_2^2 - 1)\, z_1 z_2 - (1 - \nu_1^2 - \nu_2^2)\, z_1 z_3 - (1 + \nu_1^2 - \nu_2^2)\, z_2 z_3 - 2\,\nu_2^2\, z_1 \\ & - (1 - \nu_1^2 + \nu_2^2)\, z_2 + (1 - \nu_1^2 - \nu_2^2)\, z_3 - \nu_2^2,\end{aligned} \tag{188}$$

$$M^2 = -P^2\,\nu_M^2, \qquad \nu_M^2 = \nu_1^2\, z_3^2 - (\nu_1^2 + \mu_5^2 - \mu_6^2)\, z_3 + \mu_5^2, \tag{189}$$

$$M_x^2 = -P^2\,\frac{\nu_x^2}{x(1-x)}, \qquad \nu_x^2 = x\left[\nu_2^2\, z_3^2 - (\nu_2^2 + \mu_1^2 - \mu_2^2)\, z_3 + \mu_1^2\right] + (1-x)\left[z_2^2 - \mu_{34}^2\, z_2 + \mu_4^2\right]. \tag{190}$$

In terms of scaled quantities we may rewrite the BT factor as

$$B_H = P^4\,\lambda\left(\nu_Q^2, -\nu_M^2, -\frac{\nu_x^2}{x(1-x)}\right). \tag{191}$$

Furthermore we have that

$$\lambda(\nu_Q^2, -\nu_M^2, -\frac{\nu_x^2}{x(1-x)}) = X^{-2}\,\lambda(X\,\nu_Q^2, -\,X\,\nu_M^2, -\nu_x^2) = X^{-2}\,b_H, \tag{192}$$

where $X = x(1-x)$ and numerical evaluation requires distortion across the zeros of b_H.

10.3 The analytical structure of V^{222}

Before attempting an evaluation of V^{222} it is important to know more about its analytical structure and, therefore, we start once again considering the expression for b_H; zeros of b_H that are real and inside the integration region represent apparent singularities and are an obstacle for numerical integration. In the following we classify their nature: in this representation we have introduced effective squared masses which are given by

$$\begin{aligned}M_1^2 &= \chi_1 z_1; p_2^2, m_1, m_2) = -p_2^2\, z_1^2 + (m_2^2 - m_1^2 + p_2^2)\, z_1 + m_1^2, \\ M_2^2 &= \chi_2(z_2; P^2, m_4, m_3) = -P^2\, z_2^2 + (m_3^2 - m_4^2 + P^2)\, z_2 + m_4^2, \\ M_3^2 &= \chi_3(z_3; p_1^2, m_5, m_6) = -p_1^2\, z_3^2 + (m_6^2 - m_5^2 + p_1^2)\, z_3 + m_5^2.\end{aligned} \tag{193}$$

Being functions of $\{z\}$, their sign is not constant and the following inequalities hold:

$$\begin{aligned}
M_1^2 \geq 0 \quad & \text{for} \quad p_2^2 \leq 0, \quad \lambda(-p_2^2, m_1^2, m_2^2) \leq 0, \\
& \text{or} \quad p_2^2 \geq 0, \quad \lambda(-p_2^2, m_1^2, m_2^2) \geq 0, \quad z_{1a} \leq z_1 \leq z_{1b}, \\
& \text{or} \quad p_2^2 \leq 0, \quad \lambda(-p_2^2, m_1^2, m_2^2) \geq 0, \quad z_1 \leq z_{1a}, \quad \text{or} \quad z_1 \geq z_{1b}, \\
M_2^2 \geq 0 \quad & \text{for} \quad P^2 \leq 0, \quad \lambda(-P^2, m_3^2, m_4^2) \leq 0, \\
& \text{or} \quad P^2 \geq 0, \quad \lambda(-P^2, m_3^2, m_4^2) \geq 0, \quad z_{2a} \leq z_2 \leq z_{2b}, \\
& \text{or} \quad P^2 \leq 0, \quad \lambda(-P^2, m_3^2, m_4^2) \geq 0, \quad z_2 \leq z_{2a}, \quad \text{or} \quad z_2 \geq z_{2b}, \\
M_3^2 \geq 0 \quad & \text{for} \quad p_1^2 \leq 0, \quad \lambda(-p_1^2, m_5^2, m_6^2) \leq 0, \\
& \text{or} \quad p_1^2 \geq 0, \quad \lambda(-p_1^2, m_5^2, m_6^2) \geq 0, \quad z_{3a} \leq z_3 \leq z_{3b}, \\
& \text{or} \quad p_1^2 \leq 0, \quad \lambda(-p_1^2, m_5^2, m_6^2) \geq 0, \quad z_3 \leq z_{3a}, \quad \text{or} \quad z_3 \geq z_{3b},
\end{aligned} \tag{194}$$

where $P = p_1 + p_2$ and $z_{ia,b}$ are the roots of $\chi_i = 0$. If $M_1^2, M_2^2 \geq 0$ then $M_x^2 \geq 0$. Clearly, if all masses are such that their squares are positive and $Q^2 > 0$ there are no real solutions for x to the equation $b_H = 0$. Otherwise, for $Q^2 < 0$ and positive (effective) masses squared, the solutions are given by

$$\left(M_x^2\right)_\pm = \left(\sqrt{M_3^2} \pm \sqrt{-Q^2}\right)^2. \tag{195}$$

The condition $Q^2 \geq 0$ is given by $\mathcal{P}_H(z_1, z_2, z_3) \geq 0$ with

$$\begin{aligned}
\mathcal{P}_H(z_1, z_2, z_3) = {} & p_2^2\, z_1^2 + P^2\, z_2^2 + p_1^2\, z_3^2 + 2\, p_2 \cdot P\, z_1 z_2 - 2\, p_1 \cdot p_2\, z_1 z_3 - 2\, p_1 \cdot P\, z_2 z_3 \\
& - 2\, p_2^2\, z_1 - 2\, p_2 \cdot P\, z_2 + 2\, p_1 \cdot p_2\, z_3 + p_2^2,
\end{aligned} \tag{196}$$

with $P = p_1 + p_2$. Therefore we have $Q^2 \geq 0$ for

$$\begin{aligned}
p_2^2 \geq 0 \quad & \text{and} \quad G_{12} \leq 0, \\
p_2^2 \leq 0\, (p_2^2 \geq 0) \quad & \text{and} \quad G_{12} \geq 0, \quad z_{1-} \leq z_1 \leq z_{1+}\, (z_1 \leq z_{1-} \quad \text{or} \quad z_1 \geq z_{1+}), \\
z_{1\pm} \;=\; & \frac{1}{p_2^2}\left[p_2^2 - p_2 \cdot P\, z_2 + p_1 \cdot p_2\, z_3 \pm (z_2 - z_3)\, \sqrt{G_{12}}\right].
\end{aligned} \tag{197}$$

Finally, if $M_3^2 \leq 0$ or $M_x^2 \leq 0$ there are again no real solutions. Let us assume that $M_x^2 \geq 0\, (0 \leq x \leq 1)$ and also $M_3^2 \geq 0$ and $S^2 = -Q^2 \geq 0$. We have to discuss zeros of b_H, i.e.

$$\left(M_x^2\right)_\pm = \left(M_3 \pm S\right)^2, \quad M_3 = \sqrt{M_3^2}, \quad S = \sqrt{-Q^2}. \tag{198}$$

The minimum, for $M_x^2(x)$, occurs at $x_\pm = M_1/(M_2 \pm M_1)$, where $M_i = \sqrt{M_i^2}$. Only x_+ lies between 0 and 1, corresponding to

$$\left(M_x^2\right)_{\min} = \left(M_1 + M_2\right)^2. \tag{199}$$

There are three distinct possibilities:

1. the root $(M_x^2)_+$ is below the minimum, i.e. $M_1 + M_2 - M_3 \geq S$, therefore b_H can never be zero.

2. Only one root is above the minimum, i.e. $\left(S - M_3\right)^2 \leq \left(M_1 + M_2\right)^2 \leq \left(S + M_3\right)^2$, when there are two values of x where $b_H = 0$,

$$x_\pm^+ = \frac{1}{2\, \left(S + M_3\right)^2}\, \left[\left(S + M_3\right)^2 - M_1^2 + M_2^2 \pm \lambda^{1/2}\, \left(\left(S + M_3\right)^2, M_1^2, M_2^2\right)\right]. \tag{200}$$

3. Both roots are above the minimum, i.e. $(M_1+M_2)^2 \leq (S-M_3)^2$, when we have four values of x where $b_H = 0$. The new pair of points is given by

$$x_{\pm}^{-} = \frac{1}{2\,(S-M_3)^2}\,\Big[\,(S-M_3)^2 - M_1^2 + M_2^2 \pm \lambda^{1/2}\,\Big((S-M_3)^2, M_1^2, M_2^2\Big)\Big]. \tag{201}$$

Next we study the imaginary part of $\ln U$. Rewriting U as a function of x we obtain $U(x,y;\{z\}) = U_N(x,y\,;\,\{z\})/x(1-x)$ with

$$U_N(x,y\,;\,\{z\}) = -\,(y\,Q^2 + M_3^2)\,(1-y)\,x^2 + \Big[-y^2\,Q^2 + y\,(Q^2 + M_1^2 - M_2^2 - M_3^2) + M_3^2\Big]\,x + y\,M_2^2. \tag{202}$$

There are two roots for $U_N = 0$ to be denoted $x_{L,R}$. One possible way of computing V^{222} would be to distort the integration hyper-contour. Consider the distortion for the points $x_{\pm}^{-}$: this possibility ceases when $x_{L,R}$ pinch the real x-axis at a point $\in\ [0,1]$. Given that $U_N(x,y\,;\,\{z\})$ is quadratic in x, say $U_N = ax^2 + bx + c$, this situation will occur when we simultaneously have $x_-^- = x_+^- = -\frac{b}{2\,a}$ and $b^2 = 4\,ac$. The condition for coincidence, i.e. $x_-^- = x_+^-$, is

$$S = M_1 + M_2 + M_3, \qquad S = \sqrt{-Q^2}. \tag{203}$$

The remaining two conditions, namely $\mathrm{Im}\,x_{L,R} = 0$ and $x_L = x_R = x_-^- = x_+^-$, require

$$y_{\rm th} = \frac{M_3}{M_1 + M_2 + M_3}, \tag{204}$$

and it can be easily shown that we have a pinch at $y = y_{\rm th}$. A possible way out would require distorting the $\{z\}$ hyper-contour in order to avoid the pinch at $y = y_{\rm th}$ until a true singularity appears. However it is very time consuming to build an automatized algorithm that accomplish the distortion in a proper way, i.e. that avoids crossing of cuts in the logarithms. All the attempts that we have made do not satisfy our bounds on the required CPU time for evaluating a two-loop diagram. Nevertheless we will present the main ingredients of the complete analysis, since understanding the analytical structure of the diagram has a role of its own, not bound by the method actually used in the numerical evaluation. There are also other solutions to the condition for coincidence, among which

$$S = M_1 - M_2 + M_3, \qquad S = \sqrt{-Q^2}. \tag{205}$$

Furthermore, if

$$y_{\rm pth} = \frac{M_3}{M_1 - M_2 + M_3}, \tag{206}$$

we have again $\mathrm{Im}x_{L,R} = 0$ and $x_L = x_R = x_-^- = x_+^-$. However this solution corresponds to

$$x_{\pm}^{-} = \frac{M_2}{M_2 - M_1}, \tag{207}$$

which lies outside $[0,1]$. Actually the branch points pinch the real x axis in the interval $[0,1]$ for

$$y_{1,2} = \frac{M_3\,(M_3 - M_2 + M_1) - 2\left(M_1 M_2 \pm \sqrt{\Delta}\right)}{(M_3 - M_2 + M_1)^2}, \tag{208}$$

where $\Delta = -M_1 M_2\,(M_3 - M_2)\,(M_3 + M_1)$. With considerations completely similar to the ones we are going to illustrate in the case $S = M_3 - M_1 + M_2$, it is possible to show that the values of y in Eq.(208)

are not included in $[0,1]$. Finally, the equation $x_-^- = x_+^-$ admits also the solutions $S = M_3 - M_1 - M_2$ and $S = M_3 - M_1 + M_2$. If $S = M_3 - M_1 - M_2$, the two branching points of the logarithm coincide when

$$y_{th} = \frac{M_3}{M_3 - M_1 - M_2}, \tag{209}$$

or when

$$y_{th} = \frac{M_3\left(M_3 - M_1 - M_2\right) + 2\left(M_1 M_2 \pm \sqrt{\Delta}\right)}{\left(M_3 - M_1 - M_2\right)^2}, \quad \Delta = M_1 M_2 \left(M_3 - M_1\right)\left(M_3 - M_2\right). \tag{210}$$

Since by definition $S \geq 0$ and $S \leq M_3$, the solution of Eq.(209) is larger than 1 and so it is of no interest for our discussion. The two solutions of Eq.(210) give a pinch in

$$x_L = x_R = x_-^- = x_+^- = \frac{M_2}{M_2 - M_1}, \tag{211}$$

which lies outside $[0,1]$.

If $S = M_3 - M_1 + M_2$ the two branching points of the logarithm coincide when

$$y_{th} = \frac{M_3}{M_3 - M_1 + M_2}, \tag{212}$$

or when

$$y_{th} = \frac{M_3\left(M_3 - M_1 + M_2\right) - 2\left(M_1 M_2 \pm \sqrt{\Delta}\right)}{\left(M_3 - M_1 + M_2\right)^2}, \tag{213}$$

where $\Delta = -M_1 M_2 (M_3 - M_1)\left(M_3 + M_2\right)$. In this case the solution of Eq.(212) corresponds to a pinch outside the interval $[0,1]$ on the x axis. For what concerns the two solutions of Eq.(213) they are complex if $M_3 > M_1$, since in this case the quantity Δ is negative. Let us consider what happens if $M_1 - M_2 \leq M_3 \leq M_1$. We parametrize M_3 as $M_3 = M_1 - \alpha M_2$ where $\alpha \in [0,1]$. As a consequence, the solutions of Eq.(213) will read

$$y_{th} = \frac{-\alpha\left(1-\alpha\right) M_2^2 - \left(1+\alpha\right) M_1 M_2 \pm 2\sqrt{\delta}}{\left(\alpha - 1\right)^2 M_2^2}, \quad \delta = \alpha M_1 M_2^2 \left[M_1 + \left(1-\alpha\right) M_2\right], \tag{214}$$

so that we can see immediately that the solution with the minus sign in front of the square root in Eq.(214) is negative. It is also possible to check that also the other solution is always negative; in fact the condition

$$-\alpha\left(1-\alpha\right) M_2^2 - \left(1+\alpha\right) M_1 M_2 + 2\sqrt{\delta} \leq 0 \tag{215}$$

is satisfied when $\left(M_1 - \alpha M_2\right)^2 \geq 0$, which is certainly true.

Consider now the distortion for the points $x_\pm^+$. The condition for coincidence, i.e. $x_-^+ = x_+^+$, is

$$S = M_1 + M_2 - M_3, \qquad S = \sqrt{-Q^2}. \tag{216}$$

The remaining two conditions, namely $\operatorname{Im} x_{L,R} = 0$ and $x_L = x_R = x_-^+ = x_+^+$, require

$$y = -\frac{M_3}{M_1 + M_2 - M_3} \notin [0,1]. \tag{217}$$

The condition for the coincidence of the two $x_\pm^+$ solutions is satisfied also by the choices

$$S = M_1 - M_2 - M_3\,, \quad S = M_2 - M_1 - M_3\,, \text{and} \quad S = -(M_1 + M_2 + M_3). \tag{218}$$

Since the quantity S is defined positive, the last case in Eq.(218), requiring a negative S, does not need further discussion. If $S = M_1 - M_2 - M_3$, the two $x_\pm^+$ solutions to the equation $b_H = 0$ are pinched by the branch points of the logarithm, in the interval $[0, 1]$ on the x axis, when y assumes one of the two values

$$y_{1,2} = \frac{-M_3\,(M_1 - M_2 - M_3) - 2M_1M_2 \pm 2\sqrt{\delta}}{(M_3 - M_1 + M_2)^2}, \quad \delta = -\,(M_3 - M_1)\,(M_3 + M_2)\,M_1M_2. \tag{219}$$

Since $S \geq 0$, then $M_3 \leq M_1 - M_2$ and this automatically guarantees that the values of y in Eq.(219) are real; in particular y_2, corresponding to the choice of the minus sign in front of the square root in Eq.(219), is easily seen to be negative. The solution y_1 is negative (or vanishes) if

$$-\,M_3\,(M_1 - M_2 - M_3) - 2M_1M_2 + 2\sqrt{\delta} \leq 0. \tag{220}$$

The condition in Eq.(220) is satisfied if $M_3^2(M_1 - M_2 - M_3)^2 \geq 0$, which is certainly true. We can then conclude that, if $S = M_1 - M_2 - M_3$, none of the values of y for which we have a pinch of $x_\pm^+$ is included in the interval $[0, 1]$, and so it is not necessary to distort the integration contour on the complex y plane. Finally we can repeat exactly the same discussion and reach the same conclusions in the case in which $S = M_2 - M_1 - M_3$; the necessary equations can be obtained from the ones used in the $S = M_1 - M_2 - M_3$ case by exchanging M_1 and M_2.

The general analysis will be as follows. If $Q^2 \geq 0$ and $M_3^2 \geq 0$ or $Q^2 \leq 0$ and $M_3^2 \leq 0$ there are no real solutions for x to $b_H = 0$, therefore no distortion is needed. Otherwise we have

$$\begin{aligned} &Q^2 \leq 0,\, M_3^2 \geq 0 \quad \rightarrow \quad \rho_+ = +\,(S \pm M_3)^2, \qquad S = \sqrt{-Q^2}, \quad M_3 = \sqrt{M_3^2}, \\ &Q^2 \geq 0,\, M_3^2 \leq 0 \quad \rightarrow \quad \rho_- = -\,(S \pm M_3)^2, \qquad S = \sqrt{Q^2}, \quad M_3 = \sqrt{-M_3^2}. \end{aligned} \tag{221}$$

In order to have real roots for b_H we have to require

$$\rho_+^2 - 2\,(M_1^2 + M_2^2)\,\rho_+ + (M_1^2 - M_2^2)^2 \geq 0, \quad \text{or} \quad \rho_-^2 + 2\,(N_1^2 + N_2^2)\,\rho_- + (N_1^2 - N_2^2)^2 \geq 0, \tag{222}$$

where we have introduced $N_i^2 = -M_i^2$ since, as we are going to see in more detail later on, the condition $M_x^2 = \rho_-$ implies $\left(M_1 \pm M_2^2\right)^2 \leq 0$. In the first case we obtain

$$M_1^2\,M_2^2 \leq 0, \quad \text{or} \quad M_1^2\,M_2^2 \geq 0 \quad \text{and} \quad \left\{\rho_+ \leq (M_1 - M_2)^2 \quad \text{or} \quad \rho_+ \geq (M_1 + M_2)^2\right\}, \tag{223}$$

with $M_i = \sqrt{|M_i^2|}$. In the second case we obtain

$$N_1^2\,N_2^2 \leq 0, \quad \text{or} \quad N_1^2\,N_2^2 \geq 0 \quad \text{and} \quad \left\{\rho_- \leq -\,(N_1 - N_2)^2 \quad \text{or} \quad \rho_- \geq -\,(N_1 + N_2)^2\right\}, \tag{224}$$

with $N_i = \sqrt{|N_i^2|}$. For $Q^2 \leq 0$, $M_3^2 \geq 0$ we have already covered the case $M_1^2 M_2^2 \geq 0$, as long as all the results are understood with $M_{1,2}^2 \rightarrow |M_{1,2}^2|$. The last case to be considered is $Q^2 \geq 0$ and $M_3^2 \leq 0$. Let us introduce some additional notation; the quantities S and N_3 are defined by

$$S \equiv \sqrt{P^2} > 0 \quad \text{and} \quad N_3 \equiv \sqrt{-M_3^2} > 0, \tag{225}$$

and then the dangerous denominator in the BT algorithm will read

$$b_{_H} = -4S^2N_3^2 + \left(M_x^2 + N_3^2 + S^2\right)^2 . \tag{226}$$

The apparent singularities in the numerical integration are encountered when $b_{_H}$ vanishes, and that happens when

$$M_x^2 = \frac{xM_1^2 + (1-x)\,M_2^2}{x\,(1-x)} = -\left(N_3 \pm S\right)^2 , \tag{227}$$

which is exactly the condition already found in Eq.(221). If we now impose that the two values of x at which Eq.(227) is satisfied coincide, we find that this happens when

$$\left(N_3 \pm S\right)^2 = -\left(M_1^2 + M_2^2\right) \pm 2\sqrt{M_1^2 M_2^2}. \tag{228}$$

Assuming $M_1^2 M_2^2 \geq 0$, the above equation becomes

$$\left(N_3 \pm S\right)^2 = -\left(M_1 \pm M_2\right)^2 . \tag{229}$$

Clearly this condition can be satisfied only if the square on the r.h.s. is negative, and then if the effective masses M_1 and M_2 are purely imaginary. For the sake of clarity we introduce then the following quantities: $N_1 \equiv \sqrt{-M_1^2} > 0$ and $N_2 \equiv \sqrt{-M_2^2} > 0$, so that Eq.(229) can be rewritten as $\left(S \pm N_3\right)^2 = \left(N_1 \pm N_2\right)^2$. It is then easy to see that the two roots of $b_{_H}$ coincide when S assumes one of the following values

$$S_+^- = N_1 \pm N_2 + N_3 \quad \text{or} \quad S_-^- = -(N_1 \pm N_2) + N_3, \tag{230}$$

and when S is equal to

$$S_+^+ = N_1 \pm N_2 - N_3 \quad \text{or} \quad S_-^+ = -(N_1 \pm N_2) - N_3. \tag{231}$$

It is now possible to check where the solutions of Eq.(227) are located under the assumption that S is given by one of the Eqs. (230,231). These solutions are found to be located at

$$x = \frac{N_2}{N_1 \pm N_2}, \tag{232}$$

where just the value of x corresponding to the plus sign in the denominator of Eq.(232) stays in the interval $[0,1]$ on the x axis.

The branch points for the logarithm pinch the x axis exactly at the same point; in fact, with $U = ax^2 + bx + c$, we have that

$$a = -\left(yS^2 - N_3^2\right)(1-y)\,, \quad b = -y^2S^2 + y\left(S^2 - N_1^2 + N_2^2 + N^2\right) - N_3^2, \quad c = -y\;N_2^2, \tag{233}$$

and the discriminant of the quadratic equation $U = 0$ vanishes if

$$y_{1,2} = \frac{1}{2S^2}\left[S^2 + N_3^2 - (N_1 + N_2)^2 \pm \sqrt{\rho_1}\right], \quad y_{3,4} = \frac{1}{2S^2}\left[S^2 + N_3^2 - (N_1 - N_2)^2 \pm \sqrt{\rho_2}\right], \tag{234}$$

where we have introduced

$$\rho_1 = \left[(N_1 + N_2)^2 - S^2 - N_3^2\right]^2 - 4\;N_3^2\;S^2 \quad \rho_2 = \left[(N_1 - N_2)^2 + S^2 + N_3^2\right]^2 - 4\;N_3^2\;S^2\,. \tag{235}$$

Out of this four solutions, just the first two correspond to a pinch in the $[0,1]$ interval on the x axis and they pinch the axis exactly at the value in which the zeros of $b_{_H}$ coincide (Eq.(232)).

It is now necessary to check, for each one of the coincidence conditions listed in Eqs.(230)–(231), if the values of y corresponding to a dangerous pinch on the x axis are included in the interval $[0,1]$. Let us start by taking into account the solutions $S_{\pm}^{-}$.
a) If $S = N_3 - N_1 - N_2$ the quantities y_1 and y_2 defined in Eq.(234) become

$$y_1 = y_2 = \frac{N_3}{N_3 - N_1 - N_2}. \tag{236}$$

Since $S \geq 0$ and $N_3 \geq 0$ this solution is positive, but always larger than 1.
b) If $S = N_1 - N_2 + N_3$ the quantities y_1 and y_2 defined in Eq.(234) become

$$y_{1,2} = \frac{1}{(N_1 - N_2 + N_3)^2} \left[N_3 (N_1 - N_2 + N_3) - 2N_1 N_2 \pm 2\sqrt{\rho_1} \right], \tag{237}$$

and $\rho_1 = -(N_3 - N_2) N_1 N_2 (N_3 + N_1)$. Since $S \geq 0$ we have that $N \geq N_2 - N_1$. It is immediately seen that if $N_3 > N_2$ the values of y in (237) are complex, since the quantity ρ_1 is negative. Let us see what happens when $N_2 - N_1 \leq N_3 \leq N_2$. It is convenient to parametrize the quantity N_3 as $N_3 = N_2 - \alpha N_1$ where $\alpha \in [0,1]$, so that Eq.(237) can be rewritten as

$$y_{1,2} = \frac{-\alpha (1-\alpha) N_1^2 - (1+\alpha) N_1 N_2 \pm 2\sqrt{\delta}}{(1-\alpha)^2 N_1^2}, \qquad \delta = \alpha N_2 N_1^2 \left[N_2 + (1-\alpha) N_1 \right]. \tag{238}$$

The solution y_2, that shows a minus sign in front of the square root is automatically negative. In order to see what happens in the case of the solution y_1, it is necessary to see when the inequality

$$-\alpha (1-\alpha) N_1^2 - (1+\alpha) N_1 N_2 + 2\sqrt{\delta} \leq 0 \tag{239}$$

is satisfied. It is possible to check that Eq.(239) is true if $N_3^2 (N_3 + N_1 - N_2)^2 \geq 0$, which is certainly the case.
c) For the case $S = N_3 - N_1 + N_2$ we can apply exactly the same reasoning and reach the same conclusions that have been found for the case $S = N_3 - N_2 + N_1$, no distortion of the integration contour on the x complex plane is needed. The relevant formulas for this case can be simply obtained from the formulas of the previous paragraph by exchanging N_1 with N_2.
d) If $S = N_1 + N_2 + N_3$ the quantities y_1 and y_2 defined in Eq.(234) become

$$y_1 = y_2 = \frac{N_3}{N_1 + N_2 + N_3} \equiv y_{th}; \tag{240}$$

this solution falls into the interval $[0,1]$.
e) If $S = N_1 - N_2 - N_3$ the quantities y_1 and y_2 defined in Eq.(234) become

$$y_{1,2} = \frac{1}{(N_1 - N_2 - N_3)^2} \left[-N_3 (N_1 - N_2 - N_3) - 2N_1 N_2 \pm 2\sqrt{\rho_1} \right], \tag{241}$$

and $\rho_1 = -(N_3 - N_1) N_1 N_2 (N_3 + N_2)$. The solution y_2, corresponding to the minus sign in front of the square root in Eq.(241), is negative, and does not therefore pose any problem.

The solution y_1 requires a more careful analysis; since $S \geq 0$ we have that $N_3 \leq N_1 - N_2$. The expression under square root is then positive and the solution y_1 is real. It is then necessary to find out under which conditions the numerator of the r.h.s. of Eq.(241) is negative. It is possible to verify that the condition

$$-N_3 (N_1 - N_2 - N_3) - 2N_1 N_2 + 2\sqrt{\rho_1} \leq 0 \tag{242}$$

implies $N_3^2\,(N_3+N_2-N_1)^2 \geq 0$, which is always satisfied; we do not have then to distort the integration path to avoid the solution y_1 .
f) $S=-(N_1+N_2+N_3)$ would require a negative S, which cannot occur as S is positive by definition.
g) If $S=N_2-N_1-N_3$ we can apply the same considerations written for the case $S=N_1-N_2-N_3$ exchanging everywhere N_1 with N_2.

10.4 Evaluation of V^{222}

Given the intrinsic difficulty in distorting the integration contour, in this section we introduce our alternative algorithm to evaluate V^{222}. With the help of parametrization II, introduced in Section 10.2, we can write

$$V^{222} = -\int dC_5(x,y,\{z\})\, c_q(x,y)\, Q_H^{-2}, \quad Q_H = c_q(x,y)\,\mathcal{Q}^2(\{z\}) + \sum_{i=1}^{3} c_i(x,y)\, M_i^2(\{z\}), \tag{243}$$

where the x, y dependent coefficients are

$$c_q = x\,y\,(1-x)\,(1-y), \quad c_1 = x\,y, \quad c_2 = y\,(1-x), \quad c_3 = x\,(1-x)\,(1-y), \tag{244}$$

and the $\{z\}$ dependent ones are

$$\mathcal{Q}^2 = \chi_C(z_1,z_2,z_3), \tag{245}$$

$$M_1^2 = \chi_B(p_2^2,m_1^2,m_2^2\,;\,z_1), \quad M_2^2 = \chi_B(P^2,m_4^2,m_3^2\,;\,z_2), \quad M_3^2 = \chi_B(p_1^2,m_5^2,m_6^2\,;\,z_3). \tag{246}$$

Here we have defined

$$\begin{aligned} \chi_B(p^2,m_i^2,m_j^2\,;\,z) &= -p^2\,z^2 + (p^2+m_j^2-m_i^2)\,z + m_i^2, \quad \chi_C(\{z\}) = z^t\,H\,z + 2\,K^t\,z + L, \\ H_{ij} &= k_i\cdot k_j \qquad k_1 = p_2,\, k_2 = P,\, k_3 = -p_1, \quad K_i = -2\,p_2\cdot k_i, \qquad L = p_2^2. \end{aligned} \tag{247}$$

Furthermore, we introduce

$$\mathcal{Q}^2 = \mathcal{Q}_0^2 + S, \quad \mathcal{Q}_0^2 = z^t\,H\,z + 2\,K^t\,z. \tag{248}$$

It follows that the original integral can we written as

$$\begin{aligned} V^{222} &= \frac{\partial^2}{\partial\, S^2}\int dC_5(x,y,\{z\})\, c_q^{-1}(x,y)\,\ln\, Q_H^S\mid_{S=p_2^2}, \\ Q_H^S &= c_q(x,y)\left[\mathcal{Q}_0^2(\{z\}) + S\right] + \sum_{i=1}^{3} c_i(x,y)\, M_i^2(\{z\}). \end{aligned} \tag{249}$$

Therefore, for V^{222}, our algorithm is based on numerical differentiation despite the poor reputation enjoyed by this branch of numerical analysis, at least on the real axis. For previous applications of numerical differentiation in this field we refer to [6]. In general, the second derivative of a generic function $f(x)$ can be written in terms of a so-called $(2\,N+1)$-point formula [34]

$$f^{(2)}(x) = \frac{1}{h^2}\sum_{n=-N}^{+N} c_n^N\, f(x+n\,h) + R_N(x), \qquad c_{-n}^N = c_n^N, \quad \sum_n c_n = 0. \tag{250}$$

A typical example is given by $N = 2$ where $c_0 = -30$ and $c_1 = 16, c_2 = -1$. For this case

$$R_2(x) = \frac{1}{180}\, h^6\, f^{(6)}(x) + \mathcal{O}\left(h^8\right). \tag{251}$$

The crucial point in obtaining a decent estimate of our derivative is the choice of the base interval h which is also connected with the estimate of the corresponding error on $f^{(2)}$. There are two sources of error, one related to discretization which prevents h from being large and one connected with rounding-off in evaluating f which prevents h from being too small. In our case, if $\delta_N\, f$ represents the round-off error on the $2\,N+1$ approximation to $f^{(2)}$ we select the optimal value for h as the one which minimizes $\delta_N\, f/h^2 + R_N$ and combine errors from round-off and discretization (e.g. from Eq.(251), which requires some estimate of $f^{(6)}$) in quadrature. Once a value for N is selected we obtain an approximation for V^{222} which reads as follows:

$$V^{222} \approx V^{222}_{2\,|\,N} = \frac{1}{h^2} \sum_{n=1}^{N} c_n \int dC_5(x,y,\{z\})\, c_q^{-1} \ln\left\{1 - n^2 h^2\, \frac{c_q^2}{[c_q\,(\mathcal{Q}_0^2 + p_2^2) + \mathcal{Q}_R^2]^2}\right\},$$
$$\mathcal{Q}_R^2 = \sum_{i=1}^{3} c_i(x,y)\, M_i^2(\{z\}). \tag{252}$$

As a final technical detail, we note that we always start by performing a sector decomposition to deal with common zeros of c_q and $\mathcal{Q}_R^2$ which lie at the vertices of the x, y integration square.

A potential problem of the approach based on a second derivative is that we have to deal with a function possessing integrable singularities but in a five-fold domain. As a consequence it is difficult to keep the integration (round-off) error very small and h cannot be chosen too small with an obvious effect on discretization error. Therefore we have also considered an additional approach based on third derivatives. Since

$$c_q(x,y)\, Q_H^{-2} = -\frac{1}{c_q^2}\, \frac{\partial^3}{\partial S^3} \left[c_q\, \mathcal{Q}^2 + \mathcal{Q}_R^2\right] \ln\left[c_q\, \mathcal{Q}^2 + \mathcal{Q}_R^2\right] |_{S=p_2^2}, \tag{253}$$

we may use a five-point approximation (or higher) [34] for the third derivative and obtain after straightforward algebra

$$V^{222} \approx V^{222}_{3\,|\,5} = \frac{1}{2\,h^3} \int dC_5(x,y,\{z\})\, c_q^{-1}(x,y)$$
$$\times \left\{\frac{1}{z} \ln \frac{1 - h^2 z^2/(1+hz)^2}{1 - h^2 z^2/(1-hz)^2} + 2\,h \ln \frac{1 - 4h^2 z^2}{1 - h^2 z^2}\right\} + \mathcal{O}\left(h^2\right), \tag{254}$$

where the variable z is defined by

$$z = \frac{c_q}{c_q\,(\mathcal{Q}_0^2 + p_2^2) + \mathcal{Q}_R^2}. \tag{255}$$

An higher number of points will give similar results. The advantage of Eq.(254) is that, modulo round-off errors, h can be taken to be arbitrarily small. The overall advantage of taking a third derivative is that the integrand in Eq.(254) has the form of function $\times$ ln (function), something similar to the original BT philosophy, i.e. we can write

$$V^{222} \approx \frac{1}{2\,h^2} \int dC_5(x,y,\{z\})\, c_q^{-1}(x,y) \left[4 \ln 2 + 2 \left(\frac{1}{\zeta} - 1\right) \ln(1-\zeta)\right.$$
$$\left. + \left(\frac{1}{\zeta} + 2\right) \ln\left(\zeta + \frac{1}{2}\right) - \left(\frac{1}{\zeta} - 2\right) \ln\left(\frac{1}{2} - \zeta\right) - 2 \left(\frac{1}{\zeta} + 1\right) \ln(1+\zeta)\right], \tag{256}$$

where $\zeta = h\,z$. The new kernel and its first derivative are both integrable. The discretization error will be proportional to the fifth (or higher) derivative; using a seven-point formula with coefficients $\{-1/2, 2, -5/2, 0, 5/2, -2, 1/2\}$ we obtain the following result

$$V^{222}_{3\,|\,5} = -\frac{1}{8\,h^2}\int dC_5(x,y,\{z\})\,c_q^{-1}(x,y)\left(\frac{1}{\zeta}\,L_1 + L_2\right), \tag{257}$$

where $L_i = \ln(1+X_i)$ and

$$\begin{aligned} X_1 &= 48\,\zeta^5\,(1+\delta X_1), \qquad X_2 = -60\,\zeta^4\,(1+\delta X_2),\\ \delta X_1 &= 20\,\zeta^2 + \frac{245}{3}\,\zeta^4 + \mathcal{O}\left(\zeta^5\right), \qquad \delta X_2 = \frac{28}{3}\,\zeta^2 + \frac{87}{2}\,\zeta^4 + \mathcal{O}\left(\zeta^6\right), \end{aligned} \tag{258}$$

for $\zeta \to 0$, or

$$\begin{aligned} \frac{1}{\zeta}\,L_1 + L_2 &= \left(3 - \frac{1}{\zeta}\right)\ln(1-3\,\zeta) + \left(3 + \frac{1}{\zeta}\right)\ln(1+3\,\zeta) + 4\left(\frac{1}{\zeta} - 2\right)\ln(1-2\,\zeta)\\ &- 4\left(\frac{1}{\zeta} + 2\right)\ln(1+2\,\zeta)5\left(1 - \frac{1}{\zeta}\right)\ln(1-\zeta) + 5\left(1 + \frac{1}{\zeta}\right)\ln(1+\zeta). \end{aligned} \tag{259}$$

Eq.(258) gives the estimate of the error for small ζ (showing finiteness in the limit $\zeta \to 0$) while Eq.(259) is more appropriate when ζ is finite and the argument of some logarithm crosses zero. Analogous formulae where the third derivative expression for V^{222} is given in terms of a 7-point (or higher) approximation with a discretization error proportional to the 7 th (or higher) derivative have been used and will not be reported here.

Note that sector decomposition is always applied to, say, Eq.(252) to factorize the common zeros of c_q^2 and of $[c_q\,(\mathcal{Q}_0^2 + p_2^2) + \mathcal{Q}_R^2]^2$. There are two levels of factorization, a simpler one where we only consider the x, y pair, and a more complete one where all variables are taken into account. Details of the procedure are given in Appendix D.

The same technique can be applied to other diagrams, for instance

$$V^{221} = -\int dC_4(x,y,\{z\})\,c_m(x,y)\,Q_G^{-1}, \tag{260}$$

$$Q_G = c_q(x,y)\,\mathcal{Q}^2(\{z\}) + \sum_{i=1}^{3} c_i(x,y)\,M_i^2(\{z\}) - c_m(x,y)\,M_1^2(\{z\}), \tag{261}$$

where the coefficients are now

$$\begin{aligned} &c_q = x\,(1-x)\,y\,(1-y), \quad c_m = (1-x)\,y, \quad c_1 = 1-x, \quad c_2 = x\,(1-x)\,y, \quad c_3 = x\,(1-y),\\ &M_1^2 = \chi_B(p_1^2, m_1^2, m_2^2\,;\,z_1), \quad M_2^2 = \chi_B(p_2^2, m_4^2, m_5^2\,;\,z_2), \quad M_3^2 = m_3^2, \end{aligned} \tag{262}$$

$$\mathcal{Q}^2(\{z\}) = (z_1\,p_1 - z_2\,p_2)^2 - 2\,p_1^2\,z_1 + 2\,p_1\cdot p_2\,z_2 + p_1^2. \tag{263}$$

If we introduce $M_1^2 = M_{10}^2 + S$ with $M_{10}^2 = -p_1^2 z_1^2 + (p_1^2 + m_2^2 - m_1^2) z_1$ we obtain

$$\begin{aligned} V^{221} &= \frac{\partial}{\partial S}\int dC_4(x,y,\{z\})\,\ln Q_G^S\,|_{S=m_1^2},\\ Q_G^S &= c_q(x,y)\,\mathcal{Q}^2(\{z\}) + \sum_{i=1}^{3} c_i(x,y)\,M_i^2(\{z\}) - c_m(x,y)\left[M_{10}^2(\{z\}) + S\right]. \end{aligned} \tag{264}$$

For the first derivative we will typically use a five-point rule with discretization error proportional to the fifth derivative. In Tab. 3 we have shown coefficients for numerical differentiation that are not usually found in the literature.

$n\,/\,N$	c_0	c_1	c_2	c_3	c_4	R
$2\,/\,3$	-2	1				$-\frac{7\,h^4}{120}\,f^{(7)}$
$3\,/\,7$	0	$-13/8$	1	$-1/8$		$\frac{h^2}{4}\,f^{(8)}$
$4\,/\,5$	6	-4	1			$\frac{h^2}{6}\,f^{(6)}$
$5\,/\,7$	0	$5/2$	-2	$1/2$		$\frac{h^2}{3}\,f^{(7)}$
$6\,/\,7$	-20	15	-6	1		$\frac{h^2}{4}\,f^{(8)}$
$7\,/\,9$	0	-7	7	-3	$1/2$	$\frac{5\,h^2}{12}\,f^{(9)}$

Table 3: Coefficients c_i and leading term R in the discretization error for $2\,N+1$ - point numerical differentiation of a function of one real variable, e.g. Eq.(250). The remaining coefficients for $f^{(n)}$ are $c_{-i}=-\,c_i$ for n odd and $c_{-i}=c_i$ for n even.

11 Numerical results

In this section we present numerical results for the two-loop three-point scalar functions. All the vertices are evaluated using the Korobov-Conroy [35] number theoretic method with a Monte-Carlo error estimate as supplied by the subroutine D01GDF [36], a multi-dimensional quadrature, general product region.

The estimated error and the time taken will be approximately proportional to the number of points in the chosen Korobov set times the number of random samples to be generated.

There is no ideal format for presenting numerical results of functions of so many variables and we have decided to introduce random tables, i.e. for each entry internal masses, external invariants and their signs are generated randomly and then the diagram is computed. Alternatively we have considered few physically relevant cases, extracted from processes like $Z^* \to \overline{f}f, H^* \to \overline{f}f, gg$ etc. Here the input parameter set to be used will be

$$M_{_W} = 80.380\,\mathrm{GeV}, \quad M_{_Z} = 91.1875\,\mathrm{GeV}, \quad m_b = 4\,\mathrm{GeV}, \quad m_t = 174.3\,\mathrm{GeV}, \quad M_{_H} = 150\,\mathrm{GeV}. \quad (265)$$

Kinematic configurations are further defined by the Mandelstam invariants of Eq.(8).

For most of the topologies we have two methods at our disposal and we perform a comparison; however, two results will not be shown when they agree in several digits. Results are shown in Tabs. 5–9 and, whenever needed, we fix the ultraviolet pole at $\epsilon = 1$; the unit of mass is set to 1 GeV.

Clearly, for some topology one method is better than the other and the latter is only used for internal cross-check. With so many parameters, ranging over a wide interval of values, it is hard to make an overall statement on the goodness of the results which depends on many circumstances as vicinity of a n-particle cut [37] or of a region where the diagram changes its sign and it is vanishingly small. Note that leading Landau singularities (e.g. the anomalous threshold for the one-loop vertex) do not pose a serious obstacle to numerical integration since they are rarely inside the physical region [38]; n-particle cuts may slow down the numerical evaluation whenever the algorithm used requires only absolute convergence.

As a general and self-evident rule we observe that whenever the imaginary part of a diagram is zero then all algorithms have a practically unlimited precision. To give a quantitative description we consider the diagram of Fig. 6 and evaluate it for different values of the $\overline{b}b$ invariant mass. Results and numerical

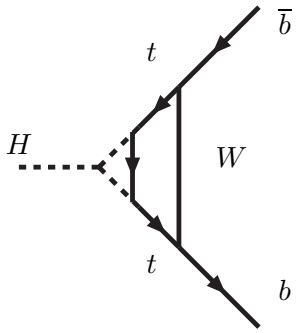

Figure 6: A two-loop vertex diagrams of the V^{231} topology for $H^* \to \overline{b}b$.

errors are given in Tab. 4 where the first row gives an invariant mass below any cut; the second row above the HH-cut; the third one above the $\overline{t}t$-cut and the last one above the $H\overline{t}t$-cut. The relative numerical error is practically zero when below any cut and 0.40% , 1.06% , 0.43% for the real part and 0.25% , 0.34% , 0.78% for the imaginary part above the cuts. Relative accuracy for the real part tends to deteriorate in the region where it changes its sign while it is increasing for the imaginary part which is becoming smaller and smaller.

For the V^{222} topology we have been able to compare our results with those of [39] where the configuration with $p_1^2 = p_2^2 = 0$ and $m_i = 150\,\mathrm{GeV}$ has been considered and where the numerical evaluation has been performed using conformal mapping and Padé approximants. The comparison is shown in Tab. 10 where the errors of [39] have been estimated by comparison of the [8/8] and [9/9] Padé approximants. Our estimate of the numerical error is done by adding in quadrature discretization and round-off errors.

12 Conclusions

Evaluating scalar diagrams at the multi-loop level is only the beginning of a complex scenario where we still have to face many (hard) technical problems before being ready to step forward. Our aim, in this paper, has been to set up a collection of algebraic-numerical algorithms to deal with arbitrary massive two-loop scalar vertices, therefore adding one more stone to the construction started in [1]. The main result, therefore, has been to assemble relatively simple expressions for scalar two-loop vertices in a systematic and coherent manner so that they can be used for practical calculations.

As explained in the Introduction, we are going to devote a forthcoming paper to the analysis of tensor integrals, i.e. of diagrams with a non-trivial spin structure. Although the main emphasis of this paper has been on proving the feasibility of a project for computing fully massive diagrams, one should not forget that QED/QCD components are integral parts of the evaluation of any realistic observable. Therefore, infrared and also collinear configurations should be treatable within the same class of algorithms, or within some extension of them. The corresponding proof is rather lengthy and, also for this reason, we decided to have a self-consistent presentation in another paper of this series.

There are six non-trivial topologies for two-loop vertices, as depicted in Fig. 7, three of them belonging to a special class – one-loop self-energy insertion – for which we have given a completely general solution in terms of the so-called BT algorithm [21]. The remaining three are, somehow, more difficult to deal with.

Here we should mention that the BT-algorithm is a general approach in the evaluation of multi-loop, multi-leg Feynman diagrams, but the general solution for the BT polynomial $\mathcal{P}$ of Eq.(266) is not known; even more important, we have fixed a guideline in our project which is based on two principles: an

algorithm for numerical evaluation of Feynman diagrams is optimal when there is a minimal number of terms in the solution, and the singularities of the diagram are not badly overestimated.

The first principle is adopted in order to avoid, as much a possible, the problem of cancellations among the (usually many) terms in the final answer. Trading one difficult original integral in favor of many easier ones with better numerical convergence most often will show a clash with the inherent existence of severe numerical cancellations. The second principle is dictated by the need of obtaining meaningful results even across thresholds, pseudo-thresholds and anomalous thresholds, and not only in asymptotic regions, s small or very large.

Therefore, for some of the diagrams, we have abandoned the BT-algorithm in favor of alternative smoothness algorithms which are defined, in general, in Eq.(2). At the same time we mention that the BT formalism becomes much less efficient under the same circumstances when other approaches, noticeably integration-by-parts formalism [40], reach the limit of manageability under the present technology in algebraic manipulation techniques [41]: it is somehow hard to accept that part of our present limitation is related to a poor level of technical handling of large systems of linear equations, however, this really represents the bottleneck of many famous approaches. In this respect difference equations could still introduce some novelty[3].

Understanding these motivations will hopefully explain our preference for algorithms anchored to specific classes of diagrams instead of pursuing the search for some universal treatment (the Holy Grail). Therefore, in our study we introduced new algorithms of smoothness and we heavily employed the procedure of extended sector decomposition in order to cure possible numerical instabilities generated by subtracted integrands, proving the relevance of the method beyond the usual treatment introduced for handling dimensionally regularized end-point singularities, of infrared or collinear nature.

Our formulation provides a systematic and economical way of evaluating a large number of complicated Feynman integrals. To a large extent our approach for solving a multi-scale problem is orthogonal to integration-by-parts techniques as applied in recent calculations. The reason is that the latter approach is naturally tailored and practically unbeatable for a massless calculation, e.g. for pure QCD/QED, or in general for a problem with very few scales, and solutions of recurrence relations for the general setup at the two-loop level are poorly known.

Another requirement that we impose in choosing a computational strategy for any given diagram is that it should work in any region, independently of the signs of the Mandelstam invariants and even in the unphysical region, e.g. below the production thresholds. Admittedly, this is a rather severe constraint; for instance there are algorithms, that we have not presented in this paper, which will describe with high accuracy the non-planar V^{222} diagram below the two-particle cut but which fail above it. The one that we have presented, although suffering from the drawbacks of numerical differentiation, is rather robust in all regions.

There are many papers in the literature dealing with two-loop vertices in one approximation or the other, but almost none presents tables of numerical results and, therefore, we had little material for comparison. For this reason we have privileged as much as possible some procedure for internal cross-check.

The complexity of the calculation increases with the number of propagators in a diagram and this is also reflected by the time needed for evaluating a six-propagator graph with respect to a four-propagator one. However, the CPU time requested by one scalar configuration should not be taken as the unit for realistic evaluation of physical observables since in the final procedure entire blocks of diagrams will be mapped into a single integral.

As a consequence, we plan to organize any realistic calculation according to building blocks that are,

[3] S. Laporta, private communication and [42].

by construction, gauge-parameter independent and will be computed within our approach. For this we need to control the gauge-parameter dependence of individual Green's functions; the tool to be employed for this purpose is represented by the use of Nielsen's identities [43].

Acknowledgments

We gratefully acknowledge discussions and comparisons with Andrei Davydychev, Misha Kalmykov, Volodya Smirnov and Oleg Tarasov. We would like to express our gratitude to Ettore Remiddi for important discussions on the evaluation of multi-loop Feynman diagrams numerically. The contribution of Stefano Actis to the general project of algebraic-numerical evaluation of Feynman diagrams and to several discussions concerning this paper is gratefully acknowledged. The work of A. F. was supported by the DFG-Forschergruppe "*Quantenfeldtheorie, Computeralgebra und Monte-Carlo-Simulation*".

A Bernstein-Tkachov functional relations

The Bernstein-Tkachov theorem [21] tells us that for any finite set of polynomials $V_i(x)$, where $x = (x_1, \ldots, x_N)$ is a vector of Feynman parameters, there exists an identity of the following form:

$$\mathcal{P}\ (x, \partial) \prod_i V_i^{\mu_i+1}(x) = B \prod_i V_i^{\mu_i}(x). \tag{266}$$

where $\mathcal{P}$ is a polynomial of x and $\partial_i = \partial/\partial x_i$; B and all coefficients of $\mathcal{P}$ are polynomials of μ_i and of the coefficients of $V_i(x)$.

For a generic quadric we have an explicit solution for the polynomial $\mathcal{P}$ which is due to F. V. Tkachov [21] (see also ref. [44] and ref. [45]):

$$G = \int_S dx\, V^\mu(x), \tag{267}$$

where the integration region is $x_i \geq 0$, $\sum_i x_i \leq 1$ and where $V(x)$ is a quadratic form of x,

$$V(x) = x^t\, H\, x + 2\, K^t\, x + L. \tag{268}$$

The solution to the problem of determining the polynomial $\mathcal{P}$ is as follows:

$$\mathcal{P} = 1 - \frac{(x + X)^t\ \partial_x}{2\ (\mu + 1)}, \qquad X^t = K^t\, H^{-1}, \qquad B = L - K^t\, H^{-1}\, K. \tag{269}$$

B is the so-called BT factor and the vector X is usually referred to as the BT co-factor.

B Complex masses

In our approach, designed for numerical evaluation of Feynman diagrams, complex masses do not pose a problem but some care has to be taken, because a complex pole does not lie on the usual physical (first) Riemann sheet. Its location is determined by the fact that it should smoothly approach the value for a stable particle when the coupling of the theory tends to zero. The complex pole is rewritten in terms of real quantities $\overline{m}_V$ and $\overline{\Gamma}_V$ as $p_V = \overline{m}_V^2 - i\overline{\Gamma}_V \overline{m}_V$. Consider for simplicity a scalar one-loop two-point function that we compute as

$$B_0(s) = \frac{2}{\epsilon} - \gamma - \ln\pi - \ln\frac{s}{\mu^2} - \int_0^1 dx\ \ln\chi(x), \quad \chi(x) = s\, x^2 + (p_{V_2} - p_{V_1} - s)\, x + p_{V_1}. \tag{270}$$

For real masses the correct procedure amounts to replace χ with $\chi - i\,\delta$, where $\delta \to 0_+$. In our case, if $\overline{\Gamma}_{V1}\overline{m}_{V1} \geq \overline{\Gamma}_{V2}\overline{m}_{V2}$ then $\mathrm{Im}\chi \geq 0$ for $0 \leq x \leq 1$. Taking into account the correct location of the complex poles implies the replacement of $\ln\chi$ with $\ln\chi - 2\,i\pi\,\theta(-\mathrm{Re}\chi)$.

C A useful integral

In this Appendix we consider a type of integral that occurs frequently in this paper and that can be evaluated by means of hypergeometric functions. Let us define

$$I = \int_0^Y dy\, y^{\epsilon/2-1}\, (a\, y + b - i\,\delta)^{-1-\epsilon}. \tag{271}$$

This integral is divergent in the limit $\epsilon \to 0$ and some care is needed in its evaluation. As a first step we write

$$I = 2\,\frac{Y^{\epsilon/2}}{\epsilon}\,b^{-1-\epsilon}\,{}_2F_1(1+\epsilon\,,\,\frac{\epsilon}{2}\,;\,1+\frac{\epsilon}{2}\,;\,-\frac{a}{b}\,Y). \tag{272}$$

It is more convenient to express this result in a different form, by using well-known properties of hypergeometric functions [31]:

$$\begin{aligned} {}_2F_1(1+\epsilon\,,\,\frac{\epsilon}{2}\,;\,1+\frac{\epsilon}{2}\,;\,-\frac{a}{b}\,Y) &= \frac{\Gamma^2\,(1+\epsilon/2)}{\Gamma\,(1+\epsilon)}\,\Big(\frac{a\,Y}{b}\Big)^{-\epsilon/2} \\ -\,\frac{\epsilon}{\epsilon+2}\,\Big(\frac{a\,Y}{b}\Big)^{-1-\epsilon}\,{}_2F_1(1+\epsilon\,,\,1+\frac{\epsilon}{2}\,;\,2+\frac{\epsilon}{2}\,;\,-\frac{b}{a\,Y}). \end{aligned} \tag{273}$$

The remaining hypergeometric function is only needed at $\mathcal{O}\,(1)$ and after collecting all terms we obtain the following expansion for the integral:

$$I = \frac{2}{\epsilon}\,a^{-\epsilon/2}\,b^{-1-\epsilon/2} - \frac{1}{b}\,\ln(1+\frac{b}{a\,Y}) + \mathcal{O}\,(\epsilon)\,. \tag{274}$$

In this way we have isolated the pole at $\epsilon = 0$.

D Integrable singularities and sector decomposition

One of the main problems in numerical multidimensional integration is to handle integrable singularities lying in arbitrary regions of the integration volume. Our experience in dealing with multi-scale Feynman integrands is such that extensions of standard techniques [46] are to be preferred to procedures that automatically adapt themselves to the rate of variation of the integrand at each point.

To give an example suppose that we have to evaluate

$$I = \int_0^1 dx \int_0^1 dy\,\frac{1}{x}\,\ln\Big[1+\frac{x}{a\,x+y}\Big], \qquad a>0. \tag{275}$$

The integral is well defined as it can be seen after performing the x-integration,

$$I = \int_0^1 dy\,\Big[\mathrm{Li}_2\,\Big(-\frac{a}{y}\Big) - \mathrm{Li}_2\,\Big(-\frac{a+1}{y}\Big)\Big], \tag{276}$$

however what we want is a numerical integration. A source of numerical instabilities is connected to the region where $x \approx y \approx 0$, since both numerator and denominator are vanishing small in the argument of the logarithm. A nice solution is to adopt a sector decomposition to factorize their common zero. We obtain

$$I = \int_0^1 dx \int_0^1 dy\,\Big[\ln\Big(1+\frac{1}{a+y}\Big) + \frac{1}{x}\,\ln\Big(1+\frac{x}{a\,x+1}\Big)\Big]. \tag{277}$$

A simple numerical exercise shows that one can gain several orders of magnitude improvement in the returned error by using Eq.(277) instead of Eq.(275). This simple example can be easily generalized to more complex situations with many variables, although in this case the number of sectors may increase considerably. For special values of external parameters a singularity may develop, for instance

$$\begin{aligned} J(a) &= \int_0^1 dx \int_0^1 dy\,\frac{1}{x}\,\ln\Big[1+\frac{x}{x+a\,y}\Big] \\ &= \int_0^1 dx \int_0^1 dy\,\Big[\ln\Big(1+\frac{1}{1+a\,y}\Big) + \frac{1}{x}\,\ln\Big(1+\frac{x}{x+a}\Big)\Big], \end{aligned} \tag{278}$$

which, after the sector decomposition shows that $a = 0$ is a singularity of J. We are going to illustrate the same technique in a more realistic example: suppose that one wants to compute

$$H = \int_0^1 dx \int_0^1 dy \, \frac{1}{x} \, \ln\Big[1 + \frac{x}{a\,x + \chi(y)}\Big], \quad \chi(y) = h\,(y - y_-)\,(y - y_+) - i\,\delta, \tag{279}$$

$\delta \to 0_+$. Suppose also that $0 < y_- < y_+ < 1$. First we split the y integral into three intervals, $[0, y_-], [y_-, y_+]$ and $[y_+, 1]$, then we change variables according to $y = y_-\,y'$, $y = (y_+ - y_-)\,y' + y_-$, and $y = (1 - y_+)\,y' + y_+$, respectively. In this way all the zeros of numerator/denominator are located at the corners of $[0, 1]^2$ and we can apply a sector decomposition to obtain 7 sectors giving the following result:

$$H = \int_0^1 dx \int_0^1 dy \, \Big[\mathcal{H}_1 + \frac{1}{x}\,\mathcal{H}_2\Big], \tag{280}$$

$$\begin{aligned}
\mathcal{H}_1 &= y_- \, \ln\Big[1 + \frac{1}{a - h\,y_+\,y_-\,(y_-\,(1 - xy) - y_+)}\Big] + \Delta y \, \ln\Big[1 + \frac{1}{a - h\,(\Delta y)^2\,(1 - xy)y}\Big] \\
&\quad + \Delta y \, \ln\Big[1 + \frac{1}{a - h\,(\Delta y)^2\,y}\Big] + (1 - y_+) \, \ln\Big[1 + \frac{1}{a + h\,(1 - y_+)^2\,x\,y^2 + h\,\Delta y\,(1 - y_+)y}\Big], \\
\mathcal{H}_2 &= y_-(1 - y) \, \ln\Big[1 + \frac{x}{a\,x - h\,y_-\,(y_-\,y - y_+]}\Big] + \Delta y \, \ln\Big[1 + \frac{x}{a\,x - h\,(\Delta y)^2}\Big] \\
&\quad + (1 - y_+) \, \ln\Big[1 + \frac{x}{a\,x + h\,(1 - y_+)\,((1 - y_+)\,y + \Delta y)}\Big],
\end{aligned} \tag{281}$$

with $\Delta y = y_+ - y_- > 0$. Once again we have been able to gain a much better numerical stability of the integrand. Note that the simple examples given in this Appendix are the prototype on which the realistic cases of evaluation via numerical differentiation (Section 10.4) or via integral representations with C_0 kernel (Appendix E) are patterned.

E The $C_0(\lambda)$-function

In this Appendix we consider a special family of integrals that often appears in our calculations and that can be easily connected to a one-loop C-function. Define

$$C_{0\,;11\,;12}(\lambda\,;\,a\ldots f) = \int dS_2\,\{1\,;\,x\,;y\}V^{-1-\lambda\,\epsilon}(x, y), \tag{282}$$

$$V(x, y) = ax^2 + by^2 + cxy + dx + ey + f - i\,\delta. \tag{283}$$

The connection with a scalar one-loop vertex is through the following identification:

$$\begin{aligned}
&a = -P_2^2, \quad b = -P_1^2, \quad c = -2\,P_1 \cdot P_2, \\
&d = M_2^2 - M_3^2 + P_2^2, \quad e = M_1^2 - M_2^2 + P_1^2 + 2\,P_1 \cdot P_2, \quad f = M_3^2.
\end{aligned} \tag{284}$$

For these functions we can use the full set of results of Sect. 4 of [3] or consider new integral representations. The new derivation is essentially similar to the one we have for the scalar one-loop vertex [47] but for keeping $\epsilon \neq 0$. Define α to be a solution of $b\,\alpha^2 + c\,\alpha + a = 0$, and introduce

$$A(y) = (c + 2\,\alpha b)\,y + d + e\,\alpha, \quad B(y) = b\,y^2 + e\,y + f. \tag{285}$$

The total result reads as follows:

$$C_n = C_{n0} - \frac{1}{2}\,\lambda\,\epsilon\,C_{n1} + \mathcal{O}\left(\epsilon^2\right), \qquad n = 0, 11, 12. \tag{286}$$

First we transform the variable y according to $y \to y + \alpha\,x$, so that $V(x,y) = A(y)\,x + B(y)$, split the integral,

$$\int_0^1 dx \int_0^x dy \longrightarrow \int_0^1 dx \int_{-\alpha x}^{\overline{\alpha} x} dy = \int_0^{\overline{\alpha}} dy \int_{y/\overline{\alpha}}^1 dx - \int_0^{-\alpha} dy \int_{-y/\alpha}^1 dx, \tag{287}$$

with $\overline{\alpha} = 1 - \alpha$ and transform again the variables: $y = \overline{\alpha}\,y'$ or $y = -\,\alpha\,y'$. Next we use

$$-\,\frac{1}{\lambda\,A\epsilon}\,\partial_x\,(A\,x + B)^{-\lambda\epsilon} = (A\,x + B)^{-1-\lambda\epsilon}, \tag{288}$$

and integrate by parts. New functions are introduced

$$A_1(y) = A(\overline{\alpha}\,y), \qquad A_2(y) = A(-\alpha\,y), \qquad B_1(y) = B(\overline{\alpha}\,y), \qquad B_2(y) = B(-\alpha\,y), \tag{289}$$

and also

$$Q_{1,2}(y) = A_{1,2}(y) + B_{1,2}(y), \quad Q_{3,4}(y) = A_{1,2}(y)\,y + B_{1,2}(y), \quad Q_{5,6}(x,y) = A_{1,2}(y)\,x + B_{1,2}(y). \tag{290}$$

The result is

$$C_{0,n} = \int_0^1 dy\,\mathcal{C}_{0,n}(y), \tag{291}$$

$$C_{11,n} = \int_0^1 dy\,\mathcal{C}^1_{11,n}(y) + \int_0^1 dy \int_y^1 dx\,\mathcal{C}^2_{11,n}(x,y), \qquad C_{12,n} = \alpha\,C_{11,n} + \int_0^1 dy\,\mathcal{C}_{12,n}(y), \tag{292}$$

Subtracted logarithms will be denoted by

$$\ln^n\,\mathcal{Q}_{1,2}(y) = \ln^n\,Q_{1,2}(y) - \ln^n\,B_{1,2}(y), \tag{293}$$

etc, and the various components are

$$\begin{aligned}
\mathcal{C}_{0,n} &= \frac{\overline{\alpha}}{A_1}\left[\ln^{n+1}\,\mathcal{Q}_1 - \ln^{n+1}\,\mathcal{Q}_3\right] + \frac{\alpha}{A_2}\left[\ln^{n+1}\,\mathcal{Q}_2 - \ln^{n+1}\,\mathcal{Q}_4\right],\\
\mathcal{C}^1_{11,n} &= \frac{\overline{\alpha}}{A_1}\left[\ln^{n+1}\,\mathcal{Q}_1 - y\,\ln^{n+1}\,\mathcal{Q}_3\right] + \frac{\alpha}{A_2}\left[\ln^{n+1}\,\mathcal{Q}_2 - y\,\ln^{n+1}\,\mathcal{Q}_4\right],\\
\mathcal{C}^2_{11,n} &= -\,\frac{\overline{\alpha}}{A_1}\,\ln^{n+1}\,\mathcal{Q}_5 - \frac{\alpha}{A_2}\,\ln^{n+1}\,\mathcal{Q}_6,\\
\mathcal{C}_{12,n} &= \frac{\overline{\alpha}^2}{A_1}\,y\left[\ln^{n+1}\,\mathcal{Q}_1 - \ln^{n+1}\,\mathcal{Q}_3\right] - \frac{\alpha^2}{A_2}\,y\left[\ln^{n+1}\,\mathcal{Q}_2 - \ln^{n+1}\,\mathcal{Q}_4\right].
\end{aligned} \tag{294}$$

In the standard analytical approach C_0 would be written as a combination of 12 di-logarithms while $C_{1,2}$ would be reduced to scalar integrals and expressed in terms of C_0 and of various B_0 functions with the usual appearance of inverse powers of G_{12}. The approach here is different and aimed to put the integrand in a form that is particular convenient for direct numerical evaluation. The coefficients $a, \ldots, f$ of Eq.(283) are usually expressed in terms of masses and momenta which, however, may depend on additional Feynman parameters.

E.1 Recovering the anomalous threshold

In Eq.(294) we have introduced extra terms in each of the integrals since their total contribution is zero. With Eq.(293) we have achieved that the residue of the poles due to $A_{1,2} = 0$ are zero. There are two cases where the A_i are nullified: the common one is due to the fact that there is a $0 \leq y_0 \leq 1$ such that $A_i(y_0) = 0$. However, when masses and momenta depend on external Feynman parameters and our C-functions are the kernel in the integral representation for a two-loop diagrams $A(y) = a_1\, y + a_0$ may become zero because $a_1 = a_0 = 0$. Even in this case our representation holds and we may encounter a real singularity only when $A_i(y) = B_i(y) = 0, \forall y$. Suppose that we are considering a one-loop C_0-function with $p_1^2 = p_2^2 = -m^2$ and $m_1 = m_3 = m, m_2 = M$. Consider now one of the terms in Eq.(294), say $\ln \mathcal{Q}_1/A_1$; we have a singularity when the zero of A_1, i.e.

$$\overline{\alpha}\, y = -\,\frac{d + e\,\alpha}{c + 2\,b\,\alpha}, \tag{295}$$

is also a zero of B_1, which may occur only if $s\,(s - 4\,m^2 + M^2) = 0$, the anomalous threshold for this configuration. The problem is more involved when masses are function of external Feynman parameters; let us consider a simple example which, however, shows all the features of more realistic ones. Suppose we have to compute

$$\int_0^1 dz\, C_0(-m^2\,,\, -m^2\,, s\,;\, m\,,\, z\,M\,,\, m). \tag{296}$$

We follow the procedure described above for the C_0 function and consider again one specific term in Eq.(294), say $\ln \mathcal{Q}_1/A_1$:

$$\begin{aligned}
I &= \int_0^1 dy \int_0^1 dz\, \frac{1}{A_1}\, \ln \mathcal{Q}_1, \qquad A_1 = \overline{\alpha}\, A_{\scriptscriptstyle T}\, (y - y_0), \qquad \mathcal{Q}_1 = 1 + \frac{(c + 2\,b\,\alpha)^2\, A_1}{B_1}, \\
B_1 &= z^2\, M^2\, s \left[\beta^2 + z^2\, M^2 - \overline{\alpha}\, (y - y_0)\, A_{\scriptscriptstyle T}\right] \\
&\quad - \overline{\alpha}\, (y - y_0)\, s \left[2\,\alpha\, m^2\, \beta^2 + 8\, m^4 - 6\, s\, m^2 + s^2 + \overline{\alpha}\, (y - y_0)\, m^2\, \beta^2\right],
\end{aligned} \tag{297}$$

where $\beta^2 = s - 4\,m^2$ and where $A_{\scriptscriptstyle T} = -\,2\,\overline{\alpha}\, m^2 + s$ and $A_1(y_0) = 0$. If $y_0 \in [0, 1]$ both numerator and denominator in the argument of the logarithm vanish inside the integration domain, i.e. for $y = y_0$ and $z = 0$. This is not yet a sign of singularity as it can be seen by using a sector decomposition (as described in Section D) after splitting the y integration interval. For instance, for $0 \leq y \leq y_0$ we change variable, $y = y_0\,(1 - y')$ and perform a sector decomposition with respect to y, z obtaining

$$\begin{aligned}
I &= -\,\frac{1}{\overline{\alpha}\, A_{\scriptscriptstyle T}} \int_0^1 dy \int_0^1 dz\, \ln\left[1 - \frac{(c + 2\,b\,\alpha)^2\, \overline{\alpha}\, A_{\scriptscriptstyle T}}{D}\right], \\
D &= y\, z^2\, M^2\, s\, (\overline{\alpha}\, y\, y_0\, A_{\scriptscriptstyle T} + \beta^2 + z^2\, y^2\, M^2) \\
&\quad + \overline{\alpha}\, y_0\, s \left[2\,\alpha\, m^2\, \beta^2 + 8\, m^4 - 6\, s\, m^2 + s^2 + \overline{\alpha}\, y\, y_0\, m^2\, \beta^2 + \cdots\right],
\end{aligned} \tag{298}$$

where only one component has been shown, the one where sector decomposition stops after the first iteration. Clearly $y = y_0, z = 0$ does not represent a singularity for I and only $A_{\scriptscriptstyle T} = 0$ does; a similar analysis applies to all terms in C_0. In conclusion, for the numerical evaluation of two-loop diagrams which are based on the integral representation of C_0 just described, a sector decomposition will give a much better numerical stability.

In another example we consider cases where there is no singularity but numerical instabilities may occur at the end points of the integration region in the external parameters. Also here some additional

work is needed, essentially another sector decomposition is requested. Let us give a simple but realistic example: suppose that we have to compute the following integral,

$$I = \int_0^1 dx_1 \int_0^{x_1} dx_2\, J(x_1, x_2), \qquad J(x_1, x_2) = \int_0^1 dy_1 \int_0^{y_1} dy_2\, V^{-1}, \tag{299}$$

where V is a quadratic form in the variables x_1 and x_2 of the kind of Eq.(283), with coefficients

$$\begin{aligned} &a = x_2\,(1-x_1)^2\,h_{11}, \quad b = x_2\,(1-x_1)^2\,h_{22}, \quad c = 2\,x_2\,(1-x_1)^2\,h_{12}, \\ &d = (1-x_2)\left[F - 2\,x_2\,(1-x_1)\,S_1\right], \quad e = -2\,x_2\,(1-x_1)\,(1-x_2)\,S_2, \quad f = x_2\,(1-x_2)^2\,S. \end{aligned} \tag{300}$$

Clearly $V = 0$ for $x_1 = x_2 = 1$. A simple sector decomposition gives

$$I = \int_0^1 dx_1 \int_0^1 dx_2\, x_2\, J(1 - x_1\,x_2, 1 - x_2). \tag{301}$$

In evaluating the internal C_0-function in Eq.(299) we obtain a factorization:

$$A_i(y) = x_2\,\mathcal{A}_i(y), \qquad B_i(y) = x_2^2\,(1-x_2)\,\mathcal{B}_i(y), \qquad i = 1, 2, \tag{302}$$

where $h_{22}\,\alpha^2 + 2\,h_{12}\,\alpha + h_{11} = 0$ and

$$\begin{aligned} \mathcal{A}_{1,2} &= F \pm 2\,x_1\,x_2\,(1-x_2)\left[\overline{\alpha}\,(\alpha\,h_{22} + h_{12})\,x_1\,y - S_1 - \alpha\,S_2\right], \\ \mathcal{B}_1 &= S + \overline{\alpha}\,x_1\,y\left[\overline{\alpha}\,h_{22}\,x_1\,y - 2\,S_2\right], \quad \mathcal{B}_2 = S + \alpha\,x_1\,y\left[\alpha\,h_{22}\,x_1\,y + 2\,S_2\right]. \end{aligned} \tag{303}$$

After that the numerical integration in Eq.(299) is free from instabilities.

Our result for the C-functions has the same range of validity of the scalar one-loop vertex, i.e. p_1 and/or p_2 and/or P time-like, p_1, p_2 and P space-like. Indeed the original derivation does not make any reference to the actual values of the internal masses, as long as they are real. For complex masses and space-like p_1, p_2 and P the scene changes with respect to the one-loop case since here the effective, $x_1, \ldots, x_n$-dependent, internal masses do not necessarily have a positive value for the real part of their squared values. Once again the presence of an anomalous threshold corresponds to a situation where simultaneously a denominator as well as the argument of the corresponding logarithms can be zero. In this case sector decomposition should be applied or the methods of [3] should be used.

F Landau equations for V^{121}

Starting with this Section we discuss the Landau equations and their solutions for the six topologies that one encounters in two-loop vertices. Their relevance is obvious, as one cannot safely attempt numerical integration before knowing something about the analytical structure of the diagrams. Furthermore these solutions are notoriously hard to derive with standard methods [48].

The Landau equations for the V^{121} topology of Fig. 7(a) are

$$\begin{aligned} &\alpha_1\,(q_1^2 + m_1^2) = 0, && \alpha_2\,((q_1 - q_2)^2 + m_2^2) = 0, \\ &\alpha_3\,((q_2 - p_2)^2 + m_3^2) = 0, && \alpha_4\,((q_2 - P)^2 + m_4^2) = 0, \end{aligned} \tag{304}$$

and also

$$\alpha_1 q_{1\mu} + \alpha_2 (q_1 - q_2)_\mu = 0, \qquad -\alpha_2 (q_1 - q_2)_\mu + \alpha_3\,(q_2 - p_2)_\mu + \alpha_4\,(q_2 - P)_\mu = 0. \tag{305}$$

The leading Landau singularity occurs for $\alpha_i \neq 0, \forall i$. We multiply the two equations Eq.(305) by $q_{1\mu}$, $q_{2\mu}$, $p_{2\mu}$ and P_μ respectively. This gives an homogeneous system of eight equations.

$$\begin{pmatrix} q_1\cdot q_1 & q_1\cdot(q_1-q_2) \\ q_1\cdot q_2 & q_2\cdot(q_1-q_2) \\ q_1\cdot p_2 & p_2\cdot(q_1-q_2) \\ q_1\cdot P & P\cdot(q_1-q_2) \end{pmatrix} \begin{pmatrix} \alpha_1 \\ \alpha_2 \end{pmatrix} = 0 \qquad \begin{pmatrix} -q_1\cdot(q_1-q_2) & q_1\cdot(q_2-p_2) & q_1\cdot(q_2-P) \\ -q_2\cdot(q_1-q_2) & q_2\cdot(q_2-p_2) & q_2\cdot(q_2-P) \\ -p_2\cdot(q_1-q_2) & p_2\cdot(q_2-p_2) & p_2\cdot(q_2-P) \\ -P\cdot(q_1-q_2) & P\cdot(q_2-p_2) & P\cdot(q_2-P) \end{pmatrix} \begin{pmatrix} \alpha_2 \\ \alpha_3 \\ \alpha_4 \end{pmatrix} = 0.$$

If we are looking for a solution where all the α_i are different from zero then the singularity will occur for

$$\begin{aligned} &q_1^2 = -m_1^2 && q_2^2 = -m_3^2 - p_2^2 + 2\,q_2\cdot p_2, \\ &q_1\cdot q_2 = \tfrac{1}{2}\,(m_2^2 - m_1^2 - m_3^2 - p_2^2 + 2\,q_2\cdot p_2) && P\cdot q_2 = \tfrac{1}{2}\,(P^2 - m_3^2 + m_4^2 - p_2^2 + 2\,q_2\cdot p_2). \end{aligned}$$

After inserting these relations the compatibility between the first two equations requires the condition

$$q_2\cdot p_2 = \frac{1}{2}\,(p_2^2 - (m_1+m_2)^2 + m_3^2). \tag{306}$$

As a result, it follows that $\alpha_1 = m_2/m_1\,\alpha_2$. If we use these relations in the next two equations, we obtain the following conditions:

$$q_1\cdot p_2 = \frac{m_1}{2(m_1+m_2)}\,(p_2^2 - (m_1+m_2)^2 + m_3^2), \quad q_1\cdot P = \frac{m_1}{2(m_1+m_2)}\,(P^2 - (m_1+m_2)^2 + m_4^2). \tag{307}$$

By inserting these values in the last four equations we obtain the condition for a proper solution; therefore, for arbitrary masses, the leading Landau singularity occurs for:

$$P^2 = \frac{1}{2\,m_3^2}\left[(-p_2^2 - (m_1+m_2)^2 + m_3^2)\,(-p_1^2 + m_3^2 - m_4^2) + 2\,m_3^2\,(p_1^2 + p_2^2) \pm (\lambda_1\,\lambda_2)^{1/2}\right], \tag{308}$$

where $\lambda_1 = \lambda(-p_1^2, m_3^2, m_4^2)$ and $\lambda_2 = \lambda(-p_2^2, (m_1+m_2)^2, m_3^2)$.

G Landau equations for V^{131}

The Landau equations for this topology (see Fig. 7(c)) are as follows

$$\begin{aligned} &\alpha_1\,(q_1^2 + m_1^2) = 0, && \alpha_2\,((q_1-q_2)^2 + m_2^2) = 0, \\ &\alpha_3\,(q_2^2 + m_3^2) = 0, && \alpha_4\,((q_2+p_1)^2 + m_4^2) = 0, && \alpha_5\,((q_2+P)^2 + m_5^2) = 0, \end{aligned} \tag{309}$$

and also

$$\alpha_1 q_{1\mu} + \alpha_2 (q_1-q_2)_\mu = 0, \quad -\alpha_2 (q_1-q_2)_\mu + \alpha_3\,q_{2\mu} + \alpha_4\,(q_2+p_1)_\mu + \alpha_5\,(q_2+P)_\mu = 0. \tag{310}$$

We recall that the leading Landau singularity occurs for $\alpha_i \neq 0, \forall i$. We multiply the two equations Eq.(310) by $q_{1\mu}$, $q_{2\mu}$, $p_{1\mu}$ and P_μ respectively. This gives the following homogeneous system of eight equations

$$\begin{pmatrix} q_1\cdot q_1 & q_1\cdot(q_1-q_2) \\ q_1\cdot q_2 & q_2\cdot(q_1-q_2) \\ q_1\cdot p_1 & p_1\cdot(q_1-q_2) \\ q_1\cdot P & P\cdot(q_1-q_2) \end{pmatrix} \begin{pmatrix} \alpha_1 \\ \alpha_2 \end{pmatrix} = \begin{pmatrix} -q_1\cdot(q_1-q_2) & q_1\cdot q_2 & q_1\cdot(q_2+p_1) & q_1\cdot(q_2+P) \\ -q_2\cdot(q_1-q_2) & q_2\cdot q_2 & q_2\cdot(q_2+p_1) & q_2\cdot(q_2+P) \\ -p_1\cdot(q_1-q_2) & p_1\cdot q_2 & p_1\cdot(q_2+p_1) & p_1\cdot(q_2+P) \\ -P\cdot(q_1-q_2) & P\cdot q_2 & P\cdot(q_2+p_1) & P\cdot(q_2+P) \end{pmatrix} \begin{pmatrix} \alpha_2 \\ \alpha_3 \\ \alpha_4 \\ \alpha_5 \end{pmatrix} = 0.$$

A proper solution will occur for

$$\begin{array}{lll} q_1^2 = -m_1^2 & q_2^2 = -m_3^2, & \\ q_1 \cdot q_2 = \frac{1}{2}\,(m_2^2 - m_1^2 - m_3^2) & p_1 \cdot q_2 = \frac{1}{2}\,(-p_1^2 + m_3^2 - m_4^2) & P \cdot q_2 = \frac{1}{2}\,(-P^2 + m_3^2 - m_5^2). \end{array}$$

Compatibility between the first two equations further requires the condition $m_3 = m_1 + m_2$; as a consequence, it follows that $\alpha_1 = m_2/m_1\,\alpha_2$. If we use these relations in the next two equations, we further obtain

$$q_1 \cdot p_1 = \frac{m_1}{2(m_1+m_2)}\,(-p_1^2 + (m_1+m_2)^2 - m_4^2), \quad q_1 \cdot P = \frac{m_1}{2(m_1+m_2)}\,(-P^2 + (m_1+m_2)^2 - m_5^2). \tag{311}$$

By putting these values in the last four equations, we finally derive the condition for a proper solution; therefore, for general masses, the leading Landau singularity occurs for:

$$p_2^2 = \frac{1}{2\,m_3^2}\left[(-p_1^2+(m_1+m_2)^2-m_4^2)\,(-P^2+(m_1+m_2)^2-m_5^2)+2\,(m_1+m_2)^2\,(p_1^2+P^2) \pm (\lambda_1\,\lambda_2)^{1/2}\right] \tag{312}$$

where $\lambda_1 = \lambda(-p_1^2, m_3^2, m_4^2)$ and $\lambda_2 = \lambda(-P^2, m_3^2, m_5^2)$.

H Landau equations for V^{221}

The Landau equations for this topology (see Fig. 7(b)) are as follows:

$$\begin{array}{lll} \alpha_1\,(q_1^2 + m_1^2) = 0, & \alpha_2\,((q_1+p_1)^2 + m_2^2) = 0, & \alpha_3\,((q_1-q_2)^2 + m_3^2) = 0, \\ \alpha_4\,((q_2+p_1)^2 + m_4^2) = 0, & \alpha_5\,((q_2+P)^2 + m_5^2) = 0, & \end{array} \tag{313}$$

and also

$$\begin{aligned} &\alpha_1 q_{1\mu} + \alpha_2 (q_1+p_1)_\mu + \alpha_3 (q_1-q_2)_\mu = 0, \\ &-\alpha_3 (q_1-q_2)_\mu + \alpha_4\,(q_2+p_1)_\mu + \alpha_5\,(q_2+P)_\mu = 0. \end{aligned} \tag{314}$$

The leading Landau singularity occurs for $\alpha_i \neq 0, \forall i$. We multiply the two equations Eq.(314) by $q_{1\mu}$, $q_{2\mu}$, $p_{1\mu}$ and $p_{2\mu}$, respectively. This gives an homogeneous system of eight equations

$$\begin{pmatrix} q_1\cdot q_1 & q_1\cdot(q_1+p_1) & q_1\cdot(q_1-q_2) \\ q_2\cdot q_1 & q_2\cdot(q_1+p_1) & q_2\cdot(q_1-q_2) \\ p_1\cdot q_1 & p_1\cdot(q_1+p_1) & p_1\cdot(q_1-q_2) \\ p_2\cdot q_1 & p_2\cdot(q_1+p_1) & p_2\cdot(q_1-q_2) \end{pmatrix} \begin{pmatrix} \alpha_1 \\ \alpha_2 \\ \alpha_3 \end{pmatrix} = 0$$

$$\begin{pmatrix} -q_1\cdot(q_1-q_2) & q_1\cdot(q_2+p_1) & q_1\cdot(q_2+P) \\ -q_2\cdot(q_1-q_2) & q_2\cdot(q_2+p_1) & q_2\cdot(q_2+P) \\ -p_1\cdot(q_1-q_2) & p_1\cdot(q_2+p_1) & p_1\cdot(q_2+P) \\ -p_2\cdot(q_1-q_2) & p_2\cdot(q_2+p_1) & p_2\cdot(q_2+P) \end{pmatrix} \begin{pmatrix} \alpha_3 \\ \alpha_4 \\ \alpha_5 \end{pmatrix} = 0.$$

If all α_i are different from zero, the singularity will occur for

$$\begin{array}{ll} q_1^2 = -m_1^2 & q_2^2 = -m_4^2 - p_1^2 - 2\,q_2\cdot p_1, \\ q_1\cdot p_1 = \frac{1}{2}\,(m_1^2 - m_2^2 - p_1^2) & q_1\cdot q_2 = -\frac{1}{2}\,(m_1^2 - m_3^2 + m_4^2 + p_1^2 + 2\,q_2\cdot p_1) \\ q_2\cdot p_2 = \frac{1}{2}\,(m_4^2 - m_5^2 + p_1^2 - P^2). & \end{array}$$

Compatibility between the first three and between the 5^{th}, 6^{th} and 8^{th} equation requires the conditions

$$q_2\cdot p_1 = -p_1^2 + \frac{1}{4\,m_2^2}\left[(p_1^2+m_1^2-m_2^2)\,(m_2^2-m_3^2+m_4^2) \pm (\lambda_1\,\lambda_2)^{1/2}\right]$$
$$q_1\cdot p_2 = -\frac{1}{2}(P^2-p_1^2-p_2^2) + \frac{1}{4\,m_4^2}\left[(-p_2^2+m_4^2-m_5^2)\,(m_2^2-m_3^2+m_4^2) \pm (\lambda_1\,\lambda_3)^{1/2}\right] \qquad (315)$$

where $\lambda_1 = \lambda(m_2^2, m_3^2, m_4^2)$, $\lambda_2 = \lambda(-p_1^2, m_1^2, m_2^2)$ and $\lambda_3 = \lambda(-p_2^2, m_4^2, m_5^2)$. By inserting these values in the remaining equations, we obtain that the compatibility requires:

$$P^2 = -\frac{1}{4\,m_2^2\,m_4^2}\Big[(m_2^2-m_3^2+m_4^2)\,(p_1^2+m_1^2-m_2^2)\,(-p_2^2+m_4^2-m_5^2) - 4\,m_2^2\,m_4^2\,(p_1^2+p_2^2) \qquad (316)$$
$$+ r\,s\,(m_2^2-m_3^2+m_4^2)\,(\lambda_2\,\lambda_3)^{1/2} + r\,(p_1^2+m_1^2-m_2^2)\,(\lambda_1\,\lambda_3)^{1/2} + s\,(-p_2^2+m_4^2-m_5^2)\,(\lambda_1\,\lambda_2)^{1/2}\Big]$$

where $r, s = \pm 1$. These are the four possibilities for the leading Landau singularity of the diagram.

I Landau equations for V^{231}

The Landau equation for this topology (see Fig. 7(e)) are as follows:

$$\begin{array}{lll} \alpha_1\,(q_1^2+m_1^2)=0, & \alpha_2\,((q_1+P)^2+m_2^2)=0, & \alpha_3\,((q_1-q_2)^2+m_3^2)=0, \\ \alpha_4\,(q_2^2+m_4^2)=0, & \alpha_5\,((q_2+p_1)^2+m_5^2)=0, & \alpha_6\,((q_2+P)^2+m_6^2)=0, \end{array} \qquad (317)$$

and also

$$\alpha_1 q_{1\mu} + \alpha_2 (q_1+P)_\mu + \alpha_3 (q_1-q_2)_\mu = 0,$$
$$-\alpha_3 (q_1-q_2)_\mu + \alpha_4\, q_{2\mu} + \alpha_5\,(q_2+p_1)_\mu + \alpha_6\,(q_2+P)_\mu = 0. \qquad (318)$$

The leading Landau singularity occurs for $\alpha_i \neq 0, \forall i$. We multiply the two equations Eq.(318) by $q_{1\mu}$, $q_{2\mu}$, $p_{1\mu}$ and P_μ, respectively. This gives an homogeneous system of eight equations. If all α_i are different from zero we may use

$$\begin{array}{lll} q_1^2 = -m_1^2 & q_2^2 = -m_4^2, & q_1\cdot q_2 = \frac{1}{2}\,(m_3^2-m_1^2-m_4^2) \\ q_1\cdot P = \frac{1}{2}\,(-P^2+m_1^2-m_2^2) & q_2\cdot p_1 = \frac{1}{2}\,(-p_1^2+m_4^2-m_5^2) & q_2\cdot P = \frac{1}{2}\,(-P^2+m_4^2-m_6^2). \end{array}$$

Compatibility requires first of all that

$$P^2 = -\frac{1}{2\,m_3^2}\Big[-(m_1^2-m_3^2-m_4^2)\,(m_2^2-m_3^2-m_6^2) + 2\,m_3^2\,(m_4^2+m_6^2) \pm (\lambda_1\,\lambda_2)^{1/2}\Big] \qquad (319)$$

where $\lambda_1 = \lambda(m_1^2, m_3^2, m_4^2)$ and $\lambda_2 = \lambda(m_2^2, m_3^2, m_6^2)$. By inserting back this result into the system we obtain the following condition:

$$q_1\cdot p_1 = \frac{1}{4\,m_4^2}\Big[(m_1^2-m_3^2+m_4^2)\,(-p_1^2+m_4^2-m_5^2) \pm (\lambda_1\,\lambda_3)^{1/2}\Big]. \qquad (320)$$

A proper solution requires yet another relation among the physical parameters. Therefore we have four possibilities in searching for the leading Landau singularity of the diagram:

$$P^2 = -\frac{1}{2\,m_3^2}\Big[-(m_1^2-m_3^2-m_4^2)\,(m_2^2-m_3^2-m_6^2) + 2\,m_3^2\,(m_4^2+m_6^2) + (\lambda_1\,\lambda_2)^{1/2}\Big]$$
$$p_2^2 = \frac{1}{4\,m_3^2\,m_4^2}\Big[(m_1^2-m_3^2-m_4^2)\,(m_2^2-m_3^2-m_6^2)\,(p_1^2+m_4^2+m_5^2) - 4\,m_3^2\,m_4^2\,(m_5^2+m_6^2)$$
$$\pm(m_1^2-m_3^2-m_4^2)\,(\lambda_2\,\lambda_3)^{1/2} \mp (m_2^2-m_3^2-m_6^2)\,(\lambda_1\,\lambda_3)^{1/2} - (p_1^2+m_4^2+m_5^2)\,(\lambda_1\,\lambda_2)^{1/2}\Big]$$

$$
\begin{aligned}
P^2 &= -\frac{1}{2\,m_3^2}\Big[-(m_1^2-m_3^2-m_4^2)\,(m_2^2-m_3^2-m_6^2)+2\,m_3^2\,(m_4^2+m_6^2)-(\lambda_1\,\lambda_2)^{1/2}\Big]\\
p_2^2 &= \frac{1}{4\,m_3^2\,m_4^2}\Big[(m_1^2-m_3^2-m_4^2)\,(m_2^2-m_3^2-m_6^2)\,(p_1^2+m_4^2+m_5^2)-4\,m_3^2\,m_4^2\,(m_5^2+m_6^2)\\
&\quad \mp(m_1^2-m_3^2-m_4^2)\,(\lambda_2\,\lambda_3)^{1/2}\mp(m_2^2-m_3^2-m_6^2)\,(\lambda_1\,\lambda_3)^{1/2}+(p_1^2+m_4^2+m_5^2)\,(\lambda_1\,\lambda_2)^{1/2}\Big]
\end{aligned}
\tag{321}
$$

where we have defined $\lambda_3 = \lambda(-p_1^2, m_4^2, m_5^2)$. The upper(lower) sign refers to the $+(-)$ sign in eq. Eq.(320).

J Landau equations for V^{222}

The Landau equations for this topology (see Fig. 7(f)) are as follows:

$$
\begin{array}{lll}
\alpha_1\,(q_1^2+m_1^2)=0, & \alpha_2\,((q_1-p_2)^2+m_2^2)=0, & \alpha_3\,((q_1-q_2+p_1)^2+m_3^2)=0,\\
\alpha_4\,((q_1-q_2-p_2)^2+m_4^2)=0, & \alpha_5\,(q_2^2+m_5^2)=0, & \alpha_6\,((q_2-p_1)^2+m_6^2)=0,
\end{array}
\tag{322}
$$

and also

$$
\begin{aligned}
&\alpha_1 q_{1\mu}+\alpha_2(q_1-p_2)_\mu+\alpha_3(q_1-q_2+p_1)_\mu+\alpha_4(q_1-q_2-p_2)_\mu=0,\\
&-\alpha_3(q_1-q_2+p_1)_\mu-\alpha_4\,(q_1-q_2-p_2)_\mu+\alpha_5\,q_{2\mu}+\alpha_6(q_2-p_1)_\mu=0.
\end{aligned}
\tag{323}
$$

The leading Landau singularity occurs for $\alpha_i \neq 0, \forall i$. The strategy for determining the solutions is, as usual, to multiply the two equations Eq.(323) by $q_{1\mu}$, $q_{2\mu}$, $p_{1\mu}$ and $p_{2\mu}$ respectively. This gives an homogeneous system of eight equations. However, finding the general solution of these equations is an arduous task and even so we do not learn much and, for V^{222}, it is more convenient to study occurrence of singularities directly in terms of distortion of the integration hyper-contour. However, some physically significant case can be discussed. We split our system into two systems of four equations and derive α_1 and α_5; in this way we obtain two homogeneous systems, $\mathcal{S}_{1,2}$, each containing three equations with unknowns $\alpha_2, \alpha_3, \alpha_4$ and $\alpha_3, \alpha_4, \alpha_6$. The two conditions for non trivial solutions are giving raise to the same quartic equation in $p_1 \cdot q_1$. If we consider a configuration with

$$
p_1^2 = p_2^2 = -m^2, \qquad m_2 = m_6 = M, \qquad m_i = m\ (i \neq 2, 6),
\tag{324}
$$

a solution is, for instance, $p_1 \cdot q_1 = m^2 + 1/2\,(P^2 + M^2)$. Inserting back this relation into our systems we may solve for α_2, α_3 and derive a non-zero α_4 under the condition $P^2 = -\,M^2 = -\,4\,m^2$.

K Tables of numerical results

$M(\bar{b}b)$ [GeV]	$\mathrm{Re}\, V$	$\Delta\,\mathrm{Re}\, V$	$\mathrm{Im}\, V$	$\Delta\,\mathrm{Im}\, V$
200	-0.04913523	0.5×10^{-9}	0	0
350	-0.1552182	0.6227×10^{-3}	-0.2036244	0.5153×10^{-3}
400	0.0552437	0.5846×10^{-3}	-0.1546848	0.5263×10^{-3}
500	0.0751724	0.3209×10^{-3}	-0.0330644	0.2564×10^{-3}

Table 4: Numerical results for the topology V^{231} of Fig. 6 as a function of the $\bar{b}b$ invariant mass. Real and imaginary parts are in units of 10^{-8}. Δ is the estimate of the absolute error.

s_p/M	s_1/M_1	s_2/M_2	m_1	m_2	m_3	m_4	$\mathrm{Re}\, V^{121}$	$\mathrm{Im}\, V^{121}$
$H^* \to ZZ$								
$+/2\,M_Z$	$+/M_Z$	$+/M_Z$	M_H	M_H	M_Z	M_H	$-0.473001 \pm 2.4 \times 10^{-6}$	0
$+/\sqrt{4.5}\,M_Z$	$+/M_Z$	$+/M_Z$	M_H	M_H	M_Z	M_H	$-0.472906 \pm 1.4 \times 10^{-6}$	0
$+/\sqrt{5}\,M_Z$	$+/M_Z$	$+/M_Z$	M_H	M_H	M_Z	M_H	$-0.472845 \pm 2.2 \times 10^{-6}$	0
$+/\sqrt{8}\,M_Z$	$+/M_Z$	$+/M_Z$	M_H	M_H	M_Z	M_H	$-0.472922 \pm 2.1 \times 10^{-6}$	0
$+/\sqrt{20}\,M_Z$	$+/M_Z$	$+/M_Z$	M_H	M_H	M_Z	M_H	$-0.476661 \pm 1.7 \times 10^{-6}$	0
$+/\sqrt{100}\,M_Z$	$+/M_Z$	$+/M_Z$	M_H	M_H	M_Z	M_H	$-0.492846 \pm 2.8 \times 10^{-4}$	$-0.041473 \pm 3.0 \times 10^{-6}$
$+/\sqrt{400}\,M_Z$	$+/M_Z$	$+/M_Z$	M_H	M_H	M_Z	M_H	$-0.460821 \pm 5.8 \times 10^{-4}$	$-0.097880 \pm 9.6 \times 10^{-6}$

Table 5: Numerical results for the topology V^{121} of Fig. 7(a). All masses are in GeV and Mandelstam invariants are defined in Eq.(8). The ultraviolet pole is $\epsilon = 1$ and the unit of mass is also 1 GeV. The process to which the diagram belongs is specified with input parameters given in Eq.(265).

s_p/M	s_1/M_1	s_2/M_2	m_1	m_2	m_3	m_4	m_5	$\mathrm{Re}\, V^{131}$	$\mathrm{Im}\, V^{131}$
Random									
$+/95$	$-/22$	$-/87$	4	18	43	3	57	0.00580331(7)	$-0.00013086(9)$
								0.00580328(2)	$-0.00013082(2)$
$-/58$	$-/6$	$-/67$	24	18	88	72	93	0.001206431(2)	0
								0.001206427(8)	0
$Z^* \to \overline{b}b$									
$+/100$	$+/m_b$	$-/m_b$	M_W	M_W	M_Z	m_b	M_Z	0.2480028×10^{-2}	0
$+/300$	$+/m_b$	$-/m_b$	M_W	M_W	M_Z	m_b	M_Z	$0.12228(6) \times 10^{-2}$	$0.27345(7) \times 10^{-2}$
								$0.122334(6) \times 10^{-2}$	$0.27334(1) \times 10^{-2}$
$+/800$	$+/m_b$	$-/m_b$	M_W	M_W	M_Z	m_b	M_Z	$-0.2183(9) \times 10^{-3}$	$0.84447(12) \times 10^{-3}$
								$-0.21744(6) \times 10^{-3}$	$0.84378(8) \times 10^{-3}$
$Z^* \to \overline{t}t$									
$+/500$	$+/m_t$	$-/m_t$	M_W	M_W	M_Z	m_t	M_Z	$0.16720(6) \times 10^{-4}$	$0.673497(7) \times 10^{-3}$
								$0.16717(3) \times 10^{-4}$	$0.673475(5) \times 10^{-3}$

Table 6: Numerical results for the topology V^{131} of Fig. 7(c). All masses are in GeV and Mandelstam invariants are defined in Eq.(8). First entry is obtained with method I of Section 6.1, second entry is obtained with method II of Section 6.2. The ultraviolet pole is $\epsilon = 1$ and the unit of mass is also 1 GeV. 'Random' implies that all entries are generated randomly, otherwise the process to which the diagram belongs is specified with input parameters given in Eq.(265).

s_p/M	s_1/M_1	s_2/M_2	m_1	m_2	m_3	m_4	m_5	$\mathrm{Re}\, V^{141}$	$\mathrm{Im}\, V^{141}$
Random									
$+/76$	$+/83$	$+/90$	43	50	80	35	89	$0.3269872(1) \times 10^{-6}$	0
								$0.3269872(1) \times 10^{-6}$	0
$+/27$	$+/6$	$-/44$	54	28	94	51	32	$0.1327195(1) \times 10^{-6}$	0
								$0.1327195(1) \times 10^{-6}$	0
$+/43$	$-/52$	$-/77$	10	5	21	5	9	$-0.136824(8) \times 10^{-5}$	$0.600728(2) \times 10^{-5}$
								$-0.13682(4) \times 10^{-5}$	$0.60072(4) \times 10^{-5}$
$+/82$	$+/33$	$-/95$	97	15	56	93	0	$0.2209(2) \times 10^{-7}$	$0.53471(4) \times 10^{-6}$
								$0.2208360(8) \times 10^{-7}$	$0.5347270(6) \times 10^{-6}$
$Z^* \to \bar{t}t$									
$+/500$	$+/m_t$	$+/m_t$	M_W	M_Z	M_W	m_b	M_W	$0.96881(21) \times 10^{-8}$	$-0.131428(23) \times 10^{-7}$
								$0.96866(4) \times 10^{-8}$	$-0.131401(3) \times 10^{-7}$
$+/800$	$+/m_t$	$+/m_t$	M_W	M_Z	M_W	m_b	M_W	$0.4803(13) \times 10^{-8}$	$-0.5335(12) \times 10^{-8}$
								$0.4815(1) \times 10^{-8}$	$-0.5326(1) \times 10^{-8}$

Table 7: Numerical results for the topology V^{141} of Fig. 7(d). All masses are in GeV and Mandelstam invariants are defined in Eq.(8). First entry is obtained with method I of Section 8.1, second entry is obtained with method II of Section 8.2. The ultraviolet pole is $\epsilon = 1$ and the unit of mass is also 1 GeV. 'Random' implies that all entries are generated randomly, otherwise the process to which the diagram belongs is specified with input parameters given in Eq.(265).

s_p/M	s_1/M_1	s_2/M_2	m_1	m_2	m_3	m_4	m_5	$\mathrm{Re}\, V^{221}$	$\mathrm{Im}\, V^{221}$
Random									
$+/10.1$	$+/1.51$	$+/1.52$	1.1	2.2	2.5	4.4	5.5	$-0.113675(2)$	$-0.004701(1)$
$-/85$	$+/36$	$+/86$	6.5	4.2	8.2	5.6	7.2	$0.002310(2)$	$-0.001084(3)$
$Z^* \to \overline{b}b$									
$+/\sqrt{8}\, m_b$	$+/m_b$	$+/m_b$	M_W	m_t	M_Z	m_t	M_W	$-0.511(3) \times 10^{-4}$	0
$+/\sqrt{1000}\, m_b$	$+/m_b$	$+/m_b$	M_W	m_t	M_Z	m_t	M_W	$-0.5253(3) \times 10^{-4}$	0
$+/\sqrt{5000}\, m_b$	$+/m_b$	$+/m_b$	M_W	m_t	M_Z	m_t	M_W	$-0.6122(2) \times 10^{-4}$	0
$Z^* \to \overline{t}t$									
$+/\sqrt{5}\, m_t$	$+/m_t$	$+/m_t$	M_W	m_b	M_Z	m_b	M_W	$0.2232(2) \times 10^{-3}$	$-0.1819(3) \times 10^{-3}$
$+/\sqrt{8}\, m_t$	$+/m_t$	$+/m_t$	M_W	m_b	M_Z	m_b	M_W	$0.2067(4) \times 10^{-3}$	$-0.1470(3) \times 10^{-3}$
$+/\sqrt{20}\, m_t$	$+/m_t$	$+/m_t$	M_W	m_b	M_Z	m_b	M_W	$0.1638(2) \times 10^{-3}$	$-0.9395(15) \times 10^{-4}$

Table 8: Numerical results for the topology V^{221} of Fig. 7(b). All masses are in GeV and Mandelstam invariants are defined in Eq.(8). 'Random' implies that all entries are generated randomly, otherwise the process to which the diagram belongs is specified with input parameters given in Eq.(265).

s_p/M	s_1/M_1	s_2/M_2	m_1	m_2	m_3	m_4	m_5	m_6	$\mathrm{Re}\, V^{231}$	$\mathrm{Im}\, V^{231}$
Random										
$-/60$	$+/48$	$+/29$	7.5	4.9	1.6	5.9	3.5	3	$0.1353(3) \times 10^{-5}$	$-0.413(7) \times 10^{-6}$
$-/39$	$+/85$	$-/93$	3.3	0.2	8.8	7	7.7	7	$-0.983(2) \times 10^{-7}$	$-0.6672(1) \times 10^{-6}$
$-/2$	$+/86$	$+/43$	4.3	5.7	4.6	8.5	6.2	2.8	$0.7469(7) \times 10^{-5}$	
$Z^* \to \overline{b}b$										
$+/100$	$+/m_b$	$+/m_b$	m_b	m_b	M_Z	m_b	M_Z	m_b	$0.5021(2) \times 10^{-7}$	$-0.1633(2) \times 10^{-7}$
$+/200$	$+/m_b$	$+/m_b$	m_b	m_b	M_Z	m_b	M_Z	m_b	$0.984(1) \times 10^{-8}$	$0.5450(6) \times 10^{-8}$
$Z^* \to \overline{t}t$										
$+/\sqrt{8}\, m_t$	$+/m_t$	$+/m_t$	m_t	m_t	M_Z	m_t	M_Z	m_t	$0.1487(8) \times 10^{-8}$	$0.1357(6) \times 10^{-9}$
$+/\sqrt{20}\, m_t$	$+/m_t$	$+/m_t$	m_t	m_t	M_Z	m_t	M_Z	m_t	$0.169(1) \times 10^{-9}$	$0.185(1) \times 10^{-9}$
$H^* \to \overline{b}b$										
$+/200$	$+/m_b$	$+/m_b$	M_H	M_H	m_t	m_t	M_W	m_t	$-0.4913523 \times 10^{-9}$	0
$+/350$	$+/m_b$	$+/m_b$	M_H	M_H	m_t	m_t	M_W	m_t	$-0.1560(12) \times 10^{-8}$	$-0.2039(8) \times 10^{-8}$
$+/400$	$+/m_b$	$+/m_b$	M_H	M_H	m_t	m_t	M_W	m_t	$0.554(7) \times 10^{-9}$	$-0.1544(6) \times 10^{-8}$
$+/500$	$+/m_b$	$+/m_b$	M_H	M_H	m_t	m_t	M_W	m_t	$0.756(4) \times 10^{-9}$	$0.329(5) \times 10^{-9}$

Table 9: Numerical results for the topology V^{231} of Fig. 7(e). All masses are in GeV and Mandelstam invariants are defined in Eq.(8). 'Random' implies that all entries are generated randomly, otherwise the process to which the diagram belongs is specified with input parameters given in Eq.(265).

$s = -P^2$	$\mathrm{Re}\, V^{222}$	$\Delta\, \mathrm{Re}\, V^{222}$	$\mathrm{Im}\, V^{222}$	$\Delta\, \mathrm{Im}\, V^{222}$
$4.0\, m^2$	0.73312	1.8×10^{-8}	0	0
	0.7331	1.4×10^{-4}		
$4.5\, m^2$	0.61645	1.3×10^{-9}	−0.33495	1.2×10^{-7}
	0.6216	7.8×10^{-3}	−0.3402	7.1×10^{-3}
$5.0\, m^2$	0.51844	2.6×10^{-8}	−0.43100	2.7×10^{-7}
	0.5203	4.0×10^{-3}	−0.4442	9.3×10^{-3}
$8.0\, m^2$	0.14555	6.8×10^{-6}	−0.5460	4.9×10^{-5}
	0.1455	2.0×10^{-3}	−0.5491	4.0×10^{-3}
$20.0\, m^2$	−0.2047	8.0×10^{-5}	−0.1876	3.8×10^{-4}
	−0.2058	5.4×10^{-4}	−0.1864	3.7×10^{-4}
$100.0\, m^2$	−0.0382	3.2×10^{-4}	0.0152	3.3×10^{-3}
	−0.0385	1.0×10^{-4}	0.0162	7.1×10^{-5}
$400.0\, m^2$	−0.0036	1.3×10^{-2}	0.0051	8.3×10^{-3}
	−0.00324	3.6×10^{-6}	0.00507	1.9×10^{-5}

Table 10: Comparison with the numerical results of [39] for the topology V^{222} of Fig. 7(e) in units of 10^{-9}. The common mass is $m = 150\,\mathrm{GeV}$ and $p_1^2 = p_2^2 = 0$. First entry is from [39], second entry is our result. Δ is the estimate of the absolute error.

References

[1] G. Passarino, Nucl. Phys. B **619** (2001) 257 [arXiv:hep-ph/0108252].

[2] G. Passarino and S. Uccirati, Nucl. Phys. B **629** (2002) 97 [arXiv:hep-ph/0112004].

[3] A. Ferroglia, M. Passera, G. Passarino and S. Uccirati, Nucl. Phys. B **650** (2003) 162 [arXiv:hep-ph/0209219].

[4] A. Ferroglia, G. Passarino, M. Passera and S. Uccirati, *Prepared for 31st International Conference on High Energy Physics (ICHEP 2002), Amsterdam, The Netherlands*;
A. Ferroglia, G. Passarino, S. Uccirati and M. Passera, Nucl. Instrum. Meth. A **502** (2003) 391.

[5] A. I. Davydychev and V. A. Smirnov, arXiv:hep-ph/0210171;
Z. Bern, Nucl. Phys. Proc. Suppl. **117** (2003) 260 [arXiv:hep-ph/0212406];
K. G. Chetyrkin and T. Seidensticker, Phys. Lett. B **495** (2000) 74 [arXiv:hep-ph/0008094];
V. A. Smirnov and E. R. Rakhmetov, Theor. Math. Phys. **120** (1999) 870 [Teor. Mat. Fiz. **120** (1999) 64] [arXiv:hep-ph/9812529];
J. Fleischer, A. V. Kotikov and O. L. Veretin, Nucl. Phys. B **547** (1999) 343 [arXiv:hep-ph/9808242];
A. T. Suzuki, A. G. Schmidt and R. Bentin, Nucl. Phys. B **537** (1999) 549 [arXiv:hep-th/9807158];
J. Fleischer and M. Tentyukov, arXiv:hep-ph/9802244;
A. Frink, Nucl. Instrum. Meth. A **389** (1997) 339 [arXiv:hep-ph/9611378];
J. Fleischer, Int. J. Mod. Phys. C **6** (1995) 495;
A. Frink, U. Kilian and D. Kreimer, Nucl. Phys. B **488** (1997) 426 [arXiv:hep-ph/9610285];
A. Czarnecki, U. Kilian and D. Kreimer, Nucl. Phys. B **433** (1995) 259 [arXiv:hep-ph/9405423];
B. A. Kniehl, Phys. Lett. B **237** (1990) 127;
G. J. Burgers, Phys. Lett. B **164** (1985) 167.

[6] A. Ghinculov and Y. Yao, Phys. Rev. D **63** (2001) 054510 [hep-ph/0006314];
A. Ghinculov and Y. Yao, Mod. Phys. Lett. A **15** (2000) 1967 [hep-ph/0004201];
A. Ghinculov and Y. Yao, Mod. Phys. Lett. A **15** (2000) 925 [hep-ph/0002211];
A. Ghinculov and Y. Yao, Nucl. Phys. B **516** (1998) 385 [hep-ph/9702266].

[7] A. Ferroglia, G. Passarino, M. Passera and S. Uccirati, Tensor Integrals for Two-Loop Two and Three Point Feynman Diagrams, work in preparation.

[8] A. Ferroglia, G. Passarino, M. Passera and S. Uccirati, Two-Loop Vertices in Quantum Field Theory: Infrared Divergent Configurations, work in preparation.

[9] R. Bonciani, P. Mastrolia and E. Remiddi, arXiv:hep-ph/0311145.

[10] A. I. Davydychev and M. Y. Kalmykov, arXiv:hep-th/0303162.

[11] J.A. Vermaseren, math-ph/0010025.

[12] A. Ferroglia, G. Passarino, M. Passera and S. Uccirati, $\mathcal{G}raph\mathcal{S}hot$, a FORM package for automatic generation of one- and two-loop Feynman diagrams, work in progress.

[13] G. Passarino and S. Uccirati, $\mathcal{T}op\mathcal{S}ide\mathcal{F}$, a FORTRAN code for numerical evaluation of one- and two-loop Feynman diagrams, work in progress.

[14] M. Tentyukov and J. Fleischer, Comput. Phys. Commun. **132** (2000) 124 [arXiv:hep-ph/9904258];
J. Kublbeck, H. Eck and R. Mertig, Nucl. Phys. Proc. Suppl. **29A** (1992) 204;
J. Fleischer and O. V. Tarasov, Comput. Phys. Commun. **71** (1992) 193;
S. A. Larin, F. V. Tkachov and J. A. M. Vermaseren, NIKHEF-H-91-18;
S. G. Gorishnii, S. A. Larin, L. R. Surguladze and F. V. Tkachov, Comput. Phys. Commun. **55** (1989) 381.

[15] G. Goldberg, Phys. Rev. D **32** (1985) 3331.

[16] V. A. Smirnov, Nucl. Phys. Proc. Suppl. **116** (2003) 417 [arXiv:hep-ph/0209295].

[17] O. V. Tarasov, Nucl. Phys. B **480** (1996) 397 [arXiv:hep-ph/9606238].

[18] T. Gehrmann and E. Remiddi, Nucl. Phys. B **601** (2001) 287 [arXiv:hep-ph/0101124].

[19] S. Laporta, Int. J. Mod. Phys. A **15** (2000) 5087 [arXiv:hep-ph/0102033].

[20] P. A. Baikov, Phys. Lett. B **385** (1996) 404 [arXiv:hep-ph/9603267];
V. A. Smirnov and M. Steinhauser, arXiv:hep-ph/0307088.

[21] F. V. Tkachov, Nucl. Instrum. Meth. A **389** (1997) 309 [hep-ph/9609429];
L. N. Bertstein, Functional Analysis and its Applications, **6**(1972)66.

[22] R.J. Eden, P.V. Landshoff, D.I. Olive, and J.C. Polkinghorne, *The Analytic S-Matrix*, Cambridge Univ. Press, 1966.

[23] P. Mastrolia and E. Remiddi, Nucl. Phys. B **664** (2003) 341 [arXiv:hep-ph/0302162];
M. Caffo, arXiv:hep-ph/0311052;
S. P. Martin, Phys. Rev. D **68** (2003) 075002 [arXiv:hep-ph/0307101];
R. Bonciani, P. Mastrolia and E. Remiddi, Nucl. Phys. B **661** (2003) 289 [arXiv:hep-ph/0301170];
M. Caffo, H. Czyz and E. Remiddi, Nucl. Phys. Proc. Suppl. **116** (2003) 422 [arXiv:hep-ph/0211178];
M. Caffo, H. Czyz and E. Remiddi, Nucl. Instrum. Meth. A **502** (2003) 613 [arXiv:hep-ph/0211171];
M. Caffo, H. Czyz and E. Remiddi, Nucl. Phys. B **634** (2002) 309 [arXiv:hep-ph/0203256];
T. Gehrmann and E. Remiddi, Nucl. Phys. Proc. Suppl. **89** (2000) 251 [arXiv:hep-ph/0005232];
T. Gehrmann and E. Remiddi, Nucl. Phys. B **580** (2000) 485 [arXiv:hep-ph/9912329];
M. Caffo, H. Czyz, S. Laporta and E. Remiddi, Nuovo Cim. A **111** (1998) 365 [arXiv:hep-th/9805118].

[24] G. Passarino and M. Veltman, Nucl. Phys. B **160** (1979) 151;
D. Bardin and G. Passarino, *The standard model in the making: Precision study of the electroweak interactions*, *Oxford, UK: Clarendon (1999).*

[25] S. Catani and M. H. Seymour, arXiv:hep-ph/9609521;
S. Catani, S. Dittmaier, M. H. Seymour and Z. Trocsanyi, Nucl. Phys. B **627** (2002) 189 [arXiv:hep-ph/0201036];
S. Dittmaier, Nucl. Phys. B **565** (2000) 69 [arXiv:hep-ph/9904440].

[26] T. Binoth and G. Heinrich, Nucl. Phys. B **585** (2000) 741 [arXiv:hep-ph/0004013];
A. Denner, M. Melles and S. Pozzorini, Nucl. Phys. B **662** (2003) 299 [arXiv:hep-ph/0301241].
K. Hepp, Commun. Math. Phys. **2** (1966) 301.

[27] L.D. Landau, Nucl. Phys. **13** (1959) 181.

[28] G. 't Hooft and M. Veltman, Nucl. Phys. B **44** (1972) 189.

[29] J. van der Bij and M. J. Veltman Nucl. Phys. B **231** (1984) 205

[30] P. Cvitanovic and T. Kinoshita, Phys. Rev. D **10** (1974) 3978.

[31] R. Erdelyi et al., *Higher Transcendental Functions vol. 2*, Bateman Manuscript Project (*McGraw-Hill 1953*);
L. J. Slater, *Generalized Hypergeometric Functions* Cambridge Univ. Press, 1966.

[32] L. Lewin, *Poly-logarithms and Associated Functions*, North Holland (New York 1981).

[33] A. Ghinculov and J. J. van der Bij, Nucl. Phys. B **436** (1995) 30 [arXiv:hep-ph/9405418].

[34] M. Abramowitz and I. A. Stegun, *Handbook of Mathematical Functions*, Dover 1970.

[35] N. M. Korobov, Dokl. Acad. Nauk USSSR **115** (1957) 1062;
H. Conroy, J. Chem. Phys **47** (1967) 5307;
R. Cranley and T. N. L. Patterson, SIAM J. Numer. Anal. **137** (1976) 904.

[36] NAG Fortran Library, Mark 19, The Numerical Algorithms Group Ltd, Oxford UK. 1999.

[37] R. E. Cutkosky, J. Math. Phys. **1** (1960) 429;
G. 't Hooft and M. J. Veltman, *In Louvain 1973, Particle Interactions At Very High Energies, Part B, New York 1973, 177-322 and CERN Geneva - CERN 73-9.*

[38] D. Kershaw, Phys. Rev. D **5** (1972) 1976.

[39] O. V. Tarasov, arXiv:hep-ph/9505277.

[40] F. V. Tkachov, New methods for evaluation of multi-loop Feynman diagrams, PhD thesis, INR, Moscow, March 1984;
F. V. Tkachov, Phys. Lett. B **100** (1981) 65;
K. G. Chetyrkin and F. V. Tkachov, Nucl. Phys. B **192** (1981) 159;
F. V. Tkachov, Theor. Math. Phys. **56** (1983) 866 [Teor. Mat. Fiz. **56** (1983) 350].

[41] F. V. Tkachov, arXiv:hep-ph/0202033.

[42] S. Laporta, arXiv:hep-ph/0311065.

[43] P. A. Grassi, B. A. Kniehl and A. Sirlin, Phys. Rev. D **65** (2002) 085001 [arXiv:hep-ph/0109228];
P. Gambino and P. A. Grassi, Phys. Rev. D **62** (2000) 076002 [arXiv:hep-ph/9907254];
N. K. Nielsen, Nucl. Phys. B **101** (1975) 173.

[44] D. Y. Bardin, L. V. Kalinovskaya and F. V. Tkachov, hep-ph/0012209.

[45] G. Passarino, J. Phys. G **29** (2003) 121 [arXiv:hep-ph/0101299].

[46] P. J. Davis and P. Rabinowitz, *Numerical Integration*, Blaisdell Publishing Company 1967.

[47] G. 't Hooft and M. Veltman, Nucl. Phys. B **153** (1979) 365.

[48] A. C. Wu, Phys. Rev. D **9** (1974) 370.

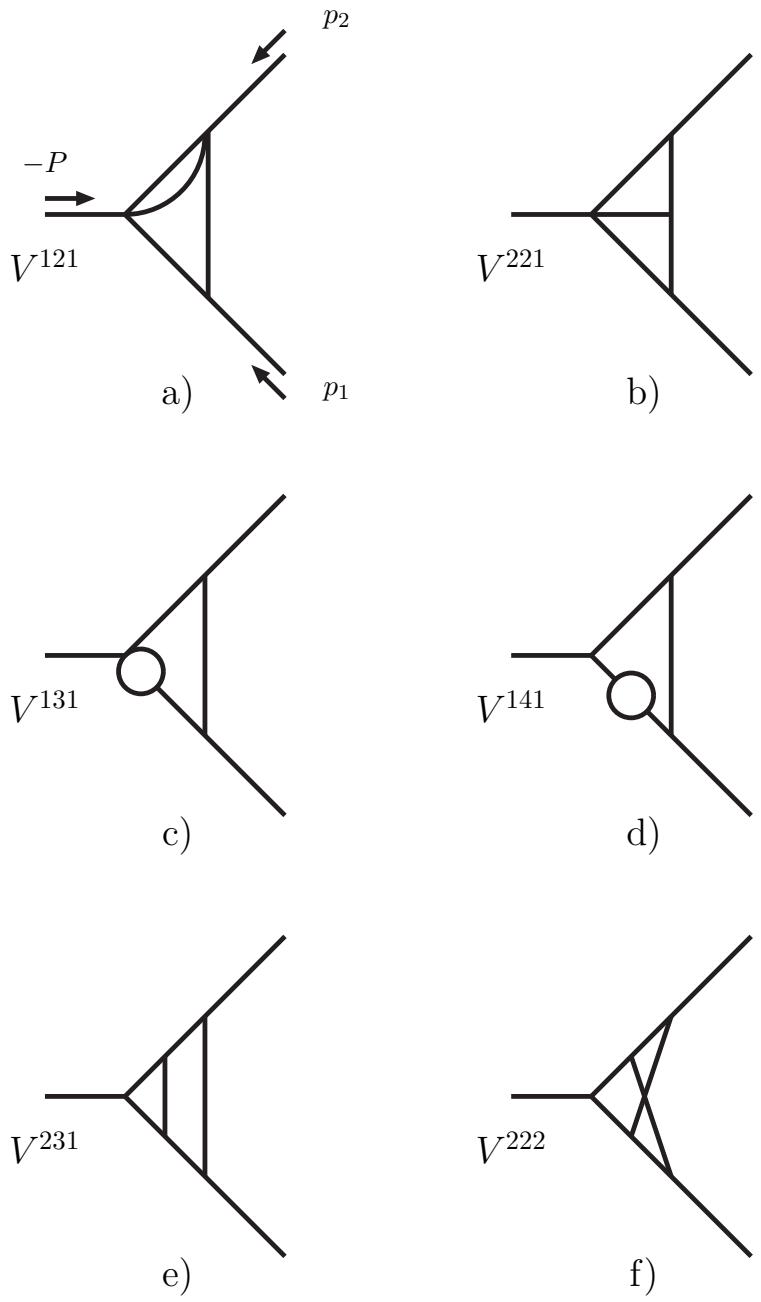

Figure 7: The irreducible two-loop vertex diagrams $V^{\alpha\beta\gamma}$ ($\gamma \neq 0$). External momenta are flowing inward.